

Stephen F. Austin State University

**SFA ScholarWorks**

---

Electronic Theses and Dissertations

---

8-2023

## Reservoir Characterization of the Utica Shale Play Using Well Log Data in Columbiana, Ohio

Tyler L. West

Stephen F Austin State University, Westtl@outlook.com

Follow this and additional works at: <https://scholarworks.sfasu.edu/etds>



Part of the [Geology Commons](#)

[Tell us](#) how this article helped you.

---

### Repository Citation

West, Tyler L., "Reservoir Characterization of the Utica Shale Play Using Well Log Data in Columbiana, Ohio" (2023). *Electronic Theses and Dissertations*. 507.

<https://scholarworks.sfasu.edu/etds/507>

This Thesis is brought to you for free and open access by SFA ScholarWorks. It has been accepted for inclusion in Electronic Theses and Dissertations by an authorized administrator of SFA ScholarWorks. For more information, please contact [cdsscholarworks@sfasu.edu](mailto:cdsscholarworks@sfasu.edu).

---

## Reservoir Characterization of the Utica Shale Play Using Well Log Data in Columbiana, Ohio

### Creative Commons License



This work is licensed under a [Creative Commons Attribution-Noncommercial-No Derivative Works 4.0 License](https://creativecommons.org/licenses/by-nc-nd/4.0/).



Reservoir Characterization of the Utica Shale Play Using Well Log Data in Columbiana,  
Ohio

By

Tyler West, Bachelor of Science

Presented to the Faculty of the Graduate School of  
Stephen F. Austin State University  
In Partial Fulfillment  
Of the Requirements

For the Degree of  
Master of Science in Geology

STEPHEN F. AUSTIN STATE UNIVERSITY  
August 2023

Reservoir Characterization of the Utica Shale Play Using Well Log Data in Columbiana,  
Ohio

By

Tyler West, Bachelor of Science

APPROVED:

---

Dr. Julie Bloxson, Thesis Director

---

Dr. Mindy Faulkner, Committee Member

---

Dr. LaRell Nielson, Committee Member

---

Dr. Robert Friedfeld, Committee Member

---

Sheryll Jerez, Ph.D.  
Interim Dean of Research and Graduate Studies

## **ABSTRACT**

The Ordovician Utica shale play is rapidly developing throughout the Appalachian Basin. The play is a mixed carbonate-siliciclastic system that grades from primarily carbonates at its base in the Lexington/Trenton limestones into primarily shale within the Utica shale. As of January 2021, it is the third highest-producing dry shale gas play in the contiguous U.S., although it is known to produce wet gas and oil in various parts of the basin. In addition to being an unconventional reservoir, the Utica shale, an informal unit in Ohio where the main fairway is located, is a known source rock for much of the Paleozoic strata across the Appalachian Basin, including multiple lower Paleozoic sandstone and carbonate units. Although some data are available on this play, models that scale from well site through basin are not publicly available. The objective of this research was the production of a petrophysical reservoir model capable of reflecting the geology, geomechanics, and geochemistry across Columbian County, Ohio, and the surrounding area as a part of a larger effort to create a scalable model that will encompass the entire Utica shale Play. Well logs, X-ray diffraction (XRD), X-ray fluorescence (XRF), and total organic carbon (TOC) data were utilized to create a model in Interactive Petrophysics (I.P.) 2021. Seismic and core data within the area is sparse, therefore the Schmoker and Hester method was utilized to estimate TOC from the readily available well logs and then calibrated with the core data available.

Lithology changes in the study area appear to correlate with known fault trends, structural highs correlating with carbonate-rich siliciclastics or thickened carbonate platform, and siliciclastic poor or thin shale intervals. Areas with increased clay content are adjacent to these structural highs and correlate with increased levels of TOC, creating localized sub-basins, or "sweet spots," that are localized rather than extensive throughout the area. These appear to be depositional lows, potentially influenced by Proterozoic basement features and faults that would have been reactivated during the Taconic Orogeny. This study expands the current knowledge regarding the Utica shale by modeling the relationship between lithology, eustatic sea level changes, prevalence of organic material, and basin subsidence. These data will assist oil and gas developers with future hydrocarbon exploration and production.

## CONTENTS

<b>ABSTRACT.....</b>	<b>iii</b>
<b>TABLE OF FIGURES.....</b>	<b>vii</b>
<b>LIST OF TABLES .....</b>	<b>xii</b>
<b>TABLE OF ABBREVIATIONS.....</b>	<b>xiii</b>
<b>TABLE OF EQUATIONS .....</b>	<b>xiv</b>
<b>1 INTRODUCTION.....</b>	<b>1</b>
<b>2 PREVIOUS STUDIES AND RESEARCH.....</b>	<b>5</b>
<b>3 GEOLOGIC SETTING .....</b>	<b>8</b>
<b>4 STRATIGRAPHY .....</b>	<b>13</b>
<b>5 METHODS.....</b>	<b>19</b>
<b>5.1 Data and Methodology Workflow .....</b>	<b>19</b>
<b>5.2 Data Correction and Synthetic Curve Generation.....</b>	<b>24</b>
<b>5.3 Clay Content .....</b>	<b>26</b>
<b>5.4 TOC and Pyrite Calculations .....</b>	<b>31</b>
<b>5.5 Silica Content Calculation .....</b>	<b>37</b>
<b>5.6 Volumetric Cross Section (U).....</b>	<b>38</b>
<b>5.7 Porosity, Saturation, and Deterministic Mineral Determination .....</b>	<b>38</b>
<b>5.8 GIS Mapping .....</b>	<b>50</b>
<b>6 RESULTS .....</b>	<b>51</b>
<b>6.1 Tracker Well.....</b>	<b>51</b>
<b>6.1.1 Upper Lexington Member.....</b>	<b>53</b>
<b>6.1.2 Point Pleasant Formation.....</b>	<b>54</b>
<b>6.1.3 Utica shale.....</b>	<b>56</b>
<b>6.2 Multi-well Analysis.....</b>	<b>58</b>
<b>6.2.1 Curdsville Member .....</b>	<b>59</b>



<b>6.2.2 Logana Member .....</b>	<b>69</b>
<b>6.2.3 Upper Lexington Member .....</b>	<b>78</b>
<b>6.2.4 Point Pleasant Formation.....</b>	<b>87</b>
<b>6.2.5 Utica shale.....</b>	<b>96</b>
<b>7 DISCUSSION .....</b>	<b>105</b>
<b>7.1 Model Error .....</b>	<b>105</b>
<b>7.2 Lithology Variations and Far-Field Tectonics.....</b>	<b>107</b>
<b>7.3 Eastern Ohio Fault Systems .....</b>	<b>114</b>
<b>8 CONCLUSIONS .....</b>	<b>118</b>
<b>9. FUTURE WORK .....</b>	<b>121</b>
<b>10. REFERENCES.....</b>	<b>122</b>
<b>11. APPENDIX A .....</b>	<b>130</b>
<b>12. VITA.....</b>	<b>141</b>

## TABLE OF FIGURES

<b>Figure 1:</b> Map of the Utica shale Play overlaid by the Utica Consortium assessment units, with Columbiana County outlined in red. Columbiana County is observed to be located within all three assessment units. Map modified from Patchen and Carter, 2015.....	4
<b>Figure 2:</b> Middle Ordovician paleographic map. Approximate outline of the Appalachian Basin is in red. Modified from Scotese, 2002.....	9
<b>Figure 3:</b> Map showing the positions of Taconian tectonic highlands, migrating dark-shale basins, and continental promontories during the Middle Ordovician to Early Silurian. CT = Carolina terrane; GA = Ganderia; AV = Avalonia. From Ettensohn and Lierman, 2012. ....	10
<b>Figure 4:</b> Facies map of eastern Laurentia during the Taconic tectophase of the Taconian Orogeny. (A) Facies map during the Blackriverian, with a carbonate platform (Black River Platform) visible during the late Blountian tectophase. (B) Facies map illustrating the differentiation of the Black River Platform into the Galena shelf and Trenton shelf in the northwest and the Lexington platform in the southeast. Partitioning the Galena/Trenton shelf and the Lexington platform is the Seabee Trough. From Ettensohn and Lierman, 2012.....	11
<b>Figure 5:</b> Eastern Ohio stratigraphic column representing the Upper Ordovician strata in the area. The Lexington Limestone has been divided into its respective members. Modified from Patchen and Carter, 2015.....	14
<b>Figure 6:</b> Map displaying the location of the wells in study area across eastern Ohio. The Tracker Well is represented by a red star in southeastern Portage County.....	20
<b>Figure 7:</b> Type-log for the researched units in Eastern Ohio using the Solomon Aquila E (API: 3402921476000) well. From Patchen and Carter, 2015.....	22
<b>Figure 8:</b> Example of a GR curve with clean and clay sections interpreted on the Tracker Well. ....	28

<b>Figure 9:</b> Neutron/Density crossplot illustrates the clean and clay point locations. Data from the well log were plotted with their neutron porosity value and density. The clay volume is then calculated based on the distance from the “clean” line (0% clay) and the 100% clay point. From the Interactive Petrophysics manual (Geoactive, 2023). .....	29
<b>Figure 10:</b> Log plot illustrating the GR, NPHI, and RHOB curves compared to the subsequent interpreted clay curves VCLGR and VCLND. XRD clay data was overlaid on top to calibrate the interpretation. ....	30
<b>Figure 11:</b> Log plot of the modified Schmoker and Hester curve overlaid with laboratory TOC measurements. ....	32
<b>Figure 12:</b> Log plot of the modified Passey method derived TOC curve overlaid with Laboratory TOC measurements. ....	34
<b>Figure 13:</b> Log plot of <i>TOC<sub>min</sub></i> with laboratory TOC overlaid. ....	35
<b>Figure 14:</b> Log plot of the calculated volume of pyrite in comparison to the XRD pyrite percentage. The calculated pyrite volume exhibits a relatively close fit to the XRD data, with a slight overestimation for Upper Lexington and Point Pleasant and a slight underestimation for the Utica shale. ....	37
<b>Figure 15:</b> Log plot illustrating laterolog deep (LLD), micro-spherically focused log (MSFL), calculated apparent formation and mud filtrate resistivity ( <i>R<sub>wapp</sub></i> and <i>R<sub>mfapp</sub></i> ), calculated un-invaded and flushed zone saturations ( <i>Swu</i> and <i>Sxou</i> ), calculated total and effective porosity ( <i>Phi<sub>T</sub></i> and <i>Phi<sub>e</sub></i> ), bulk volume water flushed zone ( <i>BVW<sub>sxo</sub></i> ), and calculated mineralogy for the Tracker Well.....	52
<b>Figure 16:</b> Map reflecting the mean clay content ( <i>V<sub>clay</sub></i> ; decimal) of the Curdsville Member across the research area, with Precambrian faults and known lineaments in the study area. ....	63
<b>Figure 17:</b> Map reflecting mean carbonate content ( <i>V<sub>carb</sub></i> , decimal) of the Curdsville Member across the research area, with Precambrian faults and known lineaments in the study area. ....	64
<b>Figure 18:</b> Map reflecting mean siliciclastic content ( <i>V<sub>siliciclastic</sub></i> , decimal) of the Curdsville Member across the research area, with Precambrian faults and known lineaments in the study area. ....	65

<b>Figure 19:</b> Map representing the mean pyrite content ( $V_{\text{pyrite}}$ , decimal) of the Curdsville Member across the research area, with Precambrian faults and known lineaments in the study area. ....	66
<b>Figure 20:</b> Map representing mean Total Organic Content (TOC, wt%) of the Curdsville Member across the research area with Precambrian faults and known lineaments in the study area. ....	67
<b>Figure 21:</b> Map representing the mean porosity (decimal) of the Curdsville Member across the research area with Precambrian faults and known lineaments in the study area. ....	68
<b>Figure 22:</b> Map reflecting the mean clay content ( $V_{\text{clay}}$ ; decimal) of the Logana Member across the research area, with Precambrian faults and known lineaments in the study area. ....	72
<b>Figure 23:</b> Map reflecting mean carbonate content ( $V_{\text{carb}}$ , decimal) of the Logana Member across the research area, with Precambrian faults and known lineaments in the study area. ....	73
<b>Figure 24:</b> Map reflecting mean siliciclastic content ( $V_{\text{siliciclastic}}$ , decimal) of the Logana Member across the research area, with Precambrian faults and known lineaments in the study area. ....	74
<b>Figure 25:</b> Map representing the mean pyrite content ( $V_{\text{pyrite}}$ , decimal) of the Logana Member across the research area, with Precambrian faults and known lineaments in the study area. ....	75
<b>Figure 26:</b> Map representing mean Total Organic Content (TOC, wt%) of the Logana Member across the research area with Precambrian faults and known lineaments in the study area. ....	76
<b>Figure 27:</b> Map representing the mean porosity (decimal) of the Logana Member across the research area with Precambrian faults and known lineaments in the study area. ....	77
<b>Figure 28:</b> Map reflecting the mean clay content ( $V_{\text{clay}}$ ; decimal) of the Upper Lexington Member across the research area, with Precambrian faults and known lineaments in the study area. ....	81
<b>Figure 29:</b> Map reflecting mean carbonate content ( $V_{\text{carb}}$ , decimal) of the Upper Lexington Member across the research area, with Precambrian faults and known lineaments in the study area. ....	82

<b>Figure 30:</b> Map reflecting mean siliciclastic content ( $V_{\text{siliciclastic}}$ , decimal) of the Upper Lexington Member across the research area, with Precambrian faults and known lineaments in the study area. ....	83
<b>Figure 31:</b> Map representing the mean pyrite content ( $V_{\text{pyrite}}$ , decimal) of the Upper Lexington Member across the research area, with Precambrian faults and known lineaments in the study area. ....	84
<b>Figure 32:</b> Map representing mean Total Organic Content (TOC, wt%) of the Upper Lexington Member across the research area with Precambrian faults and known lineaments in the study area. ....	85
<b>Figure 33:</b> Map representing the mean porosity (decimal) of the Upper Lexington Member across the research area with Precambrian faults and known lineaments in the study area. ....	86
<b>Figure 34:</b> Map reflecting the mean clay content ( $V_{\text{clay}}$ ; decimal) of the Point Pleasant Formation across the research area, with Precambrian faults and known lineaments in the study area. ....	90
<b>Figure 35:</b> Map reflecting mean carbonate content ( $V_{\text{carb}}$ , decimal) of the Point Pleasant Formation across the research area, with Precambrian faults and known lineaments in the study area. ....	91
<b>Figure 36:</b> Map reflecting mean siliciclastic content ( $V_{\text{siliciclastic}}$ , decimal) of the Point Pleasant Formation across the research area, with Precambrian faults and known lineaments in the study area. ....	92
<b>Figure 37:</b> Map representing the mean pyrite content ( $V_{\text{pyrite}}$ , decimal) of the Point Pleasant Formation across the research area, with Precambrian faults and known lineaments in the study area. ....	93
<b>Figure 38:</b> Map representing mean Total Organic Content (TOC, wt%) of the Point Pleasant Formation across the research area with Precambrian faults and known lineaments in the study area. ....	94
<b>Figure 39:</b> Map representing the mean porosity (decimal) of the Point Pleasant Formation across the research area with Precambrian faults and known lineaments in the study area. ....	95
<b>Figure 40:</b> Map reflecting the mean clay content ( $V_{\text{clay}}$ ; decimal) of the Utica Shale across the research area, with Precambrian faults and known lineaments in the study area. ....	99

<b>Figure 41:</b> Map reflecting mean carbonate content ( $V_{carb}$ , decimal) of the Utica Shale across the research area, with Precambrian faults and known lineaments in the study area. ....	100
<b>Figure 42:</b> Map reflecting mean siliciclastic content ( $V_{siliciclastic}$ , decimal) of the Utica Shale across the research area, with Precambrian faults and known lineaments in the study area. ....	101
<b>Figure 43:</b> Map representing the mean pyrite content ( $V_{pyrite}$ , decimal) of the Utica Shale across the research area, with Precambrian faults and known lineaments in the study area. ....	102
<b>Figure 44:</b> Map representing mean Total Organic Content (TOC, wt%) of the Utica Shale across the research area with Precambrian faults and known lineaments in the study area. ....	103
<b>Figure 45:</b> Map representing the mean porosity (decimal) of the Utica Shale across the research area with Precambrian faults and known lineaments in the study area. ....	104
<b>Figure 46:</b> Generalized facies distribution across the state for the (A) the Lexington and Trenton limestones and (B) the Point Pleasant Formation and Utica shale as determined by the well log analysis. A red box has been added in eastern Ohio to represent the research area. Modified from Bloxson et al. (2022). ....	112
<b>Figure 47:</b> Diagram illustrating the contractional overstepping between the Akron-Suffield-Smith fault system and the Highlandtown sault system. From Waid, 2018. ....	115
<b>Figure 48:</b> Fault and lineament map indicating the up-thrown and down-thrown blocks in the research area. Normal faults were interpreted from facies, and strike-slip faults were labeled from previous studies. ....	117

## LIST OF TABLES

<b>Table 1:</b> Water/clays module as displayed in Interactive Petrophysics for the Tracker Well. ....	40
<b>Table 2:</b> Sw logic/limits module as displayed in Interactive Petrophysics for the Tracker Well.....	42
<b>Table 3:</b> Sw parameters module as displayed in Interactive Petrophysics for the Tracker Well.....	44
<b>Table 4:</b> Sonic/neutron/density module as displayed in Interactive Petrophysics for the Tracker Well. ....	45
<b>Table 5:</b> Table of the mineral model for the Tracker Well, representing the selected input curves, their respective values, and the subsequent minerals for the model to calculate. ....	47
<b>Table 6:</b> Data table denoting well names, API, location, and wireline data present at each well. ....	130
<b>Table 7:</b> Data table denoting the presence of core data at each well. ....	133
<b>Table 8:</b> Data table denoting the mean mineralogy for the Curdsville Member wells utilized.....	136
<b>Table 9:</b> Data table denoting the mean mineralogy for the Logana Member wells utilized.....	137
<b>Table 10:</b> Data table denoting the mean mineralogy for the Upper Lexington wells utilized.....	138
<b>Table 11:</b> Data table denoting the mean mineralogy for the Point Pleasant wells utilized. ....	139
<b>Table 12:</b> Data table denoting the mean mineralogy for the Utica shale wells utilized. ....	140

## TABLE OF ABBREVIATIONS

Abbreviation	Data Type	Description
BSW <sub>SXO</sub>	Calculated	Bulk Volume Water Flushed Zone
DSI <sub>SYN</sub>	Calculated	Volumetric Silicon Content
DT <sub>SYN</sub>	Calculated	Synthetic Sonic Log
GEM	Wireline	Haliburton's Elemental Analysis Tool
GR	Wireline	Gamma Ray Log
LLD	Wireline	Laterolog Deep Resistivity Log
MSFL	Wireline	Micro-Spherically Focused Log Tool
NPHI	Wireline	Neutron Porosity Log
NPHI <sub>SYN</sub>	Calculated	Synthetic Neutron Porosity Log
PEF	Wireline	Photo-electric Effect Log
PEF <sub>SYN</sub>	Calculated	Synthetic PEF Log
RHOB	Wireline	Bulk Density Log
Rmfapp	Calculated	Apparent Mud Filtrate Resistivity
Rt	Wireline	Deep Resistivity Log
Rwapp	Calculated	Apparent Formation Water Resistivity
Rxo	Wireline	Flushed Zone Resistivity Log
Swu	Calculated	Un-invaded Zone Saturation
Sxou	Calculated	Flushed Zone Saturation
TOC	Laboratory	Total Organic Content
TOC <sub>MIN</sub>	Calculated	Minimum TOC Value of Schmoker and Passey.
TOC <sub>PASSEY</sub>	Calculated	Passey method calculated TOC
TOC <sub>SMKR</sub>	Calculated	Hester and Schmoker calculated TOC
U	Calculated	Volumetric Cross Section
Vcl	Calculated	Minimum Clay Volume
Vclav	Calculated	Average Clay value
VclGR	Calculated	Gamma Ray Clay Volume
VclND	Calculated	Neutron/Density Clay Volume
V <sub>PYRITE</sub>	Calculated	Volumetric Pyrite Content
XRD	Laboratory	X-ray Diffraction
XRF	Laboratory	X-ray Fluorescence



## TABLE OF EQUATIONS

<b>Equation 1</b>	$\text{NPHIsyn} = 0.00112 * \text{GR} + 0.0161$	
	Where GR is the gamma ray value in API at a given depth for the well to have NPHI calculated. It is important to note that this method causes a degree of error within the mineral model for that well, and requires the interpreter to adjust the confidence within the mineral model .....	26
<b>Equation 2</b>	$\text{PEFsyn} = 4.75 - 0.0078 * \text{GR}$	
	Where PEFsyn is the synthetic photoelectric effect curve, and G.R. is the gamma ray log response. ....	26
<b>Equation 3</b>	$\text{VclGr} = \frac{\text{Gr} - \text{GrClean}}{\text{GrClay} - \text{GrClean}}$	
	Where Gr is the log response, GrClean is the interpreted clean point, and GrClay is the interpreted max clay point. ....	27
<b>Equation 4</b>	$\text{VclND} = \frac{(\text{DenCl2} - \text{DenCl1}) \cdot (\text{Neu} - \text{NeuCl1}) - (\text{Den} \cdot \text{DenCl1}) \cdot (\text{NeuCl2} - \text{NeuCl1})}{(\text{DenCl2} - \text{DenCl1}) \cdot (\text{NeuClay} - \text{NeuCl1}) - (\text{Denclay} - \text{DenCl1}) \cdot (\text{NeuCl2} - \text{NeuCl1})}$	
	Where Neu is the neutron porosity curve, Den is the density curve, and DenCl1/NeuCl1 and DenCl2/NeuCl2 are the density and neutron values for the two ends of the clean line on the crossplot. ....	27
<b>Equation 5</b>	$\text{TOC}_{\text{SMKR}}(\text{wt}\%) = \frac{166}{\text{RHOB}} - 59.261$	
	Where RHOB is the density value from the well log. ....	31
<b>Equation 6</b>	$\text{DTsyn} = (130 * \text{NPHI}) + 40$	
	Where NPHI is the neutron porosity well log value in porosity units. ....	33
<b>Equation 7</b>	$\text{TOC}_{\text{Passey}}(\text{wt}\%) = \text{Log} \left( \frac{\text{Rdeep}}{50} \right) + 0.02 * (\text{DT} - 80) * 10^{(2.297 - 0.1688 * 10.6)}$	
	Where Rdeep is the deep resistivity value from the well log and D.T. is the sonic value. ....	33
<b>Equation 8</b>	$\text{TOCmin} = \text{Minimum}(\text{TOCSMKR}, \text{TOCPassey})$	
	Where TOCSMKR is the calculated TOC value from the Schmoker and Hester method, and TOCPassey is the TOC value calculated from the Passey method. ....	34

<b>Equation 9</b>	$V_{\text{pyrite}} = \frac{\text{TOC}_{\text{min}}}{150}$	
	Where TOCmin is the TOC value calculated from Eq. 8. ....	36
<b>Equation 10</b>	$\text{DSIsyn} = 42.1 * V_{\text{cl}} + 2.70$	
	Where DSIsyn is the calculated silicon content, and Vcl is the minimum clay volume log. ....	38
<b>Equation 11</b>	$U = \text{PEF} * \text{RHOB} + 0.1883 * 0.93423$	
	Where U is the calculated volumetric cross section, PEF is the photoelectric effect curve, and RHOB is the density curve. ....	38
<b>Equation 12</b>	$\text{Phie} = \sum V_{\text{water}_i} + \sum V_{\text{hydrocarbon}_i}$	
	Where Phie is effective porosity, $V_{\text{water}_i}$ is the $i_{\text{th}}$ mineral of type water Sxo, and $V_{\text{hydrocarbon}_i}$ is the $i_{\text{th}}$ mineral of type hydrocarbon Sxo. .... <b>Error! Bookmark not defined.</b>	
<b>Equation 13</b>	$\text{Phit} = \text{Phie} + V_{\text{cl}} * \text{PhitClay}$	
	Where Phit is total porosity, Phie is effective porosity, Vcl is wet clay volume, and PhitClay is the entered parameter total clay porosity. ....	41
<b>Equation 14</b>	$V_{\text{cl}} = \sum V_{\text{wetclay}_i}$	
	Where Vcl is the wet clay volume, and $V_{\text{wetclay}_i}$ is the $i_{\text{th}}$ mineral of type of wet clay. ....	41
<b>Equation 15</b>	$\frac{1}{R_t} = \frac{\text{PhiT}^m * S_w^n}{a * S_w}$	
	Archie PhiT equation where $R_t$ is the input resistivity curve, PhiT is the total porosity, m is the cementation factor, $S_w$ is the effective water saturation, n is the saturation exponent, and a is the tortuosity factor. ....	43
<b>Equation 16</b>	$S_w = \frac{\sum V_{\text{water}U_i}}{\sum V_{\text{water}U_i} + \sum V_{\text{hydrocarbon}U_i}}$	
	Where $S_w$ is the un-invaded zone saturation calculated from $R_t$ , $\sum V_{\text{water}U_i}$ is the $i_{\text{th}}$ mineral of type water in the un-invaded zone, and $\sum V_{\text{hydrocarbon}U_i}$ is the $i_{\text{th}}$ mineral of type hydrocarbon in the un-invaded zone. This controls the ratio of water to hydrocarbon in the model in the un-invaded zone. This formula produces an iteration loop where $S_w$ is calculated using the input $R_t$ curve and the Archie PhiT equation. ....	43
<b>Equation 17</b>	$S_{xo} = \frac{\sum V_{\text{water}_i}}{\sum V_{\text{water}_i} + \sum V_{\text{hydrocarbon}_i}}$	
	Where $S_{xo}$ is the invaded zone saturation calculated from $R_{xo}$ , $\sum V_{\text{water}_i}$ is the $i_{\text{th}}$ mineral of type water in the invaded zone, and $\sum V_{\text{hydrocarbon}_i}$ is the	

*i*th mineral of type hydrocarbon in the invaded zone. This controls the ratio of water to hydrocarbon in the model in the flushed zone. This formula produces an iteration loop where  $S_{xo}$  is calculated using the input  $R_{xo}$  curve and the Archie  $\Phi_i T$  equation. .... 43

**Equation 18**      $Den_{hydrocarbon} = \frac{5.5 * \rho_{den} * (4 - \rho_{den}) - 3}{(16 - 2.5 * \rho_{den})}$

Where  $Den_{hydrocarbon}$  is the modified density hydrocarbon equation, and  $\rho_{den}$  is the input hydrocarbon density. .... 45

## **1 INTRODUCTION**

The Ordovician Utica shale play is a rapidly developing oil and gas play extending throughout the Appalachian Basin across New York, Pennsylvania, Ohio, and West Virginia. The play is an organic-rich, mixed carbonate-siliciclastic system that grades from primarily carbonates at its base in the Lexington/Trenton limestones into primarily shale within the Utica shale (Patchen and Carter, 2015). As of March 2022, it is the third-highest producing dry shale gas play in the contiguous U.S. (Energy Information Administration, 2022), although it produces wet gas and oil in various parts of the basin (Popova, 2017). The Point Pleasant, upper Lexington/Trenton Limestones, and Logana Member of the Lexington Limestone are the most productive strata within the play (Patchen and Carter, 2015). In addition to an unconventional reservoir, the Utica shale is a known source rock for much of the Paleozoic strata across the Appalachian Basin, including multiple lower Paleozoic sandstone and carbonate units in the region (Ryder, 2008). Within Ohio, the main play fairway and the focus of this study, the Utica shale is informal and refers to the base of the Kope Formation. The shale formations within the play also show potential as target reservoirs for CO<sub>2</sub> capture and storage (CCS) once hydrocarbons are depleted. Advantages of injecting into these fractured shale formations as opposed to saline aquifers include increased storage capacity as a result of the empty pore space once occupied by oil/gas, reduced leakage risk as a result of the kerogen

providing a matrix for CO<sub>2</sub> sorption, and cost reduction due to the already present infrastructure in place at gas wells (Tao et al., 2014).

Although extensive and spanning throughout the Appalachian Basin, the strata vary both laterally and vertically in mineralogy, organic matter, and thermal maturity. Basin geometry and architecture are controlled by Ordovician tectonic forces resulting in the platform areas and depocenter locations shifting laterally and affecting observed thickness patterns and depositional environments, causing the heterogeneities observed in core, well logs, and outcrop (Patchen et al., 2006). Laterally, the different formations have noticeable organic variability throughout the basin, even within a formation itself. Within Ohio, mean total organic carbon (TOC) maps indicate that the Utica shale, Point Pleasant, and Logan Member of the Trenton Limestone are more organic-rich in central to eastern Ohio in comparison to other portions of the state, with values averaging over 2% TOC in these areas (Patchen and Carter, 2015). In addition, bulk mineralogy (including clay, carbonate, and other siliciclastics) also changes, representing the changing depositional environment. Vertically, the play transitions from a carbonate-rich, organic poor stratum at the base to an organic-rich shale at its top, with interbedding between consisting of shale, limestone, and siltstone (Patchen and Carter, 2015). It is observed that organic carbon varies throughout the basin, occurring in "sweet spots" in the Utica play compared to discrete horizons that extend throughout a basin, such as the Permian Basin Wolfcamp Shale. These "sweet spots" are effectively areas or pockets with high TOC, and are the targets for hydrocarbon exploration in the play (Patchen and

Carter, 2015). Therefore, it is crucial to take into account how the properties of the strata change laterally and vertically to better understand the depositional history of the play and produce a proper reservoir characterization model capable of locating the production zones.

The focus of this work is to model the geochemistry, geomechanics, and organic content of the Utica shale play in Columbiana County, Ohio (Figure 1) and the surrounding area using petrophysics to characterize the reservoir and better understand the relationship between play deposition and hydrocarbon accumulation. This work is part of a larger effort to create a scalable model encompassing the entire Appalachian Basin. The geochemistry, geomechanics, and organic richness of the play are primarily controlled by the strata's depositional environment and diagenetic history. Basin subsidence and eustatic sea level changes produced conditions optimal for preserving organic material and deposition of the mixed carbonate-siliciclastic system. However, these are variable both spatially and temporally. Modeling these properties will provide better insight into hydrocarbon distribution and reservoir quality for further play development and advancing our understanding of the depositional and diagenetic history of the Utica shale and Upper Ordovician Strata.

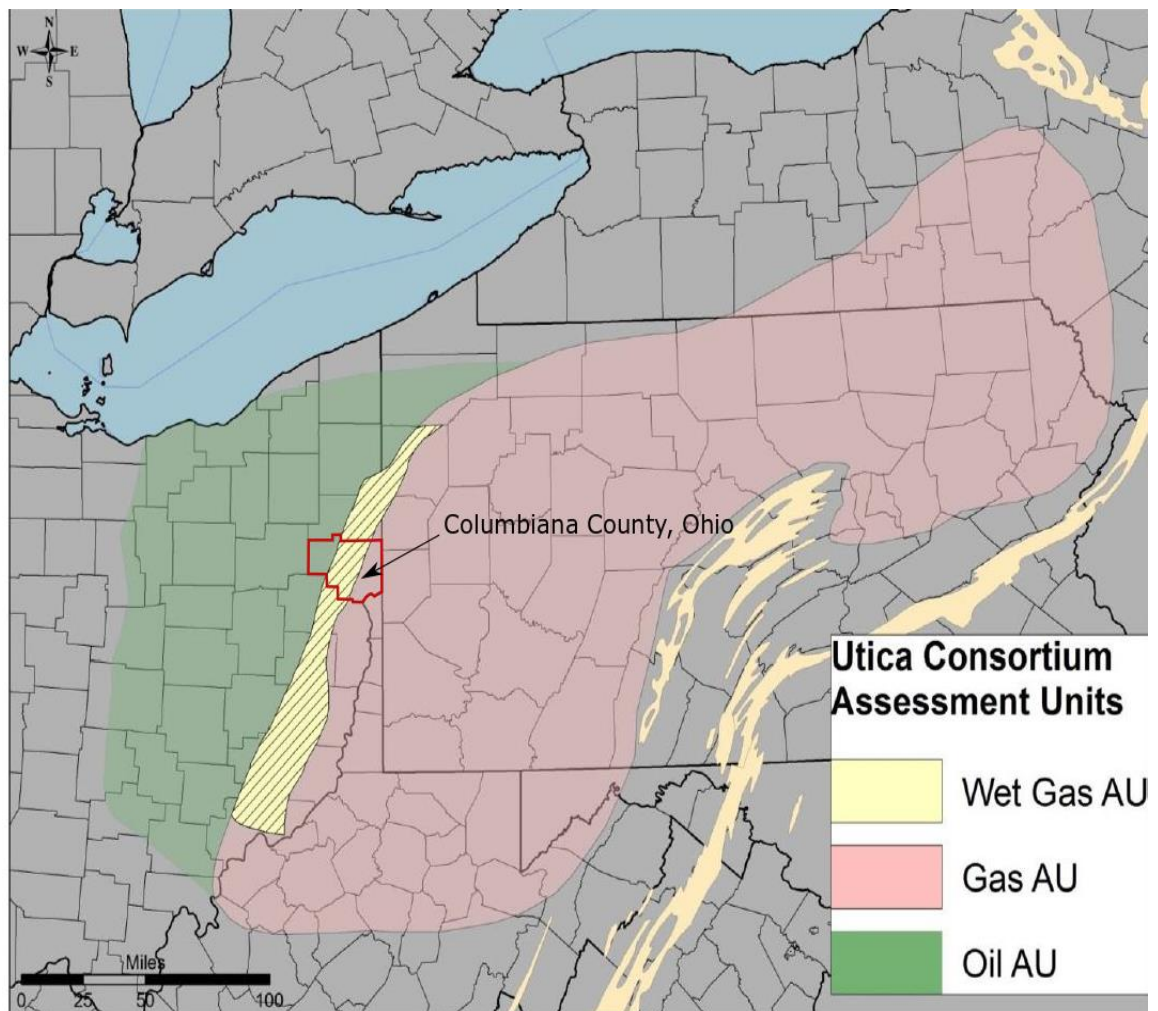


**Figure 1:** Map of the Utica shale Play overlaid by the Utica Consortium assessment units, with Columbiana County outlined in red. Columbiana County is observed to be located within all three assessment units. Map modified from Patchen and Carter, 2015.

## **2 PREVIOUS STUDIES AND RESEARCH**

An extensive study of the Utica shale Play was completed in 2015 by the Utica shale Consortium (Patchen and Carter, 2015). This study represents a coordinated effort between the Appalachian Basin Oil & Natural Gas Research Consortium (AONGRC) and the West Virginia University Shale Research, Education, Policy, and Economic Development Center. The consortium outlined three main objectives: "(1) characterize and assess the lithology, source rock geochemistry, stratigraphy, depositional environment(s) and reservoir characteristics of Utica and equivalent rocks in the northern Appalachian basin; (2) define Utica oil and gas fairways by integrating regional mapping work with drilling activity, and production tracking efforts; and (3) provide production-based and volumetric Utica resource assessments informed by geologic and geochemical data collected during this study." The focus of the Utica Playbook is on the Late Ordovician strata of the Appalachian Basin, comprised of the Kope Formation, Utica shale, Point Pleasant Formation, and Lexington/Trenton Formation (Patchen and Carter, 2015).

The Utica Playbook interprets the depositional environment for the Point Pleasant Formation, upper Lexington/Trenton Formation, and Logan Member as being a relatively shallow (likely <100 ft.), storm-dominated, carbonate shelf that experienced frequent algal blooms. Based on the fossils present within the limestone, water levels



were shallow, exposed to sunlight, and well oxygenated. Storm beds, such as those present within the Point Pleasant Formation, suggest levels well above the storm wave base. It is believed that seasonal anoxia may have been present based on frequent algal blooms (Patchen and Carter, 2015). Although previously thought to be deposited in deeper anoxic waters, the Utica shale may have been deposited in relatively shallow waters (<50 meters and commonly <30 meters) based on the occurrence of organic-rich shales immediately overlying unconformities (Smith, 2013).

The playbook also describes the mineralogy of the play, which directly plays a role in the rock mechanics of the strata and the subsequent ability to fail under hydraulic fracturing. For the Utica shale, a carbonate percentage of up to 25% is determined, indicating that clay content could be as high as 70%. This implies that despite the relatively high TOC ranges of up to 3.5% within the Utica shale, it may not fail under hydraulic stresses produced by fracking, adversely affecting its potential to be a productive play (Patchen and Carter, 2015). The underlying Point Pleasant Formation has a carbonate content ranging from 40-60%. Combined with a TOC as high as 5%, this is the target for drilling within the play (Patchen and Carter, 2015). The Upper Lexington/Trenton and Logan Formations have a carbonate content of approximately 70% and TOC as high as 5% in areas, suggesting that both formations have the potential for being productive reservoirs. The Curdsville Member, despite a carbonate content as high as 90%, has little to no TOC and is not a productive reservoir play (Patchen and Carter, 2015).

X-Ray Fluorescence (XRF) data is not available in the research area but has been collected by Barbara Kemeh of Stephen F. Austin State University for Portage County, representing the northwestern extent of the research area (Kemeh, 2021). This will provide the elemental composition of the shales in addition to calibration of the lithology model. Her work will be incorporated into this study using well log analysis and petrophysics to extrapolate composition to the remainder of the wells.

### **3 GEOLOGIC SETTING**

The Appalachian Basin is a composite foreland basin formed over approximately 340 Ma, from the late Neoproterozoic (570 Ma) to the Late Triassic (230 Ma). Formation of the basin occurred in stages, primarily produced by four nearly continuous orogenies (Taconian, Salinic, Acadian/Neoacadian, and Alleghanian) along the southeastern Laurentian Margin. However, it is strongly influenced by the relict Precambrian continental-margin architectures left from Iapetan rifting (Ettensohn and Lierman, 2012).

During the Middle Ordovician, Laurentia was located along the paleoequator (Scotese, 2003; Figure 2) in a subtropical to tropical climate (Sohrabi, 2013). At this time, the passive margin of Laurentia was an extensive carbonate platform known as the Great American Carbonate Bank, represented in eastern Ohio as the Knox Group, submerged in warm shallow water and comprised of carbonates and siliciclastics (Cornell, 2008). Along the active margin, the proto-Appalachian Mountains were forming due to the convergence between Laurentia and island arc terranes of the Iapetus. This resulted in the advent of the Taconian orogeny at approximately 472 Mya, with development of the Appalachian foreland basin continuing for nearly 200 Ma during four nearly continuous orogenies that reflect the closure of the Iapetus and Rheic oceans and the growth of Pangea (Ettensohn, 2008).

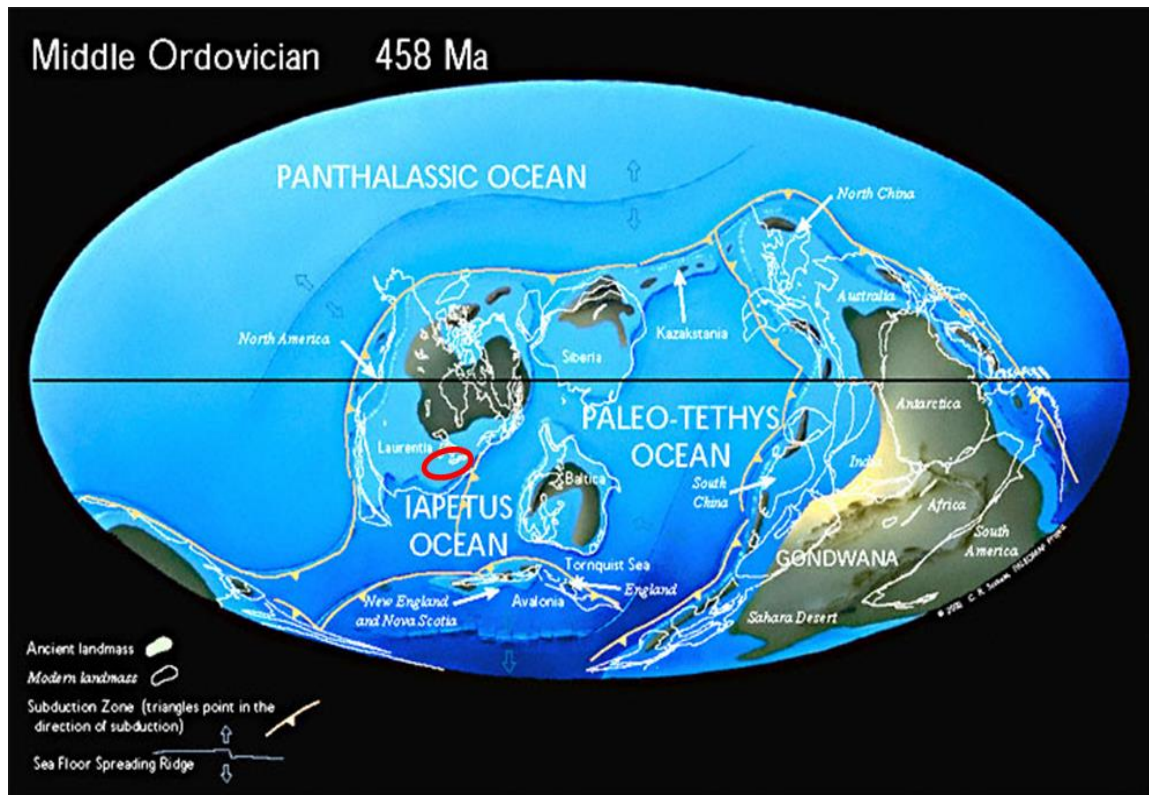


**Figure 2:** Middle Ordovician paleogeographic map. The approximate outline of the Appalachian Basin is in red. Modified from Scotese, 2002.

The second tectophase within the Taconian Orogeny is the Taconic Tectophase (Ettensohn and Lierman, 2012). Within this phase, the Lexington/Trenton, Point Pleasant, and Utica formations were deposited, occurring from the early Chatfieldian to the end of the Gamachian (Ettensohn and Lierman, 2012). The start of the tectophase is represented by the Rocklandian unconformity and the deposition of bentonites across much of the region. The resultant basin is known as the Martinsburg Foreland Basin, characterized by its dark shales (Ettensohn and Lierman, 2012; Figure 3, Figure 4). The northern part of

the basin (located in Central New York and Pennsylvania) is partitioned into a separate sub-basin by reactivated Grenvillian basement structures.

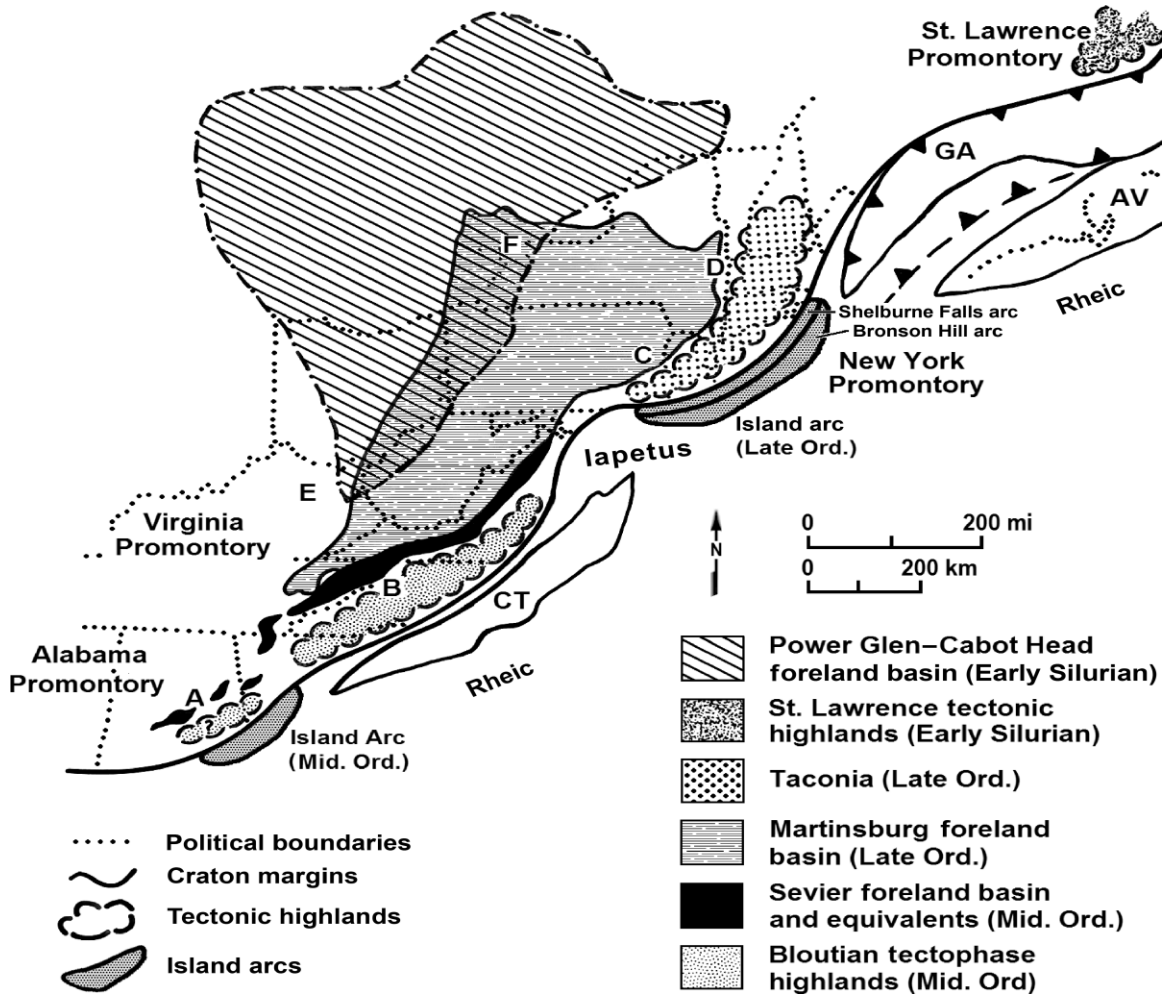


**Figure 3:** Map showing the positions of Taconian tectonic highlands, migrating dark-shale basins, and continental promontories during the Middle Ordovician to Early Silurian. CT = Carolina terrane; GA = Ganderia; AV = Avalonia. From Ettensohn and Lierman, 2012.

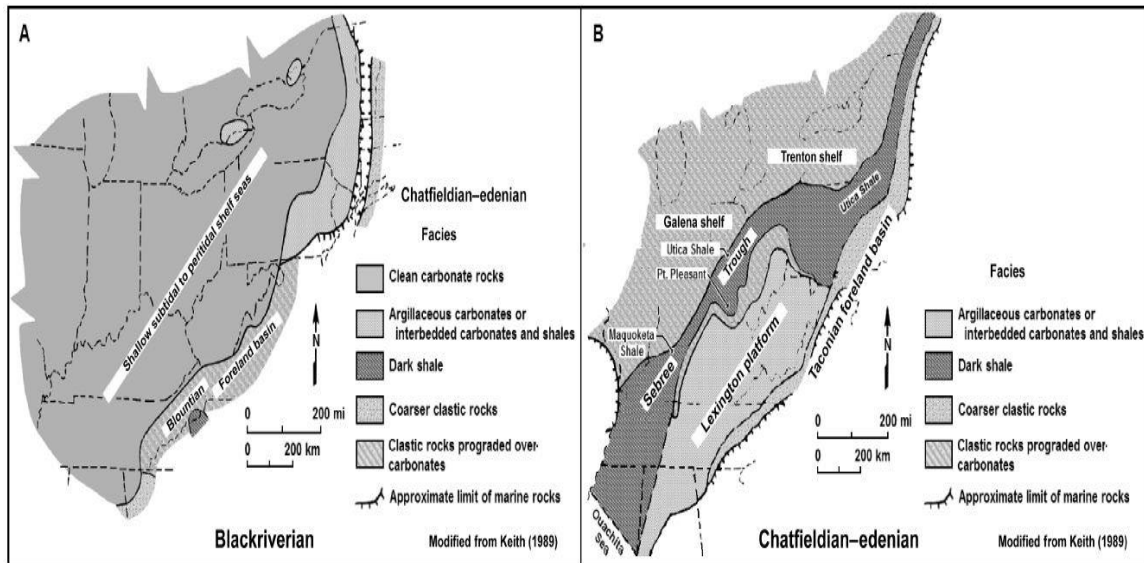


**Figure 4:** Facies map of eastern Laurentia during the Taconic tectophase of the Taconian Orogeny. (A) Facies map during the Blackriverian, with a carbonate platform (Black River Platform) visible during the late Blountian tectophase. (B) Facies map illustrating the differentiation of the Black River Platform into the Galena shelf and Trenton shelf in the northwest and the Lexington platform in the southeast. Partitioning the Galena/Trenton shelf and the Lexington platform is the Sebree Trough. From Ettensohn and Lierman, 2012.

The basin architecture during Middle Ordovician was dominated by a Black Riverian ramp to the northwest, flanked by the central Appalachian Basin along the southeastern margin and the deeper Sevier Basin farther to the east and southeast. During the Middle to Late Ordovician, the region transitioned from a passive/extensional regime to a compressive regime with the collision of the Taconic arc from the east-southeast. The resulting architecture was a broad, shallow-water carbonate ramp as epeiric seas transgressed much of the region, leading to the deposition of the Black River Group. During this time, a north-northeast-trending depocenter formed, expanding throughout

the remainder of the Ordovician Period and becoming characteristic of the central Appalachian Basin (Patchen et al., 2006). Extensive ash deposits are located throughout the carbonate ramp as a result of the volcanic island arcs formed along the Laurentian craton margin (Patchen et al., 2006).

The basin architecture continued to evolve during the Late Ordovician Trenton time with the appearance of low-relief carbonate buildups known as the Trenton and Lexington platforms. The craton-wide marine transgression continued during this time, with water depth increasing and the carbonate production keeping pace. A significant shift in paleoclimate and increased volumes of temperate-marine, fossiliferous carbonates occurred during this time (Patchen et al., 2006). A continental glaciation centered on the South Pole resulted in the cooling of surface waters and mass mortalities among marine faunas (Berry et al., 1995). Dominantly clastic muds poured in westward from the volcanic island arcs from the Taconic Mountains to the east. These muds represent the appearance of dark brown/ black shales within the region, along with continued volcanic ash deposits. As carbonates continued to deposit on the shallower carbonate platforms, deposition interbedded limestones, calcareous shales, and brown/black shales of the Point Pleasant Formation began. The intensity of the Taconic orogeny increased during Utica time, resulting in a rapid rise in sea level or increased area subsidence. This shift led to carbonate deposition being replaced with the Utica shale deposition on the platforms (Patchen et al., 2006).

## **4 STRATIGRAPHY**

The Utica shale Play encompasses all formations from the Lexington/Trenton Limestone to the Kope Formation. The primary target zone is the Logana Member of the Lexington Limestone and the base of the Point Pleasant Formation (Figure 5). It is an organic-rich, mixed carbonate-siliciclastic system that grades from primarily carbonates at its base in the Lexington/Trenton limestones into mostly shale within the Utica shale (Patchen and Carter, 2015).



Global			N.A.		Eastern Ohio
System	Series	Stage	Series	Stage	
Ordovician	Upper Ordovician	Katian	Cincinnatian	Edenian	Kope Formation
					Utica shale
			Mohawkian	Chatfieldian	Point Pleasant Formation
					Lexington Upper Member
					Logana Member
Sandbian			Turonian		Curdsville Member
					Black River Group

**Figure 5:** Eastern Ohio stratigraphic column representing the Upper Ordovician strata in the area. The Lexington Limestone has been divided into its respective members. Modified from Patchen and Carter, 2015.

The Black River Group was first described along the Black River in Oneida and Lewis Counties, NY (USGS, 2023). The depositional environment of the formation is shallow-marine, leading to the formation of a carbonate ramp with a matrix primary consisting of calcite micrite, microspar, pseudospar, and terrigenous clay minerals. Matrix dolomitization is common due to fracturing, brecciation, and vug development originating from tectonic activity (Patchen et al., 2006). The formation is primarily

composed of fine-grained and muddy shallow marine carbonates with bioturbation present. Within western and southern Ohio, the formation transitions to a fossiliferous, grainstone/packstone similar to that of the overlying Trenton. The presence of k-bentonite beds is often utilized as a key stratigraphic marker illustrating the formation contact (Patchen et al., 2006).

The Lexington/Trenton Limestone are stratigraphically equivalent carbonate platforms but vary in lithology and fossil content. The Lexington is a deeper water platform comprised of carbonate grainstones, packstones, and wackestones that are more argillaceous than the Trenton (Patchen et al., 2006). As the research area is entirely in eastern Ohio and subsequently on the Lexington Platform, this paper will only focus on the Lexington Limestone. The Lexington was first described in Lexington, Kentucky, as a thin-bedded gray limestone containing nodules at the base (USGS, 2023). It is subdivided into the Upper Lexington Member, Logan Member, and the Curdsville Member.

The basal member of the Lexington Limestone is the Curdsville Limestone Member, first described at the Curdsville Station in Mercer County, Kentucky, as a cherty crystalline limestone (USGS, 2023). The depositional environment is shallow, turbulent waters occurring during the initial transgression of the Lexington Sea. It is described by the Utica Playbook as consisting of bioclastic calcarenite, with this being sand and chert-bearing in part, with silicified fossils common. Near the top of the member, the limestone becomes irregularly bedded and finer-grained, with fossil content

increasing. TOC for the formation reaches as high as 5% in parts with carbonate content consistently exceeding 70% (Patchen and Carter, 2015). The contact with the underlying Black River Formation is generally gradational (Patchen et al., 2006).

The Logana Member was first described at the Logana Station in Jessamine County, Kentucky, as an argillaceous fossiliferous limestone (USGS, 2023). The depositional environment is interpreted to be during the culmination of the initial transgression of Lexington/Trenton time. The Utica Playbook describes it as an organic-rich argillaceous limestone and shale with TOC as high as 5%. It is laminated, containing limestone beds in the top, with some well-developed, laterally extensive brachiopod-rich beds at the base (Patchen and Carter, 2015). The contact with the underlying Curdsville Member is gradational (Patchen et al., 2006).

The Upper Lexington/Trenton Formation is an organic-rich nodular and irregularly bedded fossiliferous limestone and shale. The limestone contains both whole and broken fossils preserved in a silt to clay-sized carbonate matrix. It is less organic-rich than the overlying Point Pleasant. However, some areas have TOC as high as 4-5% (Patchen and Carter, 2015). Abundant fossils include bryozoans, brachiopods, mollusks, and trilobite fragments, with stromatoporoids and colonial corals present in zones. Bioturbation is common, with the limestones being deposited in the infralittoral zone allowing for optimum light, aeration, circulation, and nutrients to foster life. It is

observed that thickness varies throughout the formation, with intertonguing occurring with the Utica and Point Pleasant Formations (Mcdowell, 1986).

The Point Pleasant Formation was first described at Point Pleasant in the Ohio River Valley in Clermont County, Ohio as a massive blue limestone interbedded with concretion-bearing shale (USGS, 2023). It is an interbedded fossiliferous limestone, black shale, and minor siltstone, with the limestone and shale occurring in approximately equal amounts. The upper part of the formation is organic-poor, with TOC less than 1% on most samples. The lower part of the formation is organic-rich with TOC up to 4-5%. Storm beds are abundant throughout the formation, indicating it is storm-influenced (Patchen and Carter, 2015). The contact with the underlying Lexington Formation is gradational (Patchen et al., 2006).

The Utica shale was first described in Utica, New York, as a black shaly mass (Emmons, 1842). It is a black, organic-rich interbedded dark fissile shale and limey shale (varying between 10% to 60% calcite) beds (Patchen and Carter, 2015). Thin, fossiliferous (brachiopods and trilobites) beds are present within organic-rich sections of the formation, with bioturbation common (Smith, 2013). Analysis of the formation indicates that the middle portion of the Utica is organic-rich, with TOC as high as 3.5%. However, the top and bottom portions are not organic-rich, despite being a dark shale. This indicates that a high organic content is not identifiable by the darkness of samples alone within the Utica shale (Patchen and Carter, 2015). Furthermore, in Ohio, the Utica

shale is not a formal unit, rather, it is the shaley base of the Kope Formation, equivalent to the Utica shale in New York. Throughout this work the informal term will be used.

The Kope Formation was first described as shale and minor interbedded limestones in the Maysville area of Kentucky and Ohio, with the name originating from the Kope Hollow north of Levanna, Ohio (USGS, 2023). It is described by the Utica Playbook as an interbedded shale (60-80%), limestone (20-40%), and minor siltstone. It has a lower carbonate content than the underlying Utica, with TOC for the black shales reaching as high as 3% (Patchen and Carter, 2015). The contact with the underlying Utica shale has been observed to be a gradational contact (Kirchner and Brett, 2008).

## **5 METHODS**

### **5.1 Data and Methodology Workflow**

An in-depth analysis of the formation mineralogy and subsequent geomechanical properties was performed to create a reservoir model by analyzing well logs, geochemistry, X-ray diffraction (XRD), and X-ray fluorescence (XRF) data. The first step in modeling the play was data acquisition, with well logs and core data (core photos, source rock analyses, bitumen reflectance reports, and XRD data) for 31 wells publicly available from the Utica shale Consortium within the study area (Figure 6) (Patchen and Carter, 2015). Additionally, XRF data was available for the Tracker Core in the nearby Portage County (Kemeh, 2021). The Tracker Core also contained a full suite of well log data, also referred to the Tracker Well in this study, including gamma ray (GR), caliper (CAL), elemental analysis (GEM), neutron porosity (NPHI), density (RHOB), and photoelectric effect (PEF). The XRF data were used to refine the mineral model before extrapolation across the research area. The Tracker Core is housed at the Ohio Division of the Geological Survey, Columbus, Ohio. The Tracker Core and its accompanying well log data were used as the control well throughout the study area.

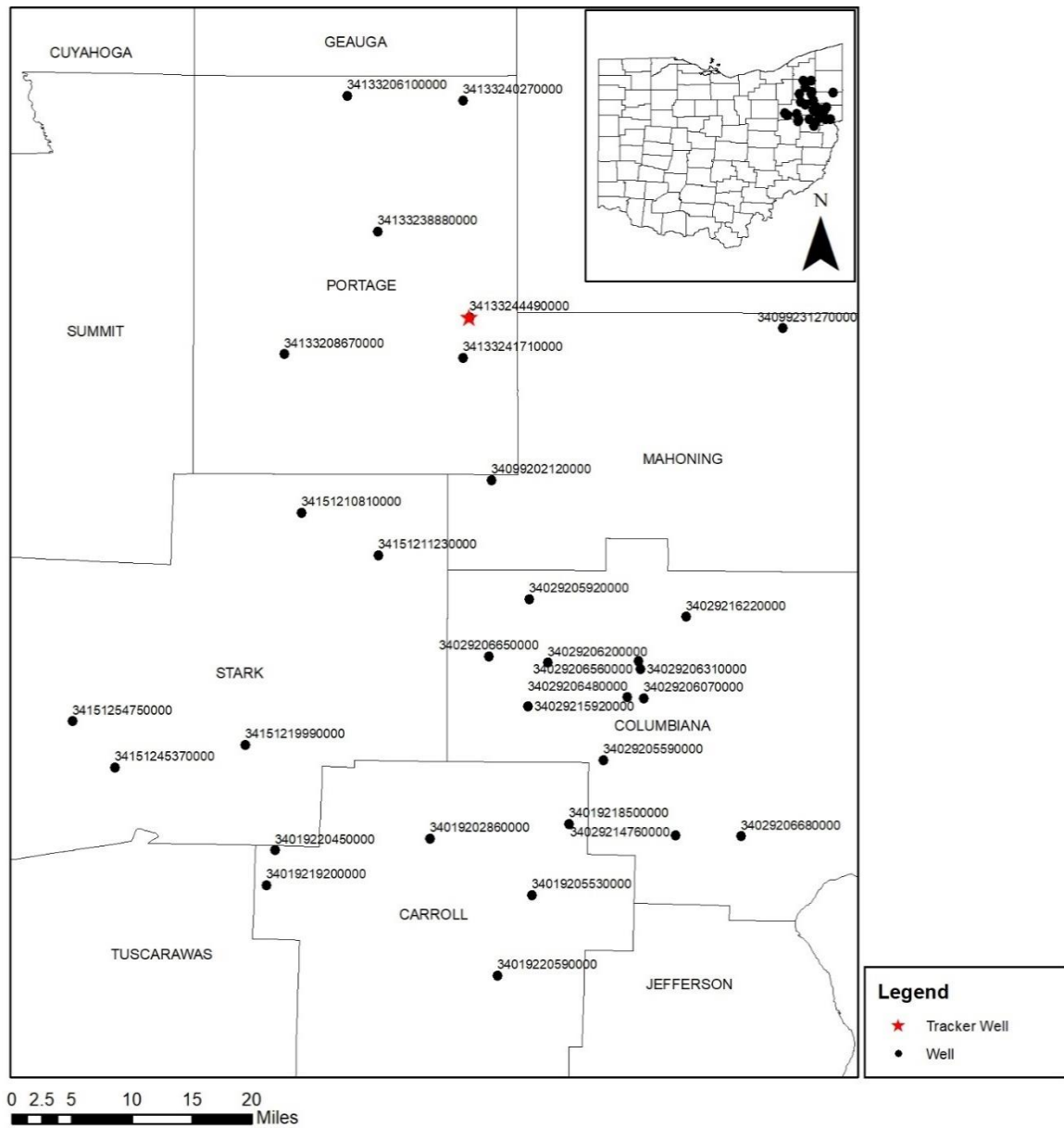


**Figure 6:** Map displaying the location of the wells in study area across eastern Ohio. The Tracker Well is represented by a red star in southeastern Portage County.

Interactive Petrophysics 2021 was utilized for petrophysical analysis. The software allows the interpreter to apply petrophysical equations to well logs and

laboratory data in order to determine mineralogy, porosity, TOC, hydrocarbon saturation, and water saturation. Several equations for clay, porosity, saturation, and total organic carbon (TOC) determination are built in, with additional equations possible by performing regressions between well logs and core data.

First, well logs and laboratory measurements were uploaded to the program. Formation boundaries then were determined for the Curdsville Member, Logana Member, Lexington Member, Point Pleasant Formation, and Utica shale using a type log of the area from the nearby Solomon Aquila E (API: 3402921476000) well (Patchen and Carter, 2015; Figure 7).



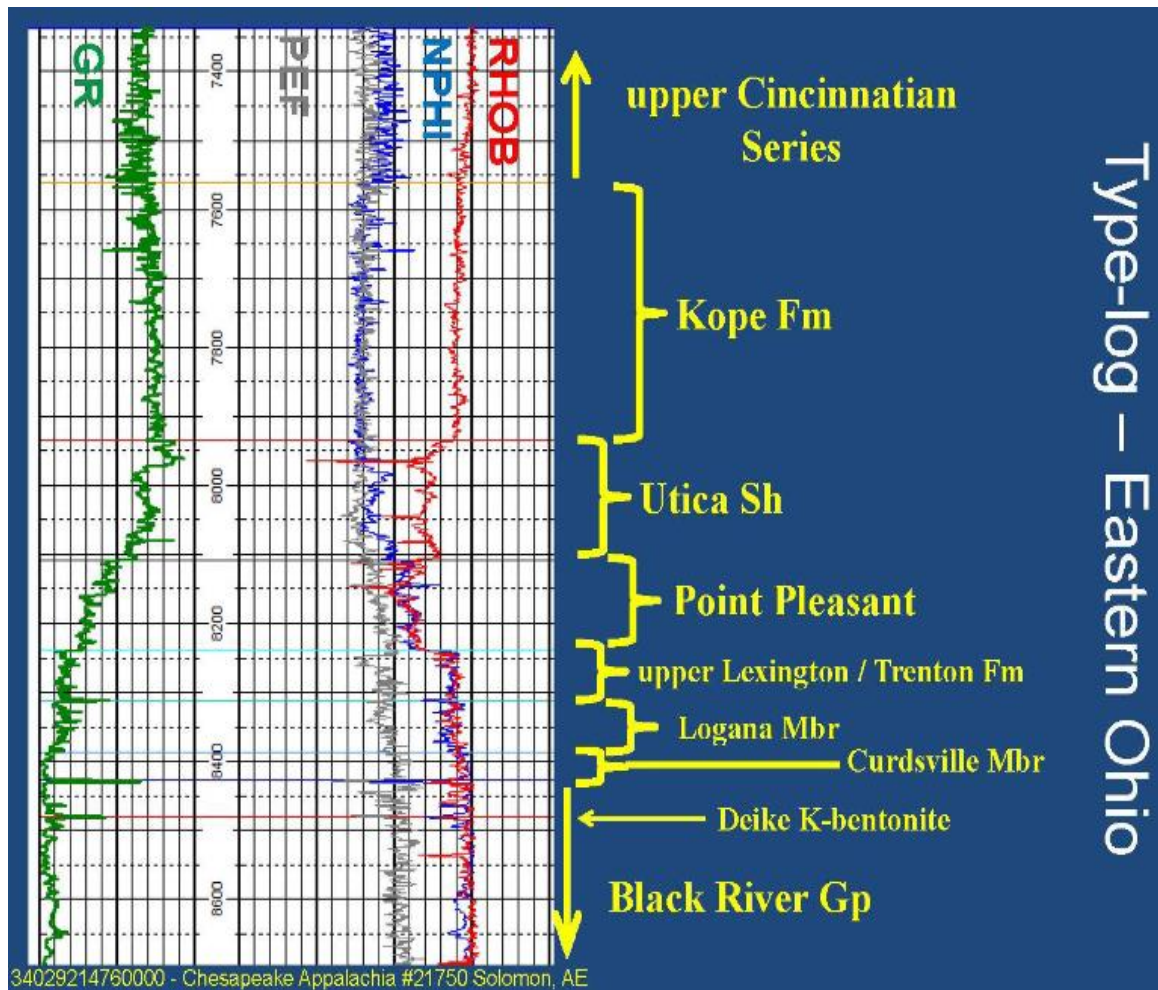


**Figure 7:** Type-log for the researched units in Eastern Ohio using the Solomon Aquila E (API: 3402921476000) well. From Patchen and Carter, 2015.

After formation boundaries were determined, data correction was performed to ensure all logs were of the same units and did not exhibit errors. Pyrolysis data, XRD, XRF, and tight rock analysis data were added to the corresponding depths in the wells, providing essential control points for the interpolation. "Clean" (little to no clay content) and 100% clay sections were determined in the clay module for each well, with the

software using pre-built clay equations to approximate clay content. XRD-derived clay content was overlaid, and clean and clay lines were refined to match the calculated clay content. The Tracker Well was then used to develop regressions to be applied to all wells in the research area. TOC was calculated by modifying the Schmoker and Hester, and Passey methods to better reflect pyrolysis data at the Tracker Core, then taking the minimum of the two curves to form one single TOC curve (Schmoker and Hester, 1983; Passey et al., 1990). A linear regression between the TOC curve and XRD-derived pyrite was performed and adjusted for fit, allowing for continuous pyrite estimation. A siliciclastic content formula was then created from the calculated clay content and the elemental analysis data from the Tracker Core. Some wells did not have PEF curves, therefore, a linear regression between the PEF and GR curves from the Tracker Core well log data was performed, allowing for synthetic PEF curves to be calculated for these wells. This was used to calculate the volumetric cross section (U) in the corresponding module in the software. These equations were then applied to all wells in the AOI to construct the model.

The mineral solver module was run for each well, which required inputting temperature data and determining the porosity, saturation parameters, and equations for the Tracker Well such that calculated porosity and saturation best reflect those provided by the tight rock analyses. These parameters were then saved and applied to all wells within the dataset. Next, the mineral model setup was performed, with density, neutron porosity, TOC, pyrite content, volumetric cross section (U), and siliciclastic content

selected as inputs. The mineralogy to be determined was defined, including clay, siliciclastics, dolomite, limestone, kerogen, pyrite, hydrocarbon saturation, and water saturation. From this, the expected real-world values of each mineral were inputted, and the mineral model ran. XRD mineralogy was overlaid to verify the mineral model, adjusting mineral end points for accuracy. Similarly, porosity and saturation data are overlaid on top of the calculated porosity and saturation, with a refinement of the initial model parameters performed for calibration.

## **5.2 Data Correction and Synthetic Curve Generation**

There are several sources of error within a well log, including variations amongst tool brands, age of data, and calibration accuracy. Throughout the area, various tools were utilized, especially associated with older wells. As a result, the response given by one tool may not easily correlate with responses in another. Older wells may have tools in counts-per-second and must be converted into the appropriate units before any equations can be applied to the curve. These wells vary by operator, with each operator having different standards for tool calibration and an accepted level of variance within the tool response. This presents a significant challenge in modeling, with some wells having density curves that contain anomalous values, which may be due to improperly scanned or tool errors. Therefore, data corrections, and sometimes culling, are required before petrophysical analysis. It is important to note that by performing these corrections, a certain level of inaccuracy exists within the analysis for such wells. This inaccuracy can

be adjusted for when the mineral model is applied to the well by adjusting the confidence values.

Several older wells had neutron porosity logs (NPHI) in counts-per-second, whereas newer wells utilized porosity units (p.u.). While both produce similar log responses, their values are significantly different. As the mineral model assigns values based on the neutron porosity value in porosity units, the older wells must first be converted to match the units of modern wells. These logs were first converted to porosity units before interpretations were made. This was done by producing a histogram of neutron porosity values at the Tracker Well already in porosity units, then overlaying the wells still in counts per second. The curve was then rescaled until the statistics of the new curve closely matched that of the control. The curve was then saved as a corrected neutron porosity curve and was used for interpretation. This same procedure was then repeated for the density log in wells containing anomalous values and saved as a corrected density curve.

Synthetic neutron porosity (NPHI) curves were created for wells without neutron porosity logs or where sections of the log were missing by performing a linear regression between gamma ray (GR) and NPHI for the Tracker Well log data, and the resulting equation was saved (Equation 1). An  $R^2$  of 0.861 was observed between the NPHI and GR curves at the Tracker Well, indicating the data is relatively close to the calculated regression.

**Equation 1**

$$NPHI_{syn} = 0.00112 * GR + 0.0161$$

The photoelectric tool (PEF) is a newer tool and is frequently not run on well sites. Numerous wells did not contain a PEF well log; a synthetic PEF was derived for these wells to be utilized in the mineral model. Linear correlation with the gamma ray tool provided the best fit with the PEF log available at the Tracker Well (Equation 2). An  $R^2$  of 0.767 was observed between the PEF and GR curves at the Tracker Well.

**Equation 2**

$$PEF_{syn} = 4.75 - 0.0078 * GR$$

**5.3 Clay Content**

The first step in creating the petrophysical model was determining the amount of clay/shale present. This was done in Interactive Petrophysics 2021 by Geoactive by first determining if the analysis is for clay volume (Vcl) or shale volume (Vsh), with the distinction being that shales are typically only 40-90% clay (Shaw, 1965). The two different calculations use different parameters within the software, specifically gamma ray for Vcl or a combination of neutron porosity and density for Vsh. The play is unconventional; therefore, clay volume (Vcl) analysis was chosen for a more in-depth analysis of the reservoirs.

Clay content was determined by taking the average of a single clay GR indicator (calculation) and a double clay neutron/density crossplot indicator (calculation).

Indicators are calculation methods and refer to the number of curves used to calculate a given factor. For example, single clay indicators rely on only one curve to calculate clay

content, while double clay indicators rely on two. Given the abundance of gamma ray, neutron porosity, and density curves throughout the research area, both a single clay indicator based on gamma ray (VclGr) and a double clay indicator from a neutron/density crossplot (VclND) were used. The VclGr indicator directly interprets clay content from the gamma ray log from a linear formula based upon a section that is “clean” (very little to no clay content) and a section that is 100% shale (Equation 3). The interpreter must first decide the GR value for a clean section and the clay section for each well (Figure 8).

The neutron/density clay volume (VclND) indicator calculated clay using a crossplot between the two curves (Figure 9). Neutron porosity and density values were plotted on a cross plot that was overlain with lines corresponding to clay volumes. The corresponding clay content was determined by the location of a datapoint on the crossplot in relation to the clean and clay points, as determined by the interpreter (Equation 4).

**Equation 3** 
$$VclGr = \frac{Gr - Gr_{Clean}}{Gr_{Clay} - Gr_{Clean}}$$

**Equation 4** 
$$VclND = \frac{(DenCl2 - DenCl1) \cdot (Neu - NeuCl1) - (Den \cdot DenCl1) \cdot (NeuCl2 - NeuCl1)}{(DenCl2 - DenCl1) \cdot (NeuClay - NeuCl1) - (Denclay - DenCl1) \cdot (NeuCl2 - NeuCl1)}$$

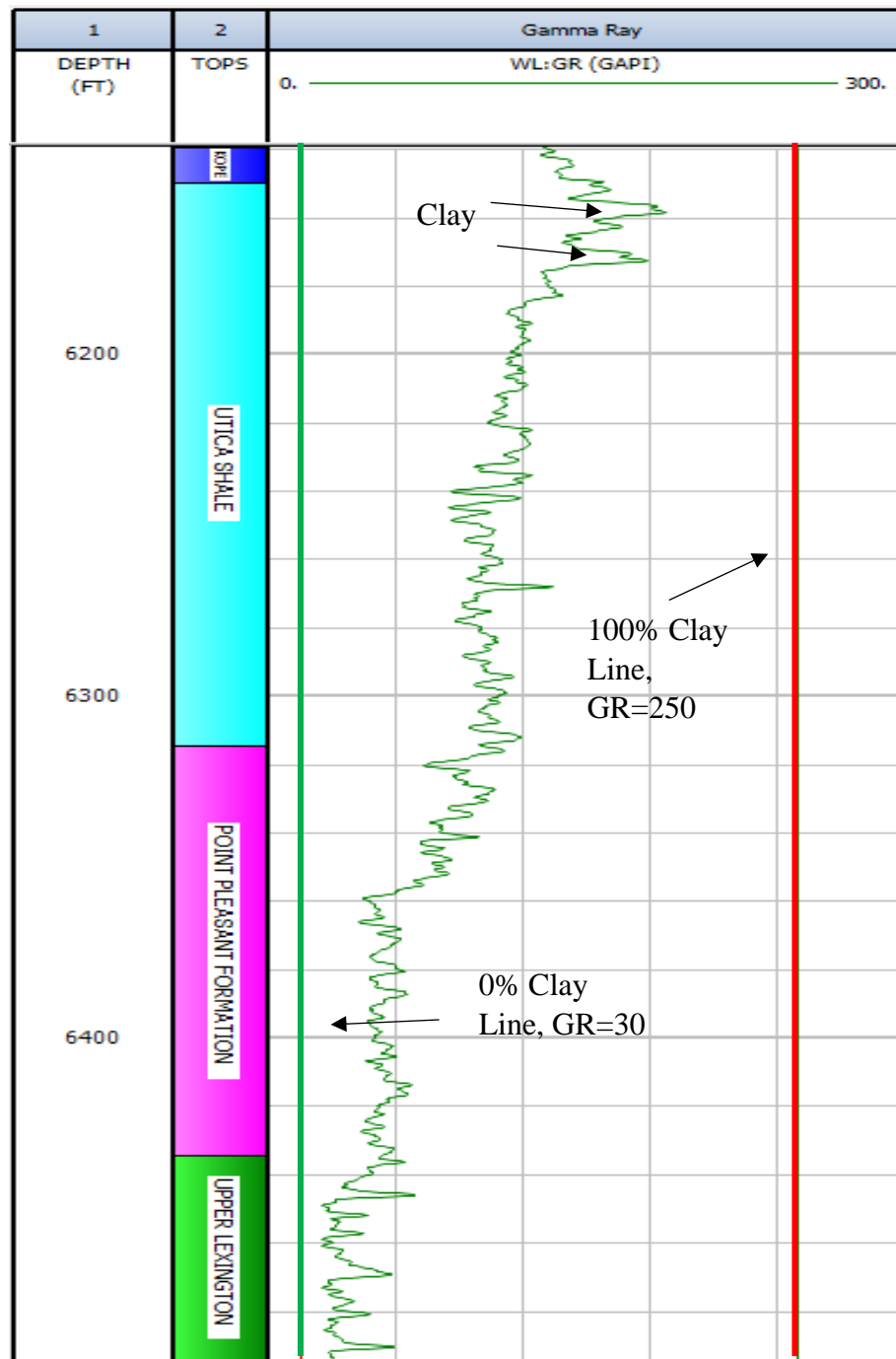


**Figure 8:** Example of a GR curve with clean and clay sections interpreted on the Tracker Well.

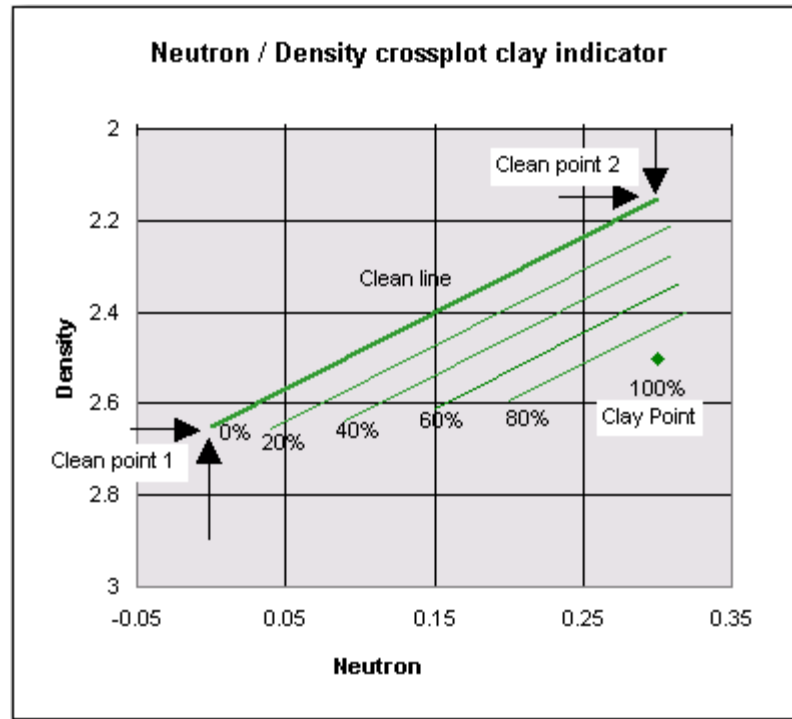


**Figure 9:** Neutron/Density crossplot illustrates the clean and clay point locations. Data from the well log were plotted with their neutron porosity value and density. The clay volume is then calculated based on the distance from the “clean” line (0% clay) and the 100% clay point. From the Interactive Petrophysics manual (Geoactive, 2023).

Two clay models were produced (VclGr and VclND). Interactive Petrophysics 2021 calculated a minimum clay curve (Vcl) by taking the lower value of the two curves for each specific depth. Average clay curve (Vclav) was calculated by taking the value of the two curves at each specific depth and producing an average from this. If only one clay indicator method is possible, Vcl and Vclav effectively equal the curve produced by the one method.



Following this step, XRD derived clay content values were overlaid on top of the two clay curves for each well, and the clean and clay points were refined so that the calculated clay curves matched the XRD clay points (Figure 10).

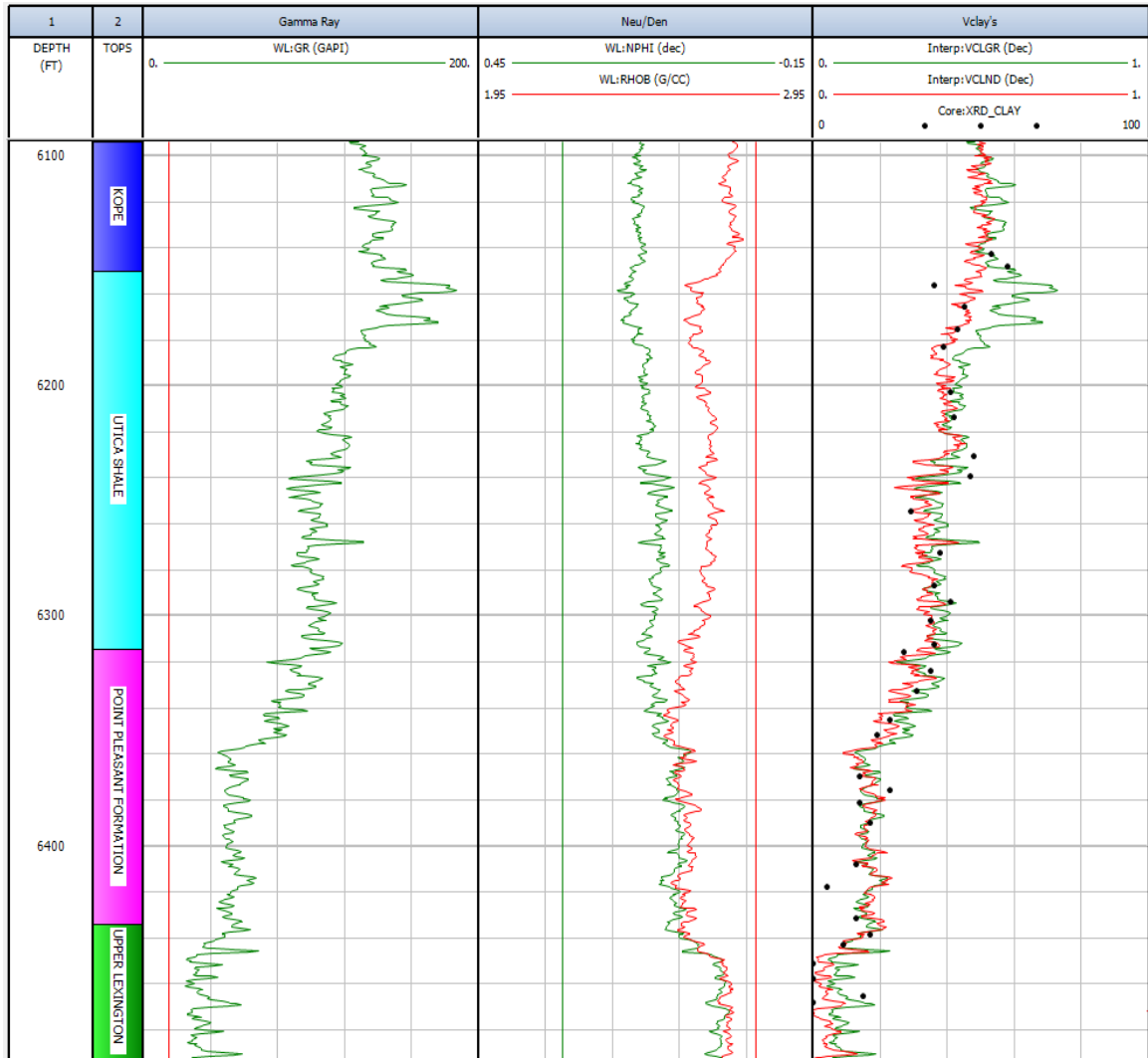


**Figure 10:** Log plot illustrating the GR, NPHI, and RHOB curves compared to the subsequent interpreted clay curves VCLGR and VCLND. XRD clay data was overlaid on top to calibrate the interpretation.

## 5.4 TOC and Pyrite Calculations

Several methods exist to calculate TOC from a variety of well logs, including resistivity, gamma ray, neutron porosity, density, or a combination of multiple logs. Linear correlations were calculated for gamma ray and neutron to the laboratory TOC measurements, with poor results. The density based Schmoker and Hester formula as well as the resistivity based Passey formula provided stronger fits to the TOC data at the Tracker than simply linear regressions with single well log curves. However, taking the minimum values of the two methods provided an even stronger correlation to the TOC data.

First, the Schmoker and Hester formula was applied to the Tracker Well and subsequently modified to better fit the TOC measurements recorded (Equation 5, Figure 11). It can be seen that the curve slightly overestimates the TOC in the Utica and Upper Lexington, while underestimating the TOC in the Point Pleasant.

**Equation 5** 
$$TOC_{SMKR}(wt\%) = \frac{166}{RHOB} - 59.261$$

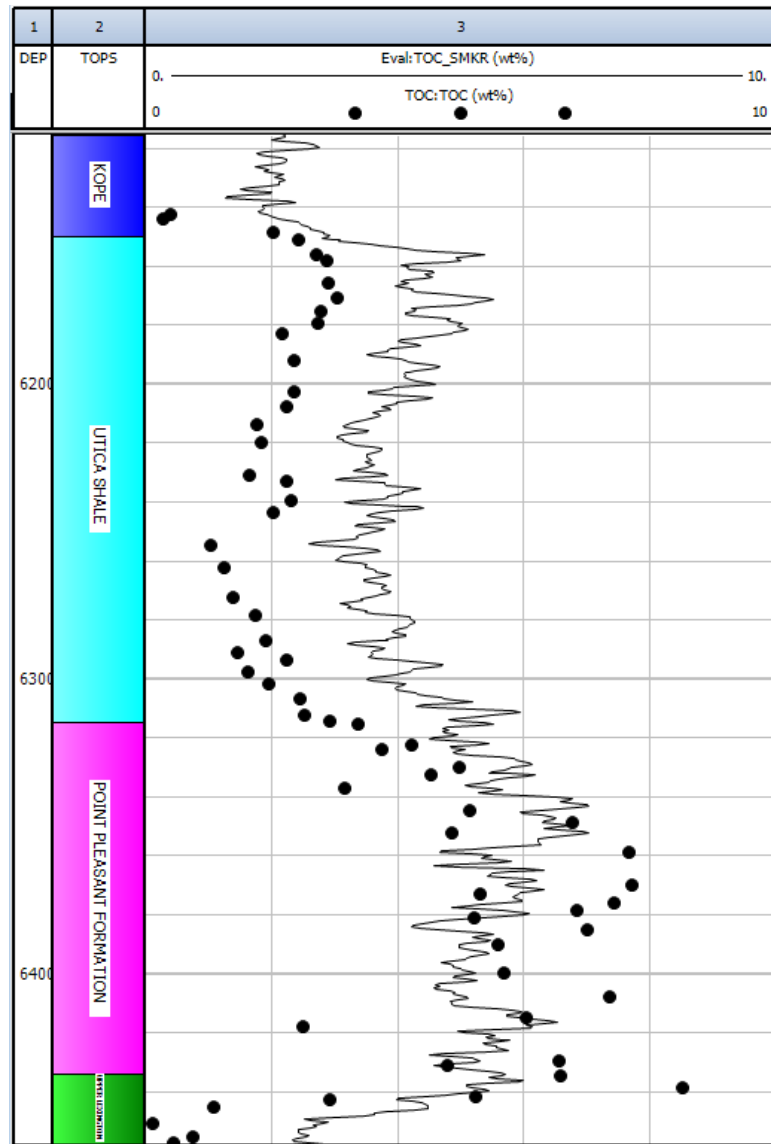


**Figure 11:** Log plot of the modified Schmoker and Hester curve overlayed with laboratory TOC measurements.

Next the Passey method was applied to wells containing resistivity and sonic data to calculate TOC. Resistivity and sonic data are not commonly available throughout the Appalachian Basin and is rare in the study area as well. Therefore, it is not possible to apply the Passey method to wells without resistivity data. For wells with resistivity data

but no sonic data, a synthetic sonic from neutron porosity formula must first be performed (Equation 6). Once this step was performed, the Passey formula was applied and modified to best fit laboratory TOC data (Equation 7). The resultant curve illustrates a strong fit with the laboratory TOC measurements for the Utica shale and Upper Lexington, but fails to accurately represent the finer TOC changes within the Point Pleasant Formation (Figure 12).

**Equation 6** 
$$DT_{syn} = (130 * NPHI) + 40$$

**Equation 7** 
$$TOC_{Passey}(wt\%) = Log\left(\frac{R_{deep}}{50}\right) + 0.02 * (DT - 80) * 10^{(2.297 - 0.1688 * 10.6)}$$

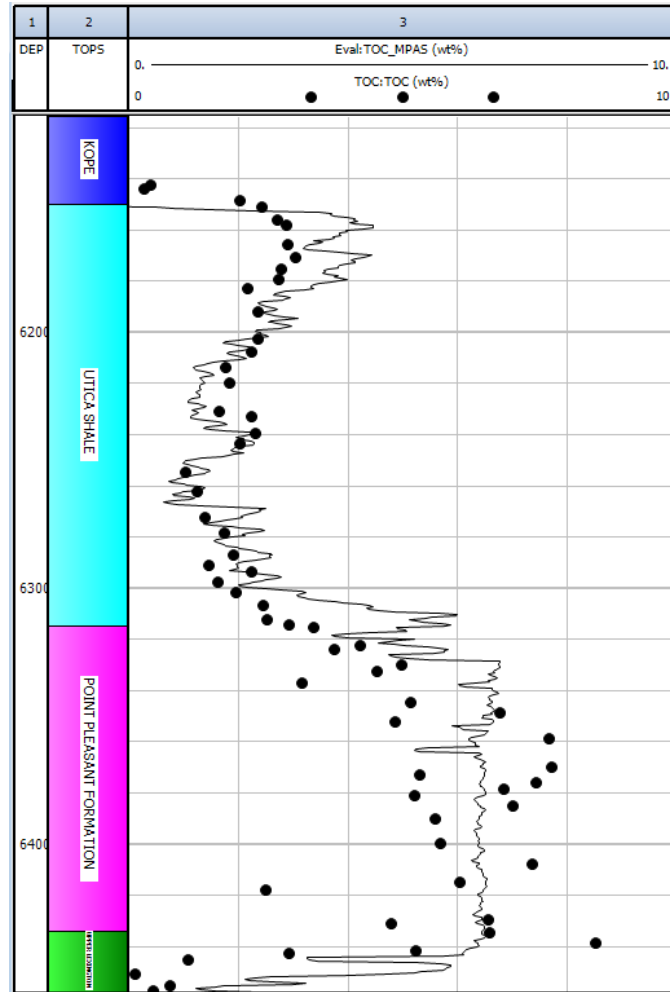


**Figure 12:** Log plot of the modified Passey method derived TOC curve overlaid with Laboratory TOC measurements.

Finally, the minimum of the formulae was taken in order to rectify the weaknesses of both methods (Equation 8). While not commonplace, it is observed that the resulting curve provided a stronger fit to the laboratory TOC measurements when compared to the individual TOC methods previously discussed alone (Figure 13).

**Equation 8**

$$TOC_{min} = \text{Minimum}(TOC_{SMKR}, TOC_{Passey})$$

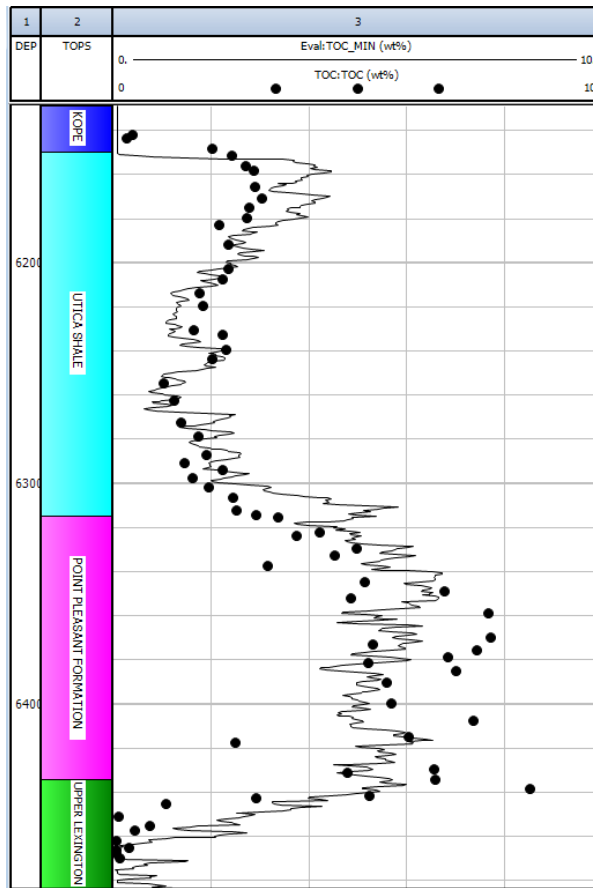


**Figure 13:** Log plot of  $TOC_{min}$  with laboratory TOC overlaid.

In the absence of resistivity data, the modified Schmoker and Hester method becomes the sole method of TOC calculation for the remaining wells, and subsequently overestimates organic content within the Utica shale and Upper Lexington, adversely affecting model accuracy.

TOC correlated with the presence of increased pyrite content within these formations. This is because the mineralization of pyrite often involves the breakdown of organic matter by sulfate-reducing bacteria, leading to anoxia within the water column.

This, in turn, coincides with the increase in the preservation and burial of organic carbon. A linear regression between the calculated TOC and XRD pyrite data were obtained, at the Tracker, with the resulting formula allowing for the estimation of pyrite across the AOI (Equation 9). It is evident from the low R-squared value ( $R^2=0.081$ ) that this linear regression appears weak. However, this equation still proves useful as it provides a relatively close fit to the XRD pyrite, typically within 1-2% of the real-world values (Figure 14).

**Equation 9**

$$V_{pyrite} = \frac{TOC_{min}}{150}$$

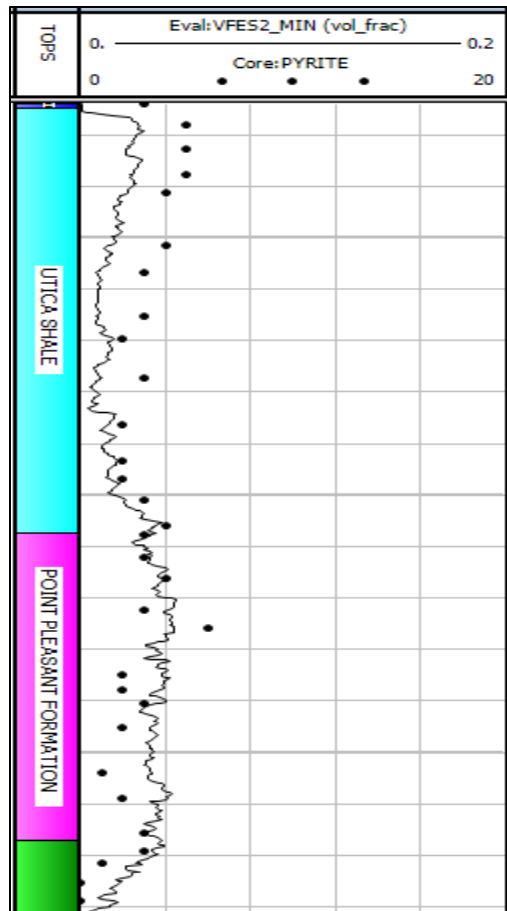


**Figure 14:** Log plot of the calculated volume of pyrite in comparison to the XRD pyrite percentage. The calculated pyrite volume exhibits a relatively close fit to the XRD data, with a slight overestimation for Upper Lexington and Point Pleasant and a slight underestimation for the Utica shale.

## 5.5 Silica Content Calculation

In order to represent siliciclastics within the mineral model, a linear regression was calculated between the calculated clay volume to the volume of silicon measured by the Halliburton GEM Elemental Analysis tool at the Tracker Well (Equation 10). This tool allows rapid and continuous evaluation of formation elemental composition (Halliburton,



2023). Alternatively, XRF derived Si produces similar results. A  $R^2$  value of 0.878 was observed between Haliburton GEM derived silica content and calculated clay content at the Tracker Well, indicating a strong fit between the data and calculated regression.

**Equation 10** 
$$DSI_{syn} = 42.1 * Vcl + 2.70$$

### **5.6 Volumetric Cross Section (U)**

The volumetric cross section, U, is calculated using the mineral solver preprocessing module within Interactive Petrophysics (Equation 11). For this module to be run, there must exist a density and PEF curve for each well, hence the importance of deriving a synthetic PEF curve.

**Equation 11** 
$$U = PEF * (RHOB + 0.1883) * 0.93423$$

### **5.7 Porosity, Saturation, and Deterministic Mineral Determination**

Before the mineral model was constructed, model parameters were determined. There are five different modules in the IP software. The zones/mixings module allows the user to apply different parameters to different zones within a well if needed. To simplify the model, only one parameter zone was applied.

The water/clays module calculated the water saturation and clay content. The parameters for water and clay resistivity, porosity, and temperature were inputted in this module. These values are unique to each well, and therefore most values were adjusted on a well-by-well basis in accordance with resistivity data and temperature logs, with an example visible below (Table 2). In this example, data was derived from the Tracker

Well, with the value of  $\Phi_{iTClay}$  (the total clay porosity) dynamically adjusted so the total and effective porosity calculated by the mineral model matched that of the porosity obtained by the tight rock analyses data when overlaid. The effective porosity,  $\Phi_{ie}$ , is the summation of the volume of water and volume of hydrocarbons as determined by the mineral model (Equation 12). Similarly, total porosity,  $\Phi_{it}$ , is the summation of the calculated effective porosity, wet clay volume, and the total clay porosity (Equation 13), with wet clay volume being the summation of the wet clay mineral type (Equation 14). This method determined the  $\Phi_{iT}$  Clay parameter which was subsequently applied to all the wells.

**Table 1:** Water/clays module as displayed in Interactive Petrophysics for the Tracker Well.

Zone	Rw	Rw	Rw	Rmf	Rmf	Rmf	Rw	Rwb	Rwb	Rmf	Rmf	Rmf	Res	Rxo	PhiT
#		Temp	Salinity Kppm		Temp	Salinity Kppm	bound	Temp	Salinity Kppm	bound	Temp	Salinity Kppm	Clay	Clay	Clay
1	0.2	150	15.2	0.05	195	53.6	0.1	60	87.8	0.1	60	87.8	1	1	0.04

**Equation 12** 
$$Phie = \sum V_{water_i} + \sum V_{hydrocarbon_i}$$

**Equation 13** 
$$Phit = Phie + Vcl * PhitClay$$

**Equation 14** 
$$Vcl = \sum V_{wetclay_i}$$

Next, the saturation parameters, equations, and limits within the Sw Logic/Limits module were defined (Table 3). It is within this step that the saturation equation, Sw (un-invaded zone saturation) method, and Sxo (flushed zone saturation) method that most accurately fits their data was determined. If resistivity data was not present for a well, it was not possible to calculate Sw and Sxo, and therefore "nocalc" was used as the method. It was determined that the Archie PhiT was the best method as the water saturation equation for wells that possess resistivity data in the research area (Equation 15). This equation is a modified form of the Archie equation, with the distinction that it uses total porosity instead of effective porosity in the calculation. The Sw method utilized is Rt, indicating that Sw will be calculated from the Rt resistivity input curve (Equation 16). Similarly, the Sxo method used is Rxo which calculates Sxo from the Rxo resistivity input curve (Equation 17).

**Table 2:** Sw logic/limits module as displayed in Interactive Petrophysics for the Tracker Well.

Zone	Sat	Sw	Sxo	OBM	Sw Sxo	m vari	Vd	Sxo	Sxo	Invasion	Phi Sw	Vd Sw	Swi
#	Equation	Method	Method	?	Inv Logic	with Vd	cutoff	Limit ?	Limit	factor	Limit	Limit	Limit
1	Archie PhT	Rt	Rxo		✓		0.6	✓	0.2	2	0	1	0

**Equation 15**

$$\frac{1}{Rt} = \frac{\Phi T^m * S_w^n}{a * S_w}$$

**Equation 16**

$$S_w = \frac{\sum V_{water} U_i}{\sum V_{water} U_i + \sum V_{hydrocarbon} U_i}$$

**Equation 17**

$$S_{xo} = \frac{\sum V_{water_i}}{\sum V_{water_i} + \sum V_{hydrocarbon_i}}$$

The Sw Parameters module is where the Archie PhiT equation parameters were modified (Table 4). Here, default values for a, m, and n were chosen. In addition, parameters were present for adjustment for other saturation equations but were not used within the research area.

**Table 3:** Sw parameters module as displayed in Interactive Petrophysics for the Tracker Well.

Zone	m	n	a	m	n	min	max	m plus	B fact	B fact	Qv	Qv 'a'	Qv 'b'	Cm*
#	source	source	factor	exponent	exponent	m value	m value	value	Juhasz	W&S		Const	Const	
1	Param	Param	1	2	2	1.5	3	0	1			0.5	-3	1

The final module is the Sonic/Neutron/Density module and is responsible for the equations governing their respective tools, if present (Figure 15). As a true sonic log is not available in the research area, only neutron and density tool equations were utilized. In the case of the Tracker Well, Halliburton was the logging contractor for the neutron tool and was characterized correctly as a neutron tool. Den Hyd Model determines the model used to calculate the apparent hydrocarbon density from the true hydrocarbon density. Here, modified has been selected as it better represents the correction from electron density to apparent density (Equation 18).

**Table 4:** Sonic/neutron/density module as displayed in Interactive Petrophysics for the Tracker Well.

Zone	Sonic	Sonic	Neu	Neu	Neu	Den Hy
#	Equ	Cp	Form Sal	Log Cont	Tool Type	Model
1	Raymer	1	✓	Halliburt	Neutron	Modified

#### Equation 18

$$Den_{hydrocarbon} = \frac{5.5 * \rho_{den} * (4 - \rho_{den}) - 3}{(16 - 2.5 * \rho_{den})}$$

Following the input of all parameters, the mineral model was then constructed (Table 6). The model behaves like a matrix of linear equations, with the software attempting to solve the equations. The mineral model estimates mineral volume fractions from this matrix, with wireline data and regressions serving as inputs, and user defined minerals and water/hydrocarbon saturation serving as outputs. These outputs are defined



by the user, and are largely based on the objective of the mineral model. For instance, an in-depth clay analysis may require a mineral model with multiple clay minerals as the output. As this research is focused on large scale mineralogy changes, the outputs are more broadly defined as siliciclastic, calcite, dolomite, clay, kerogen, pyrite, oil Sxo, and water Sxo. As the accuracy of the outputs is controlled by the number of inputs, it is not possible to subdivide further without compromising model accuracy.

The first step was to input the relevant curves available and the type of equation. For example, the RHOB log was input as a curve, and therefore it was correctly defined as a density equation. The input and synthetic logs previously calculated were used as inputs for the model. The curve labeled 1.0 was labeled as Unity. This equation is included in every model, and effectively states that the total volume of all minerals and fluids must total 1.0.



Next, the equation mode, Eq. Mode, was defined, allowing for the distinction between a “model” and “output”. Selecting “model” indicates the equation was used for solving in the mineralogy. Selecting “output” indicates that it is not used to calculate mineralogy, but instead takes the mineralogy once calculated and calculates a curve from this, such as in the case of grain density.

The confidence sets the weighting for the equations, with smaller numbers indicating a higher weight. The confidence values entered take the units of the curve. For example, a confidence value of 0.01 for the density curve would indicate it is within 0.01 g/cc<sup>-1</sup>. This is useful in situations where tool accuracy may be in question, and subsequently needs a lower weighting.

As well logging tools read into the subsurface at different distances, it is important to quantify this distance, known as the invasion factor. An invasion factor was applied for each curve, with a value of 1.0 indicating the equation is reading into the flushed zone (S<sub>xo</sub>) and therefore affected by fluids in the zone. Similarly, 0.0 would indicate the equation reads into the uninvaded zone (S<sub>w</sub>).

The mineral column was then used to define which minerals and fluids to plot. In the case of the Tracker, the mineral model is capable of plotting quartz, calcite, dolomite, clay, kerogen, pyrite, oil saturation, and water saturation. The number of minerals able to be accurately determined is controlled by the number of inputs and should be verified by

core data. The type of mineral added was then defined as either matrix, wet/dry clay, or water and hydrocarbon  $S_{xo}/S_w$ .

Interactive Petrophysics will attempt to auto generate the mineral endpoints entered. For instance, quartz has a density of  $2.65 \text{ g/cc}^{-1}$  and subsequently the software will label it as such on the RHOB graph. Some outputs were modified, such as in the case of Oil  $S_{xo}$ , where the hydrogen density changes with maturity and therefore were modified on a well-by-well basis. This step is crucial as hydrogen density is dependent on the type of hydrocarbon present at the well, be it oil, gas, or a mixture of the two. Within the research area, hydrocarbon density data are limited, therefore it was estimated by the location of the well within the hydrocarbon assessment unit map (Figure 1).

Following the completion of this step, the mineral model was run, and core data were compared with the calculated result. Adjustment to the confidence and values of the mineral end points themselves were performed such that the calculated model agreed with XRD data at the Tracker Well for clay, limestone, dolomite, pyrite, and quartz. Additionally, laboratory porosity and saturation data were overlaid for comparison with the calculated porosity and saturation. Adjustment of the PhiT Clay parameter was then performed so that the calculated total and effective porosity matched laboratory results.

At this step, the model was saved and applied to the entire dataset, with adjustments being made for each well when necessary. For wells without resistivity data available, water and hydrocarbon density were disabled as an output for the model.

Additionally, XRD data available for the wells indicates dolomite is typically less than 5%; it was difficult to accurately model dolomite in some wells where the confidence in the input data was in question. Therefore, it was decided to combine limestone and dolomite into a unified “carbonate” to improve model accuracy. This was done by disabling the dolomite output column and changing the density of limestone from 2.71 g/cc<sup>-1</sup> to 2.75 g/cc<sup>-1</sup> to account for the higher density of dolomite. This was then saved as a new discrete model used to map the mineralogy across the study area.

## **5.8 GIS Mapping**

The mean value for each calculated variable (clay, carbonate, siliciclastic, pyrite, TOC, and porosity) for each formation was exported into geospatial software ArcMap to create mineral maps using the inverse distance weighting method in geostatistical wizard. The parameter to be modeled was selected in the batch field, and smooth was selected as the neighborhood type. A prediction map was produced, and subsequently saved as a raster. The contour processing tool located in spatial analyst was then performed on the raster. From here, contours were manually adjusted to be geologically correct while still preserving the general trend of the contours. Contour to raster in the interpolation section was then performed, producing the final raster.

## **6 RESULTS**

### **6.1 Tracker Well**

The Tracker well was chosen as it is a research well consisting of the Lexington Limestone, Point Pleasant Formation and the Utica shale, providing XRD, tight rock analyses (TRA), and TOC data, with XRF performed by Barbara Kemeh of Stephen. F. Austin State University (Kemeh, 2021). The mineral model, pyrite calculations, and TOC calculations were completed in Interactive Petrophysics (Figure 15), showcasing variations throughout the formations, grading from mostly limestone in the Lexington to mostly shale in the Utica.

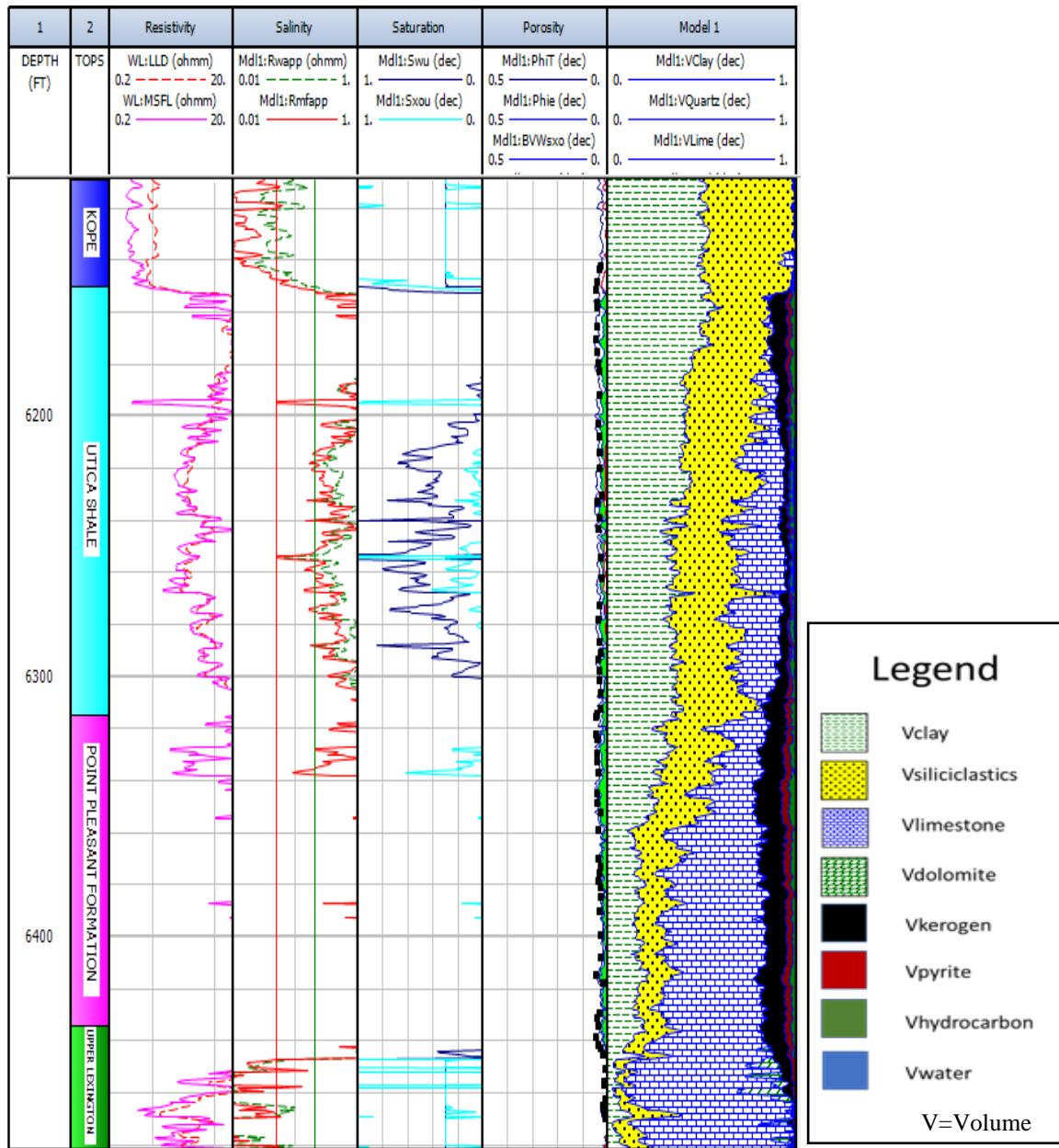


**Figure 15:** Log plot illustrating laterolog deep (LLD), micro-spherically focused log (MSFL), calculated apparent formation and mud filtrate resistivity (Rwapp and Rmfapp), calculated un-invaded and flushed zone saturations (Swu and Sxou), calculated total and effective porosity (PhiT and Phie), bulk volume water flushed zone (BVWsxo), and calculated mineralogy for the Tracker Well.

### **6.1.1 Upper Lexington Member**

XRD data from the Tracker indicates the Lexington Limestone is carbonate rich, with calcite values between 50-95%. Dolomite values are typically between 3-7%, with lows correlating to calcite rich intervals. Core data supports that clay content is discrete, occurring as localized zones and not continuous throughout the formation. When present, these clay rich zones reach in excess of 15%, with highs up to 30%. Siliciclastic content ranges from 5-25% and does not appear to strongly correlate to clay or carbonate content alone. Pyrite content appears absent in clay poor/absent zones, but has values as high as 3% in the clay rich zones indicating a possible correlation between clay deposition and pyrite. TOC data indicates organic content varies vertically, with lows of <1% prevalent throughout the formation. Organic rich intervals are present, reaching as high as 5% towards the contact with the overlying Point Pleasant. These organic rich intervals are observed to have high pyrite content, and occur in the clay rich portion of the formation. Tight rock analyses indicate a total porosity of 1-2% throughout the formation, but can reach as high as 4% in clay rich zones. Saturation data supports that the formation is primarily saturated with gas with values of over 90%, with little oil saturation present.

The mineral model for the Upper Lexington indicates that it is primarily limestone with discrete dolomite zones up to 10% present throughout. The calculated dolomite percentage is lower than the XRD dolomite, indicating additional calibration is needed. Limestone is observed to range from 60-90% throughout the formation, in line with the XRD data. Clay values are typically around 5%, with two discrete zones of 10-15% clay



observed. While the calculated clay content highs agree with the XRD, the mineral model calculates a small percentage of clay in places where the XRD data indicates there is none. Siliciclastic content ranges from 5-25% and appears to correlate stronger with clay content than carbonates, representing the siliciclastic portion of shale.

Calculated organic content in the formation is typically between 1-3%, with the upper portion of the formation more organic-rich than the lower, correlating with the available core data. TOC values increase upwards of 5% as it approaches the Point Pleasant Formation, with pyrite typically between 1-3% and correlating with TOC. Porosity values vary throughout, with lows of <1% throughout the formation and highs of 4-5% occurring near the top of the formation. The porosity is determined to be largely hydrocarbon filled, with values ranging between 2-3%. These values agree with the core data, indicating the model is properly calibrated for the formation.

#### **6.1.2 Point Pleasant Formation**

XRD data for the Point Pleasant indicates a large increase in clay content, with values ranging from 5-20% in the lower Point Pleasant and 20-40% in the upper Point Pleasant. The lower portion of the formation is calcite rich with values between 50-80%, whereas the top becomes increasingly more clay rich with calcite values of only 25-50%. Dolomite values range from 2-8%, with the highest values correlating to increased clay content in the upper portion of the formation. Siliciclastic values gradually increase from 5% at the base to as high as 25% at the top of the formation, correlating strongly with

clay content. TOC values vary throughout, ranging from 2-9% and gradually decreasing towards the contact with the overlying Utica shale. Pyrite correlates with the TOC content, with values between 1-6% throughout and highs located in organic rich zones. Porosity increases in the Point Pleasant, with values on average in excess of 5%, with a slight increase in porosity observed from the lower portion to the upper portion of the formation. This is hydrocarbon filled, with saturation data now indicating a significant increase in oil saturation upwards of 25%. Gas saturation is still dominant, with values averaging 60-70% throughout.

The mineral model indicates that the Point Pleasant Formation shifts from a primarily carbonate formation in the underlying Lexington to more clay-rich lithology. The model shows that the lower Point Pleasant contains a clay composition between 15-25% and a siliciclastic composition between 10-20%, in line with XRD values. As a result, limestone decreases compared to the Upper Lexington, with values between 50-70%. Little to no dolomite is observed to be present, in contrast to XRD dolomite values of 2-8%. A large increase in TOC is observed, with values in excess of 5% and pyrite values now as high as 4%. Hydrocarbon content is observed to reach as high as 5%, supporting this as an apparent target for exploration. Porosity values increase to as high as 6%, and coincide with the hydrocarbon content, agreeing with the saturation data.

The mineral model for the upper Point Pleasant represents a shift to a shale-dominated lithology, with clay composition between 20-40% and siliciclastics between

20-30%. Limestone composition represents 20-40% of the section, with no dolomite content calculated. TOC is observed to largely be the same as the lower Point Pleasant, with the distinction that a slightly high porosity is observed and, subsequently, more porous space for hydrocarbon saturation. Interestingly, the upper Point Pleasant is described as organic poor and often less than 1% TOC according to the Utica shale Playbook (Patchen and Carter, 2015). Despite this, the model indicates TOC as high as 5% and is verified by pyrolysis data to support it. This indicates a possible "sweet spot" in the area, with more wells in proximity needed to verify this.

### **6.1.3 Utica shale**

XRD data for the Utica shale supports an increase in clay content, with values in the lower Utica shale of 40% and gradually increasing to 60% at the top. Calcite content ranges from 5-25% and gradually decreases towards the top of the unit. Dolomite varies throughout, with values typically less than 5% and does not appear to correlate with any specific mineralogy. Siliciclastic content varies, ranging from 15-30%. Pyrite correlates strongly with TOC data, with values reaching as high as 5%. TOC data indicates a decrease in organic content compared to the Point Pleasant, with values now less than 3% and as low as 1%. Despite this decrease in TOC, pyrite values are observed to be similar or even higher than the Point Pleasant in places, with both correlating strongly to TOC. Porosity data increases compared to the Point Pleasant, with values reaching as high as 6%, indicating that increased porosity alone does not correspond to increased organic

content. Saturation data indicates a similar oil saturation compared to the Point Pleasant, but a slight decrease in gas saturation, with values from 40-65% present.

The mineral model indicates the Utica shale to have a similar composition to that of the underlying upper Point Pleasant, with the distinction that it is not as organic-rich. Clay continues to increase, reaching as high as 60%, and siliciclastics between 20-30%. Limestone is observed to fall between 10-30% on average, with a general decrease in the uppermost portion of the unit. Little to no dolomite is calculated within the formation, contradicting the dolomite content obtained via XRD data.

TOC values average 3-5%, with some intervals reaching as high as 8%, representing an overestimation of organic content compared with TOC data available in some intervals. Pyrite composition averages between 1-4% and correlates with TOC. Porosity values average approximately 5%, with hydrocarbon content ranging between 2-4% throughout the formation.

Distinct zones of little to no limestone are reported throughout, including the top of the Point Pleasant Formation and the top of the Utica shale. XRD-derived calcite data indicate that calcite values decrease in these locations to as low as 10%, but the model underestimates the content, even indicating no limestone present. XRD-derived dolomite data indicates the model fails to accurately convey the percentage of dolomite, instead resulting in a slight overestimation of the siliciclastic component compared to XRD. Overlaying the XRD data on top of each calculated mineralogy for all formations

indicates that distinct zones exist where siliciclastics are overestimated in the model, leading to an underestimation of limestone and dolomite at these segments. To correct this, mineral endpoints for the siliciclastic component were adjusted to account for the changing K-feldspar and plagioclase content. As a modified model with a unified carbonate output was utilized for the multi-well analysis, the effects of this should be mitigated.

Additionally, saturation data could not be calculated for the remaining wells as there were insufficient wells with resistivity data to build an accurate map. Rather, subsequent mapping focuses on clay, carbonate, siliciclastic, TOC, pyrite, and porosity changes.

## **6.2 Multi-well Analysis**

The modified version of the model was then applied to the other wells in the research area. The carbonates (limestone and dolostone in the Lexington) have been unified into one distinct group with a density representing the mixing. The lowermost unit to be considered will be the Curdsville Member, followed by the Logana Member, Upper Lexington Member, Point Pleasant Formation, and Utica shale. Values for each map are based on the average for each parameter, and each well was individually examined to ensure the entirety of the unit was present as to not skew the data. As some wells contain suspected tool/digitizing errors, these wells may skew the data even after rescaling the curves. These wells were not considered in the analysis if there was a

noticeable difference when compared to XRD if present and comparing the P10, P50, P90, and means of nearby wells. All data are available in the supplemental data excel files.

#### **6.2.1 Curdsville Member**

Clay content for the Curdsville ranges from 1-12%, with high concentrations located in northeast Stark County and northeast Mahoning County, where clay reaches as high as 12% (Figure 16). A northwest-to-southeast trend of lower clay content is observed between these two areas, with values less than 5% towards the southeast. A low of approximately 1% mean clay is in the western portion of Stark County, with additional well data needed to verify the accuracy of this value.

The clay-rich zone located in northeastern Stark County is observed to be bounded by faults to the immediate north and south. This may indicate this area is a structural low, allowing for increased clay deposition. This trend of increased clay content can be followed south into southern Stark and western Carroll, with further presence of lineaments alongside these clay rich wells. Additionally, the clay rich zone in Mahoning County is adjacent to a lineament to the north. Well control is sparse in this area, with more data needed to verify the clay content in this area and its relation to the local structures present.

Carbonate content across the area ranges from 65-83%, with low carbonate content located in northern Carroll County and northeastern Mahoning County (Figure

17). Carbonate-rich regions are in northern Portage County and southeastern Columbiana, with values in excess of 80%. This contrasts with the clay content, representing depositional changes across the research area due to water depth. The carbonate rich trend observed runs NW-SE, the same direction of several fault and lineament planes observed in the research area. Comparing the low carbonate region present in Carroll and Stark counties with the carbonate rich region indicates these two areas are divided by a series of fault and lineament planes. This indicates the carbonate rich region may be representative of a structural high in which carbonate deposition increased, explaining the reduced clay content in these areas. Furthermore, the clay content is the inverse of the carbonate content across the study area; where there is high carbonate content, the clay content is low, and vice versa. This further suggests bathymetric highs and lows in the study area, influencing carbonate and clay deposition.

Siliciclastic content ranges from 1-12% in the Curdsville Member, with a general increase towards the southern portion of the research area (Figure 18). A well located in northeastern Portage exhibits a value of less than 1% siliciclastic. The relatively carbonate poor region is observed to be rich in siliclastics, whereas the carbonate rich region has reduced siliclastic content. Comparing siliclastic content with clay indicates the siliciclastics are representative of increased shale content, further supporting Carroll County to be a structural low in which shale deposition was increased.

Pyrite content ranges from 1-3%, with localized highs in western Stark County, northwestern Carroll County, northeastern Columbiana County, and northeastern Portage County (Figure 19). Pyrite values appear more heterogenous due to being a diagenetic feature, forming as a result microbiological processes within the water column (Duverger et al., 2020). Pyrite formation does not appear to correlate with a specific mineralogy, nor does it correlate with proximity to known faults and lineaments. While the central Carroll well has a high observed pyrite content and is located along lineaments, nearby wells are pyrite poor or absent. It is unclear to what extent pyrite alteration at these fault zones play within the research area.

TOC values range from 0.5-5.5%, with similar trends as pyrite due to pyrite strongly correlating to TOC within the research area (Figure 20). Sweet spots are present in western Stark County, northwestern Carroll County, northeastern Columbiana County, and northeastern Portage County. TOC changes abruptly, such as in Carroll County, where a sweet spot is adjacent to an organic poor area 20 miles to the southwest. Similar to pyrite, TOC does not appear to strongly correlate with a specific mineralogy or proximity to fault zones, with organic highs and lows located across different mineralogies, and therefore different water depths. Instead, this supports TOC distribution to be heterogeneous and a result of conditions in the water column allowing for the preservation of organic content.



Porosity values range from 1-5%, with highs located in the southwest and northeast area of the research area, with western Carroll County containing values more than 5% (Figure 21). A northwest-to-southeast pattern of low porosity is observed, bisecting the two areas. Values within this region are less than 1% porosity and need additional tight rock analyses to verify the accuracy of the porosity values. The low porosity region appears bounded by faults and lineaments on either side, with an increase in porosity observed on the other side. This further supports the effect localized structures have on mineralogy and the resulting porosity distribution in the area. It is observed that as carbonate content increases, formation porosity decreases as a result.

### Curdsville Member Average Clay Map

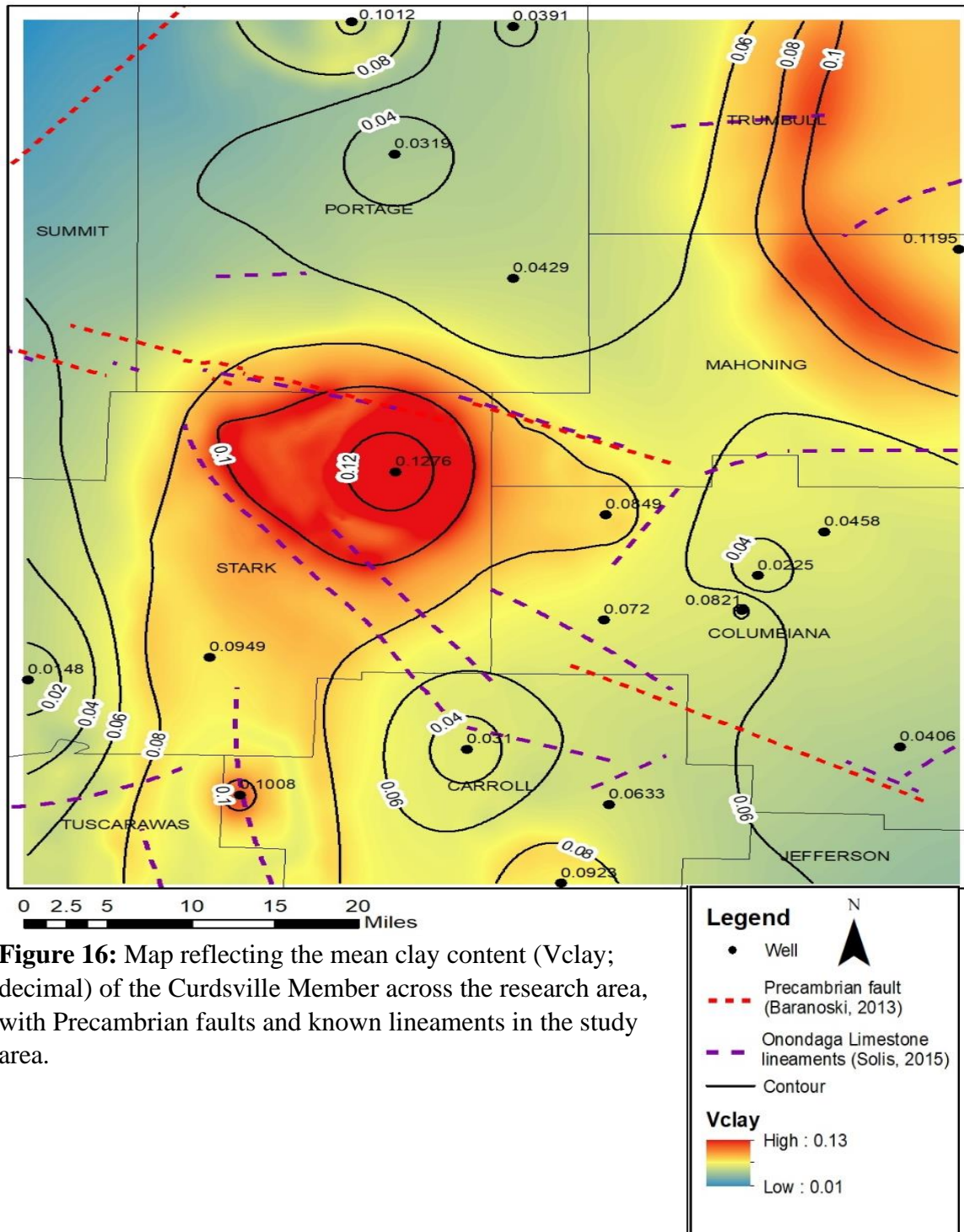


**Figure 16:** Map reflecting the mean clay content (Vclay; decimal) of the Curdsville Member across the research area, with Precambrian faults and known lineaments in the study area.

### Curdsville Member Average Carbonate Map

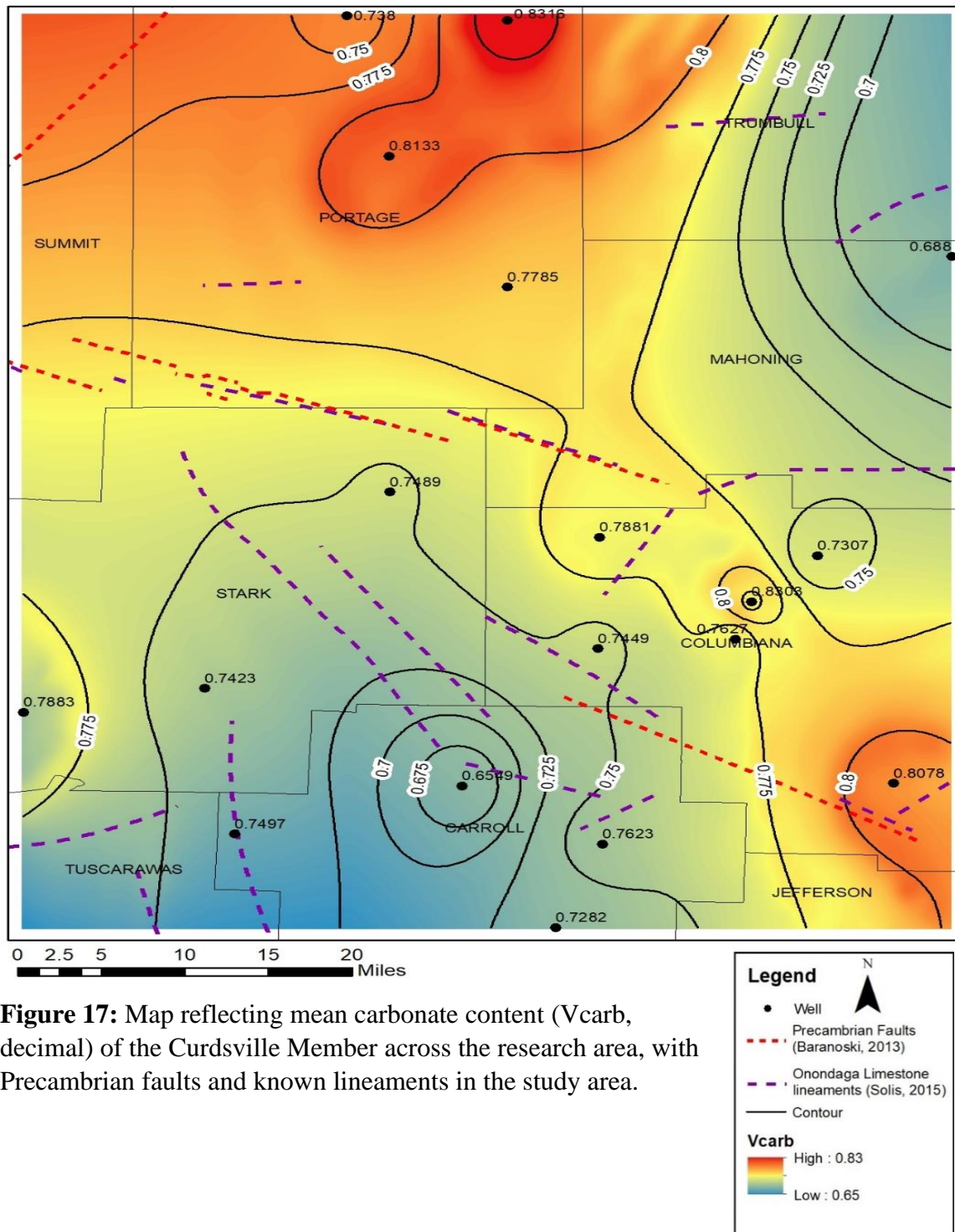


**Figure 17:** Map reflecting mean carbonate content (Vcarb, decimal) of the Curdsville Member across the research area, with Precambrian faults and known lineaments in the study area.

### Curdsville Member Average Siliciclastic Map

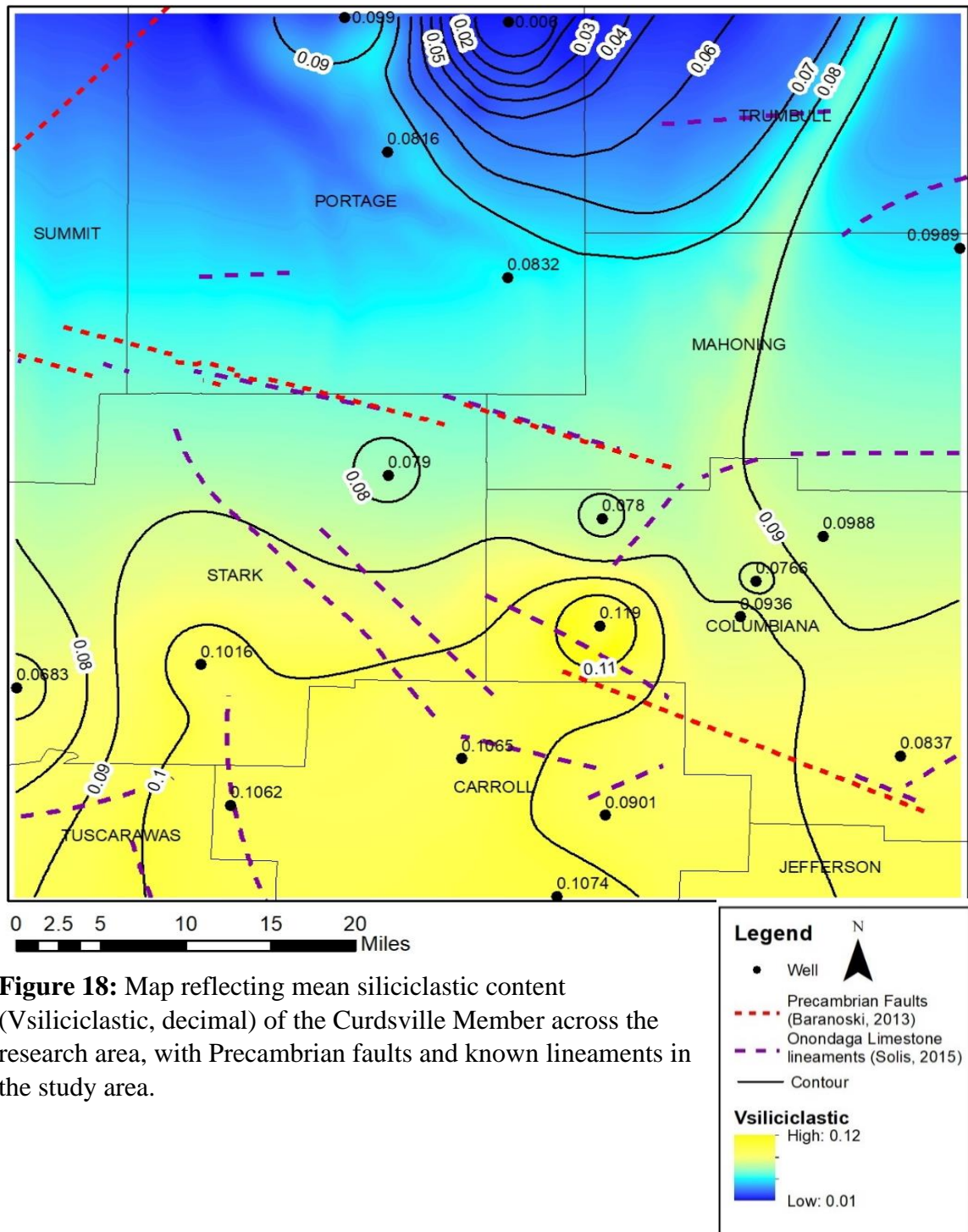


**Figure 18:** Map reflecting mean siliciclastic content (Vsiliciclastic, decimal) of the Curdsville Member across the research area, with Precambrian faults and known lineaments in the study area.



### Curdsville Member Average Pyrite Map

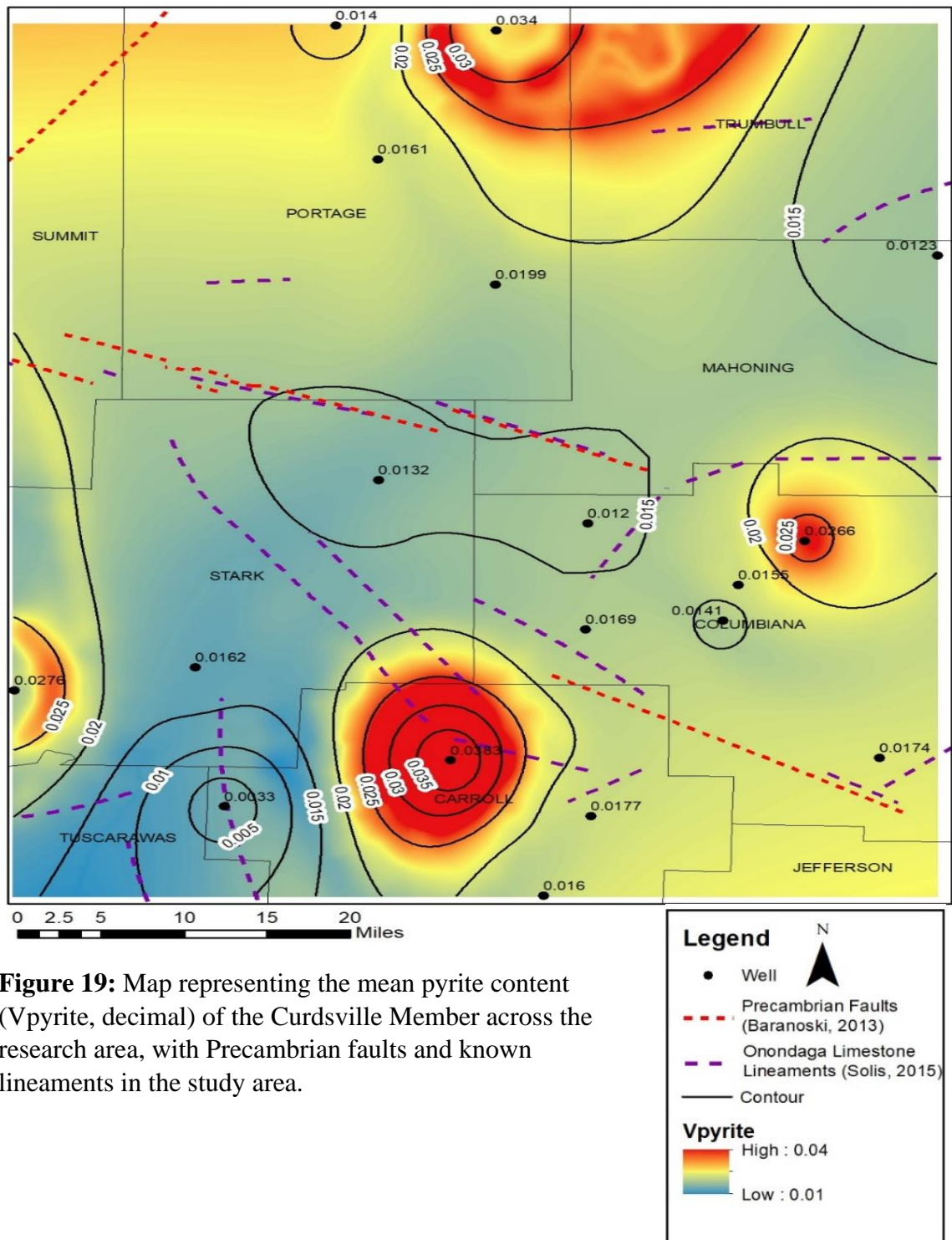
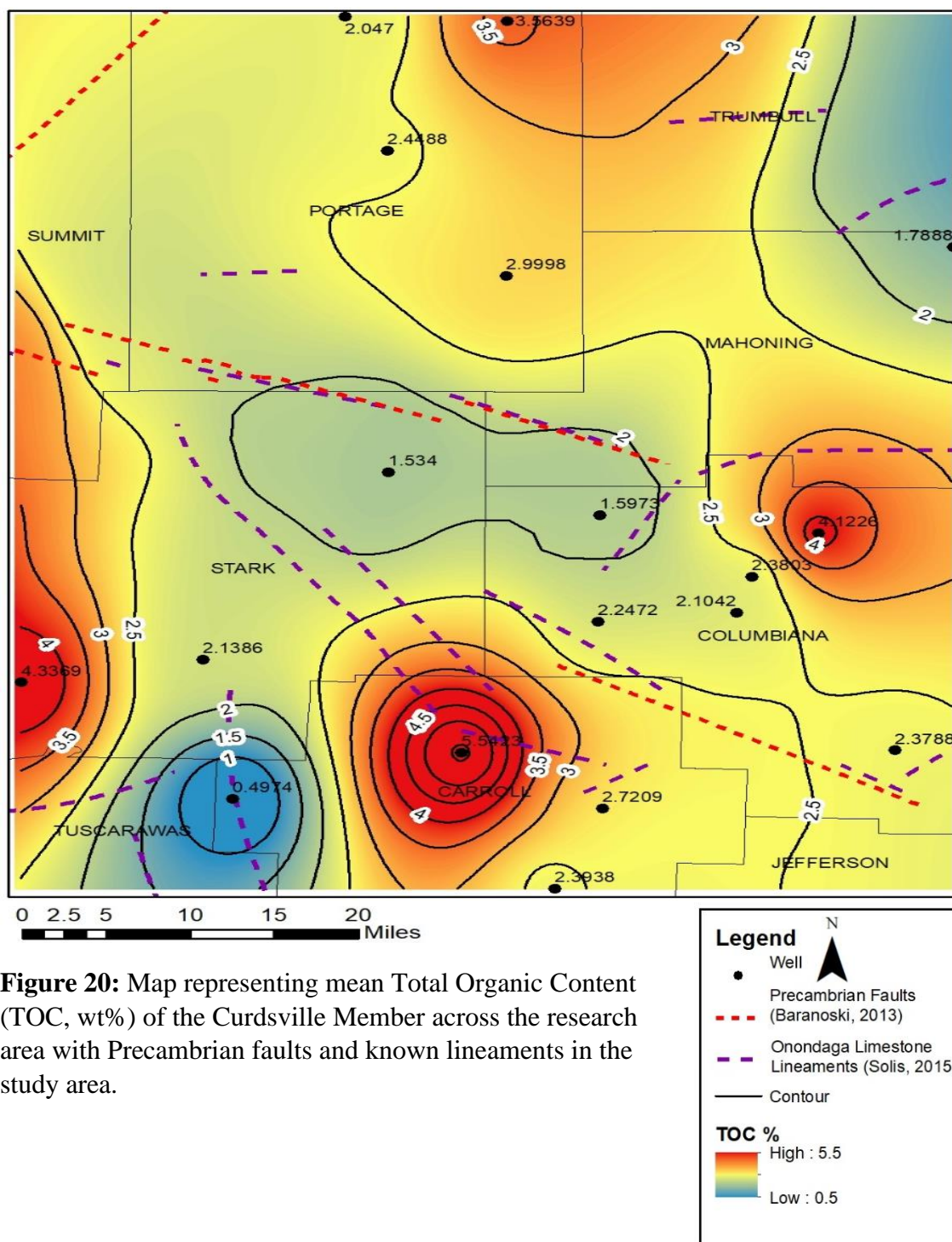


**Figure 19:** Map representing the mean pyrite content (Vpyrite, decimal) of the Curdsville Member across the research area, with Precambrian faults and known lineaments in the study area.

### Curdsville Member Average TOC (wt%) Map



### Curdsville Member Average Porosity Map

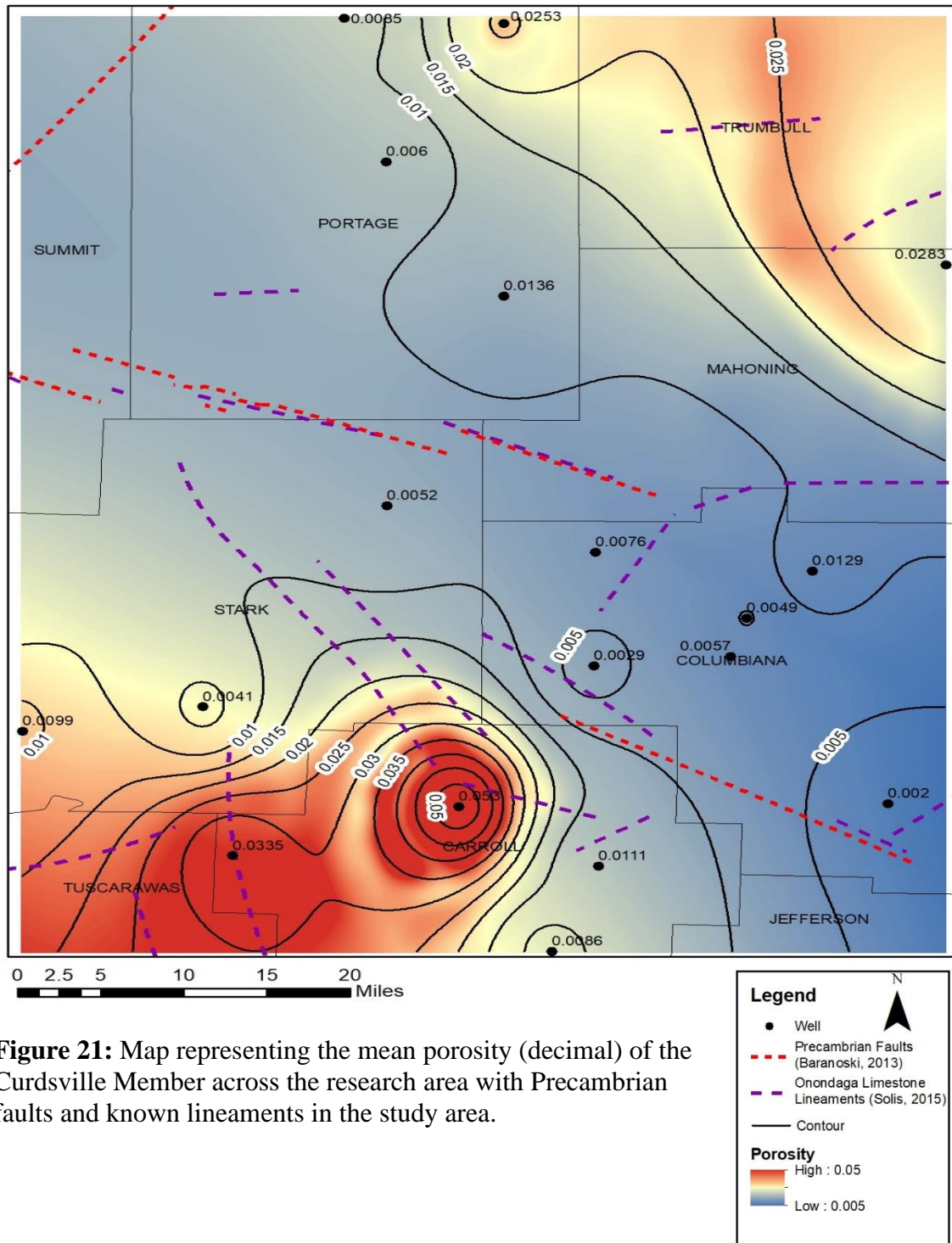


**Figure 21:** Map representing the mean porosity (decimal) of the Curdsville Member across the research area with Precambrian faults and known lineaments in the study area.

### **6.2.2 Logana Member**

Clay content ranges from 2-21%, with a strong trend of increasing clay content towards the northwest portion of the research area (Figure 22). Northern Portage County is observed to contain clay values more than 15%. Interestingly, western Stark County contains two wells with significantly different clay content averages. This abrupt change may indicate a significant depositional shift or possible error within the mineral model for one of these wells.

Clay content does not appear to be strongly affected by the location of nearby faults and lineaments in the southern portion of the research area. However, north of the faults and lineaments, clay content increases significantly. This may indicate that the northern part of the area was a bathymetric low associated with the Sebree Trough, which may have influenced clay deposition during the Late Ordovician (Bloxson, 2022; Figure 4b). The Sebree Trough is associated with the failed Reelfoot Rift in Kentucky, which continues through Ohio trending southwest to northeast. Researchers are unsure if it is a bathymetric low, or an area of non-deposition due to anoxic waters sourced from deep seated faults (Kolata et al., 2001; Ettensohn et al. 2002). There is minor influence from faulting in Stark County, with either pre- or syn-depositional movement of fault blocks creating bathymetric lows that allowed for increased clay deposition.

Carbonate content in the Logana ranges from 45-81%, with a strong increasing carbonate trend towards the southeastern portion of the research area (Figure 23). This



suggests that as clay deposition decreased, it was replaced by carbonates in the southeast. Values change relatively fast towards western Stark County and northwestern Portage County. Carbonate content follows a strong NW-SE trend. Within the southern portion of the research area, carbonate values are typically 70% or more and do not exhibit significant changes despite the prevalence of structural features within the area. The increased carbonate content towards the southeast suggests deepening of sea levels towards the northeast, further suggesting influence of the Sebree Trough and the corresponding cessation of carbonate sedimentation associated with this bathymetric low (Kolata et al., 2001).

Siliciclastic content ranges from 2-17% across the research area, with southern Carroll County and northwest Portage County containing the highest values (Figure 24). A southwest to northeast trend of lower siliciclastic values is present in the area, expanding across Stark, Eastern Portage, and Northern Columbiana counties. This map is the inverse of the carbonate content map (Figure 23), further suggesting influence of the Sebree Trough. With either a bathymetric low or non-deposition of carbonates (i.e., reef building organisms) within the trough, siliciclastics and clays are deposited (Kolata et al., 2001; Ettensohn et al. 2002).

Pyrite content ranges from 1-4%, with pyrite increasing towards the northeast portion of the research area (Figure 25). Little to no pyrite is observed in the southernmost portion of the research area, with values less than 2% on average. Pyrite

formation in the Logana is less heterogeneous than the Curdsville, instead correlating with an increase of clay content.

TOC ranges from 1-5%, with a similar trend to the mean pyrite map (Figure 26). TOC trends appear more uniform than the lower Curdsville member, with a clear trend of low organic values present from western Carroll County, through Stark County and ending in Western Columbiana County. TOC and pyrite do not appear to correlate with siliciclastic, clay, or carbonate content, nor correspond to areas bounded by faults.

Porosity values range from 0-5%, with a general increase towards the northern portion of the research area (Figure 27). Similar to the Curdsville Member, porosity is observed to be greatest when clay/siliciclastic values are high and carbonate content is low. Little to no porosity is calculated for the southern portion of the research area, with most wells having less than 2% porosity on average. Within eastern Stark and western Columbiana counties, a zone of less than 1% porosity is observed. While there are more prevalent faults and lineaments in the area with higher porosity, the general trend is low to the north and decreasing to the south. This loosely correlates to the carbonate content, suggesting that porosity may be controlled by carbonate content and a function of dissolution or a lack of clay matrix in the formation.

## Logana Member Average Clay Map

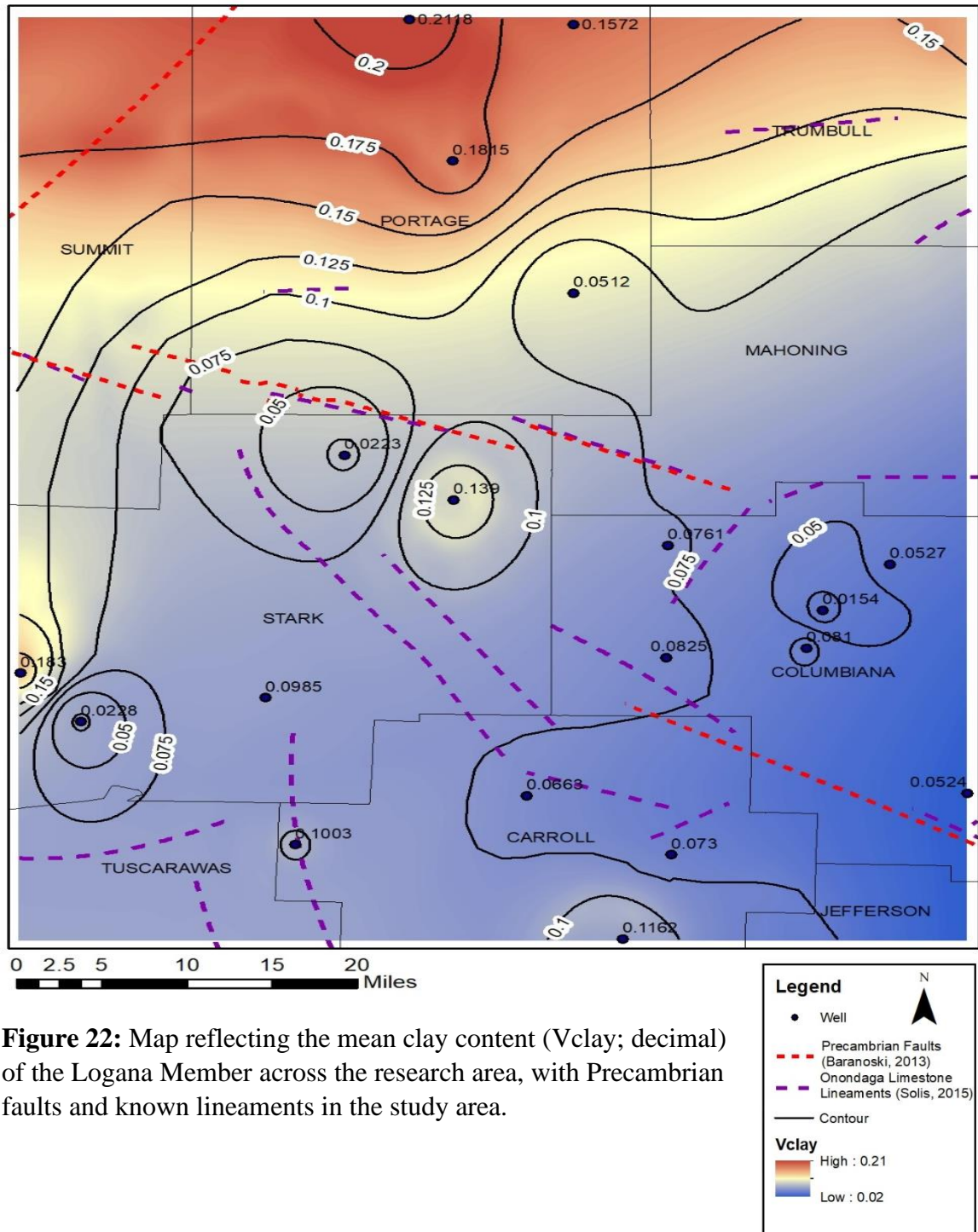


**Figure 22:** Map reflecting the mean clay content (Vclay; decimal) of the Logana Member across the research area, with Precambrian faults and known lineaments in the study area.

## Logana Member Average Carbonate Map

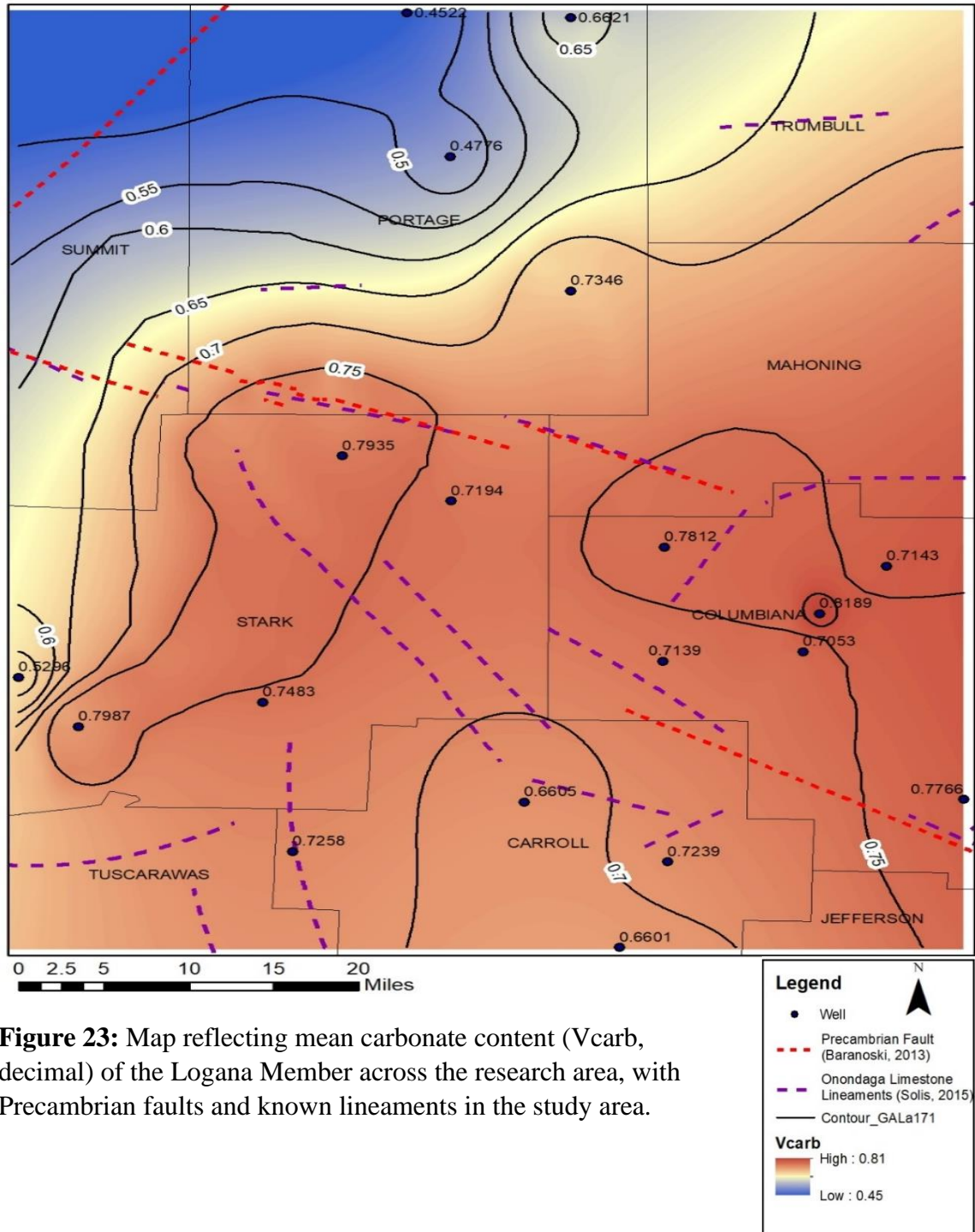


**Figure 23:** Map reflecting mean carbonate content (Vcarb, decimal) of the Logana Member across the research area, with Precambrian faults and known lineaments in the study area.

## Logana Member Average Siliciclastic Map

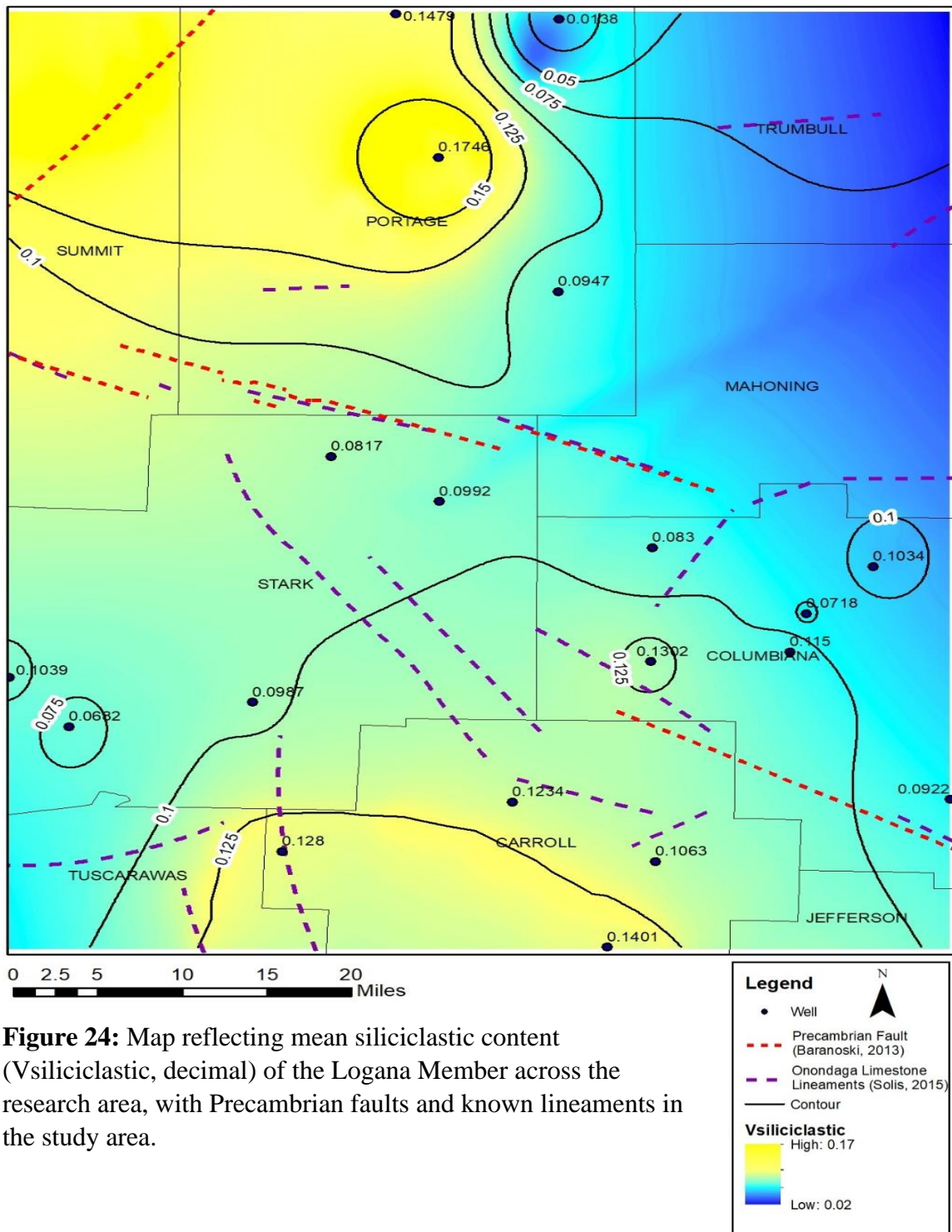


**Figure 24:** Map reflecting mean siliciclastic content (Vsiliciclastic, decimal) of the Logana Member across the research area, with Precambrian faults and known lineaments in the study area.



### Logana Member Average Pyrite Map

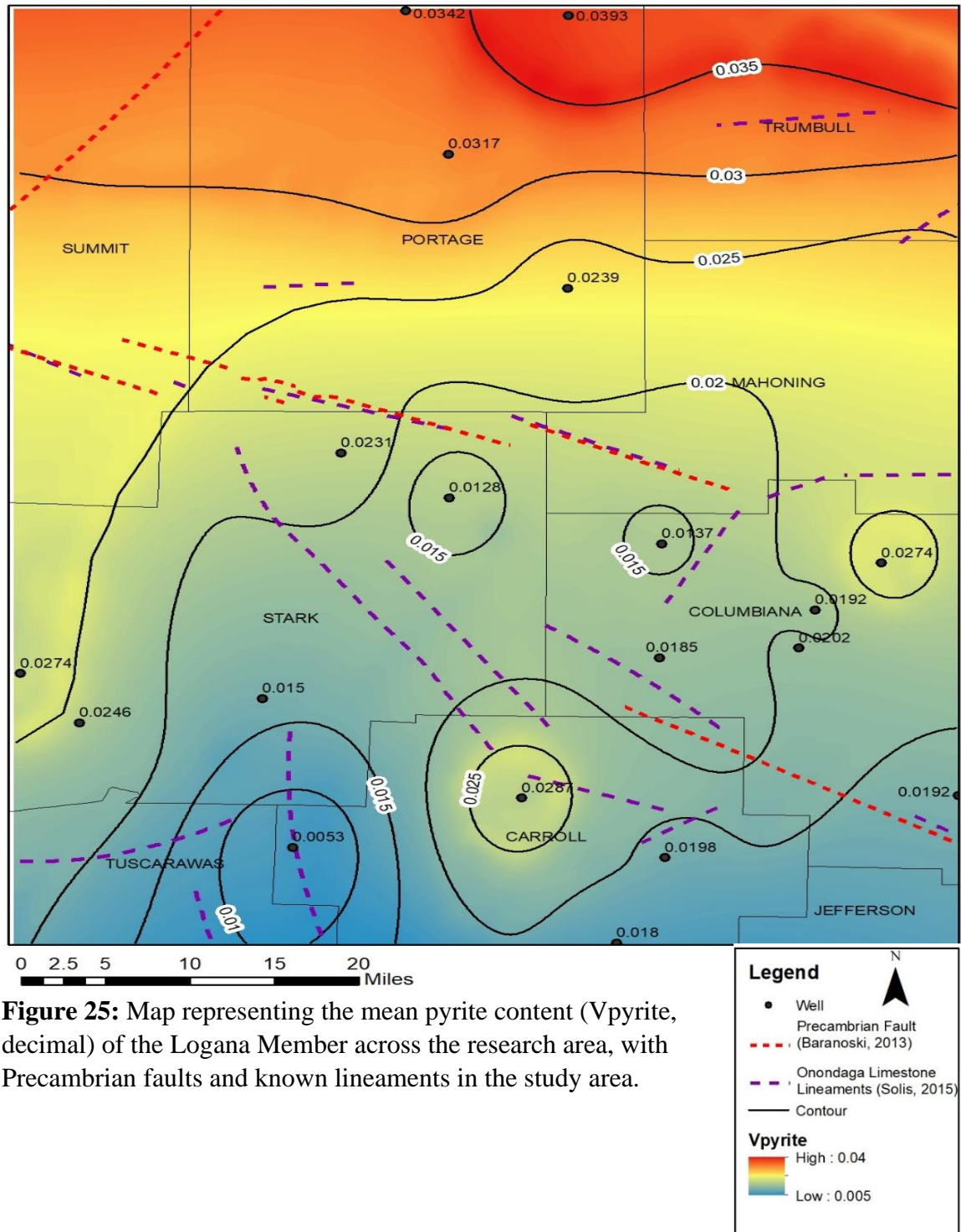


**Figure 25:** Map representing the mean pyrite content (Vpyrite, decimal) of the Logana Member across the research area, with Precambrian faults and known lineaments in the study area.

### Logana Member Average TOC (Wt %) Map

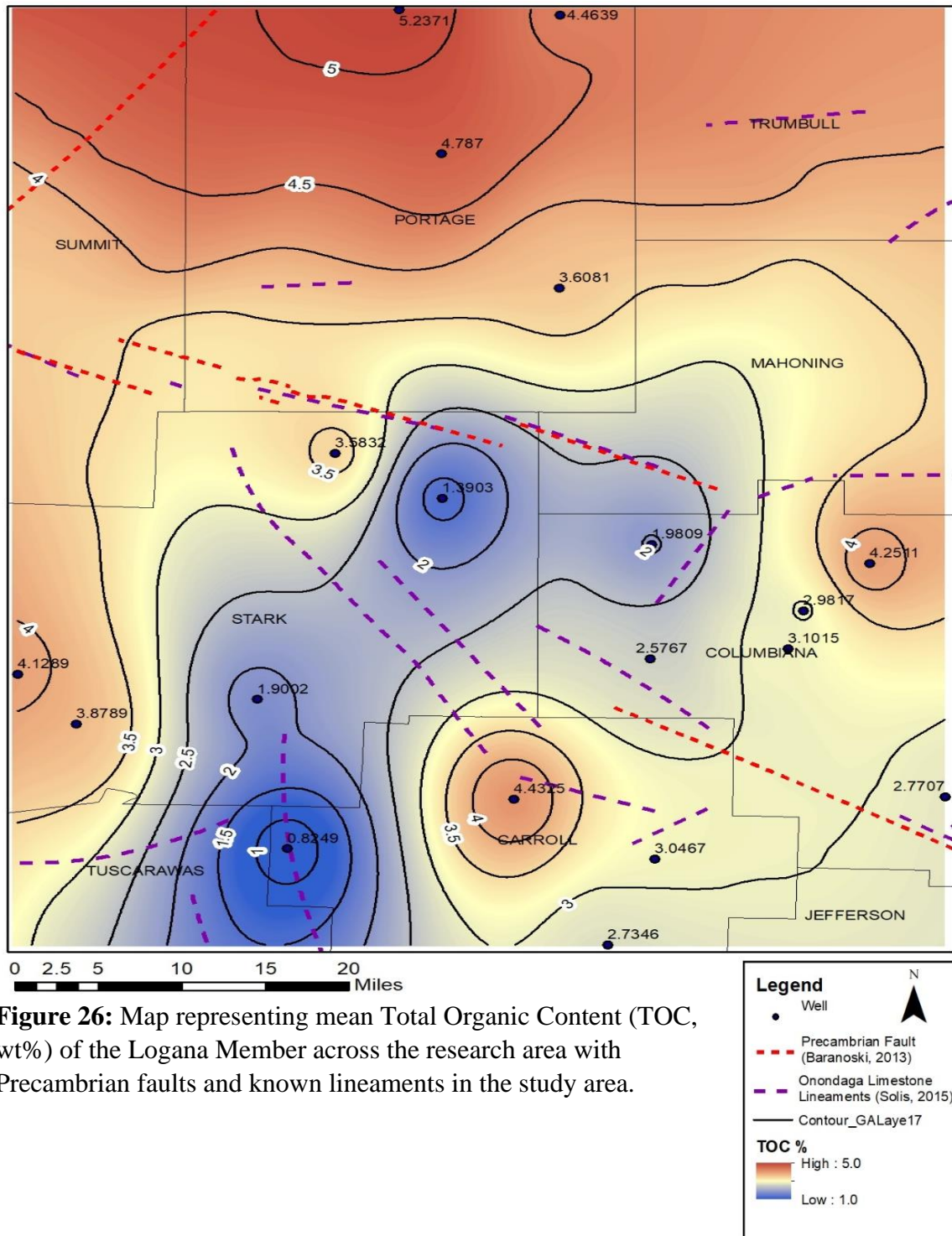


**Figure 26:** Map representing mean Total Organic Content (TOC, wt%) of the Logana Member across the research area with Precambrian faults and known lineaments in the study area.

### Logana Member Average Porosity Map

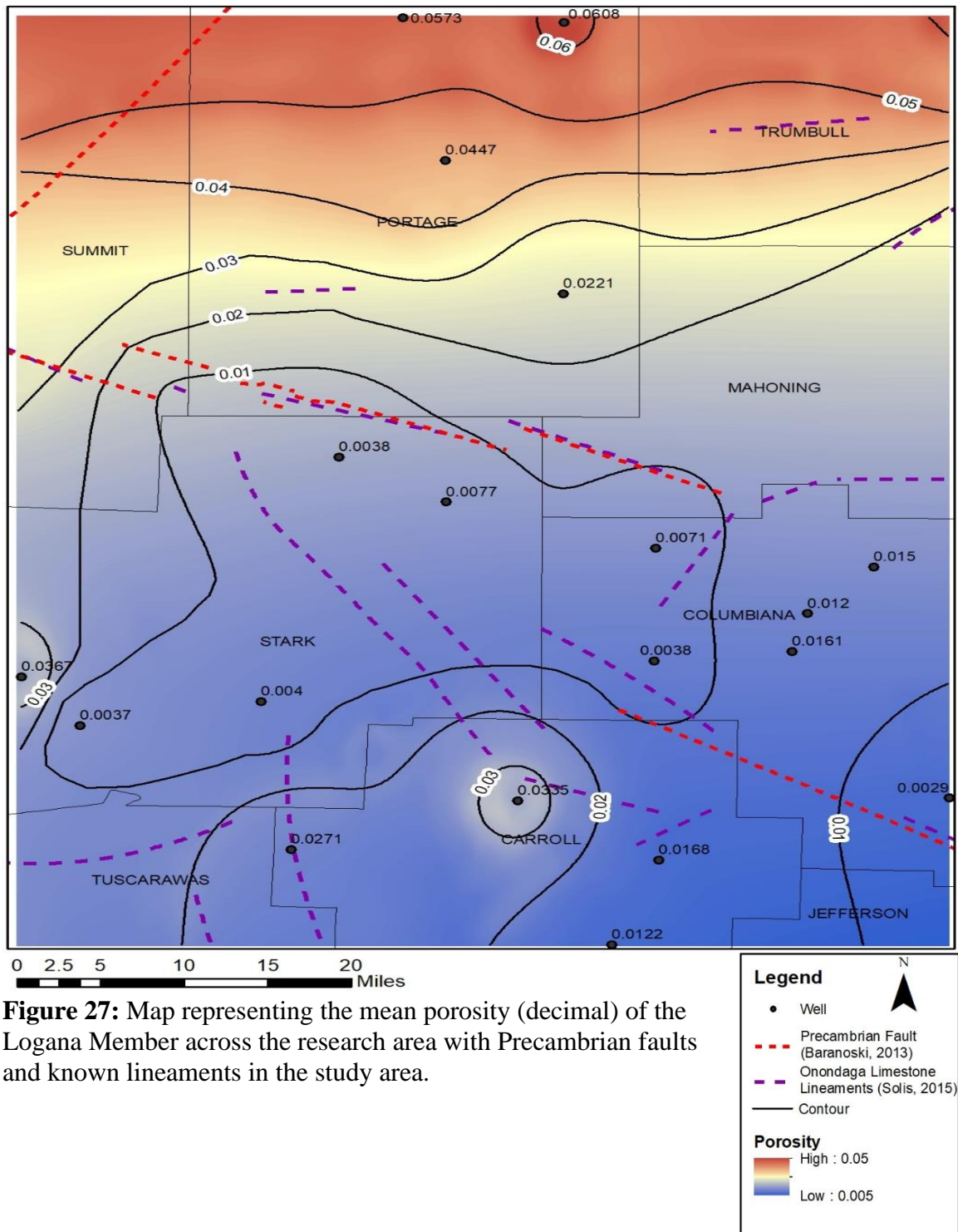


**Figure 27:** Map representing the mean porosity (decimal) of the Logana Member across the research area with Precambrian faults and known lineaments in the study area.



### **6.2.3 Upper Lexington Member**

Clay content ranges from 2-17%, with a general increasing clay trend towards the northwest portion of the research area (Figure 28). Portage County has the highest clay values in the area, with values exceeding 15%. Wells within northern Columbiana County and central Carroll County exhibit clay values as low as 2%. Low clay content is reported in the southeast portion of the research area, adjacent to faults and lineaments. While these do not appear to control clay content, north of these faults and lineaments clay content rapidly increases. This indicates a shift in the water depth, with Portage County representing a structural low allowing for increased clay deposition.

Carbonate content ranges from 44-83%, with an increasing carbonate content towards the southeast portion of the research area (Figure 29). The highest carbonate values occur in central Columbiana County, where clay content is the lowest. Similarly, the highest clay content occurs in Portage County, which exhibits the lowest carbonate values. This further supports a structural low in Portage, with a decrease in carbonates as a result. Columbiana County is observed to be a structural high and appears bounded by faults and lineaments, allowing for increased carbonate precipitation.

Siliciclastic content ranges from 2-18%, with the high values occurring in western Portage County and Carroll County (Figure 30). The same well in northeastern Portage exhibits unusually low siliciclastic content in comparison to the surrounding area as it did in the Curdsville Member analysis, further supporting the need for additional

investigation. Siliciclastic content does not appear to correlate with one mineralogy alone. Instead, a NW-SE trend of decreased siliciclastic content is observed, spanning from Columbiana to Stark counties. This area of low siliciclastic content is bounded by faults and lineaments, giving support to a structural high with siliciclastic poor carbonates present. In Portage, the siliciclastic content appears correlated with an increase in clay, representing the siliciclastic component of shale.

Pyrite content ranges from 1-4%, with Portage County containing some of the highest pyrite content in the research area (Figure 31). A localized high is located within central Carroll County, with a mean pyrite content of nearly 4%. Values in western Carroll County and southern Columbiana County indicate pyrite drops significantly, often less than 1%. Pyrite does not appear to correlate with known faults and lineaments in the southern portion of the research area, but does appear to increase north of this area and coincides with increased clay content.

TOC ranges from 0.5-6%, with a general increase observed in Portage County where values exceed 5% (Figure 32). Additionally, a localized sweet spot is present in central Carroll County and northeastern Columbiana County. Additional wells are needed to verify if these two regions are linked or represent discrete zones. TOC values rapidly drop around these sweet spots, with values of less than 1% present. A noticeable increase in TOC is observed towards the northwest, interpreted to be a structural low based on the increased clay content. However, organic poor and enriched zones are present throughout

the southern portion of the research area, despite similar carbonate content. This supports that while TOC is generally correlated with increased clay content, local variations exist even in similar mineralogic content.

Porosity values range from 1-7%, with Portage County containing the highest porosity in the research area (Figure 33). Although porosity may appear correlated with TOC in Portage County, high porosity is also present in western Carroll County which had TOC values of less than 1%. Additionally, northeastern Carroll County had TOC values of over 4%, yet porosity values were consistently less than 2%. A NW-SE trend of low porosity values is present and correlates with the presence of faults and lineaments bounding them. These porosity changes are strongly correlated with clay content, with clay rich zones containing the highest porosity. The low porosity zone in Columbiana is remarked by high carbonate values, bounded by faults and lineaments, and indicates a possible structural high where insufficient clay content is responsible for the low porosity. Adjacent to this area, porosity values increase, and coincide with an increase in clay content to the north and west.

### Upper Lexington Member Average Clay Map

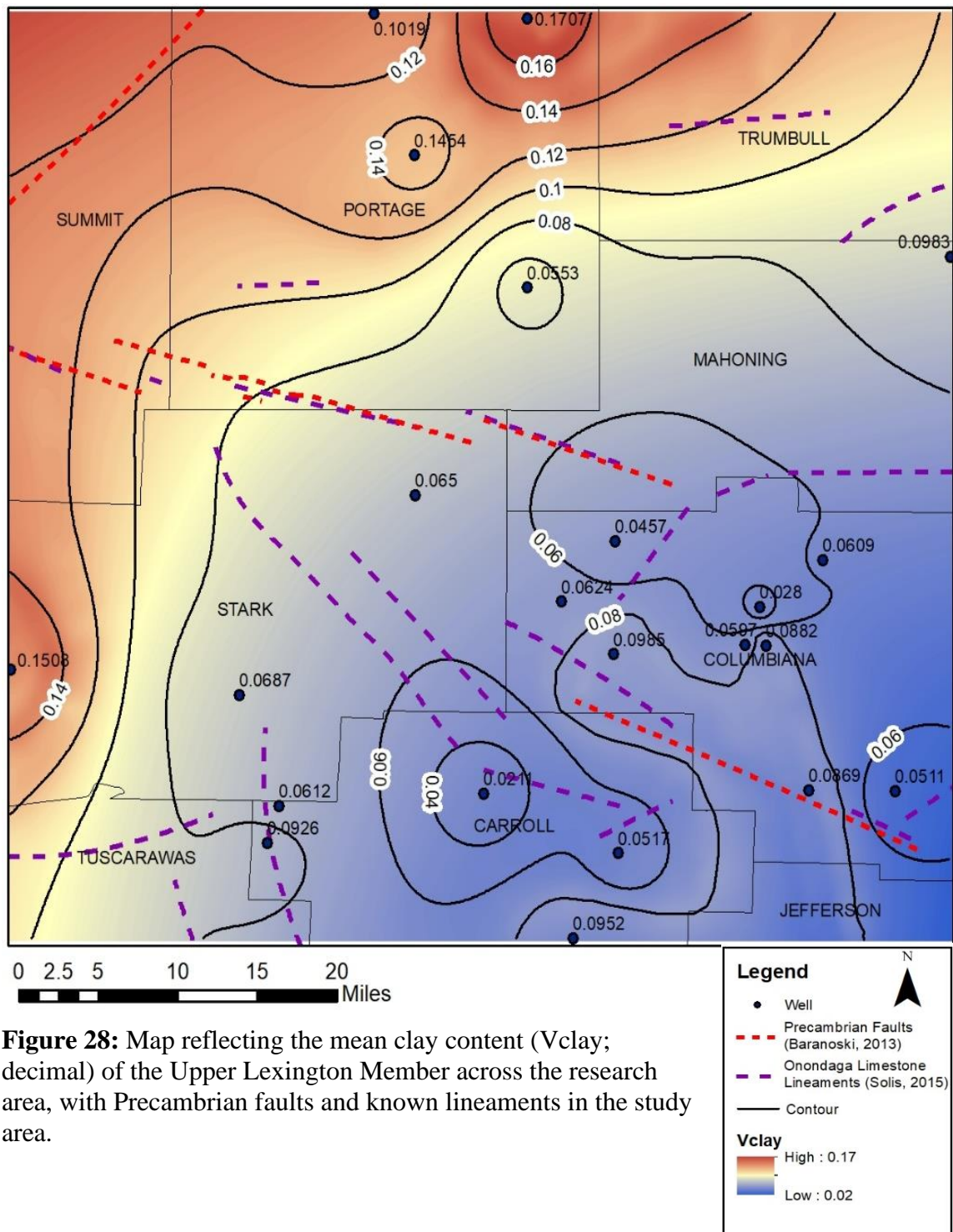
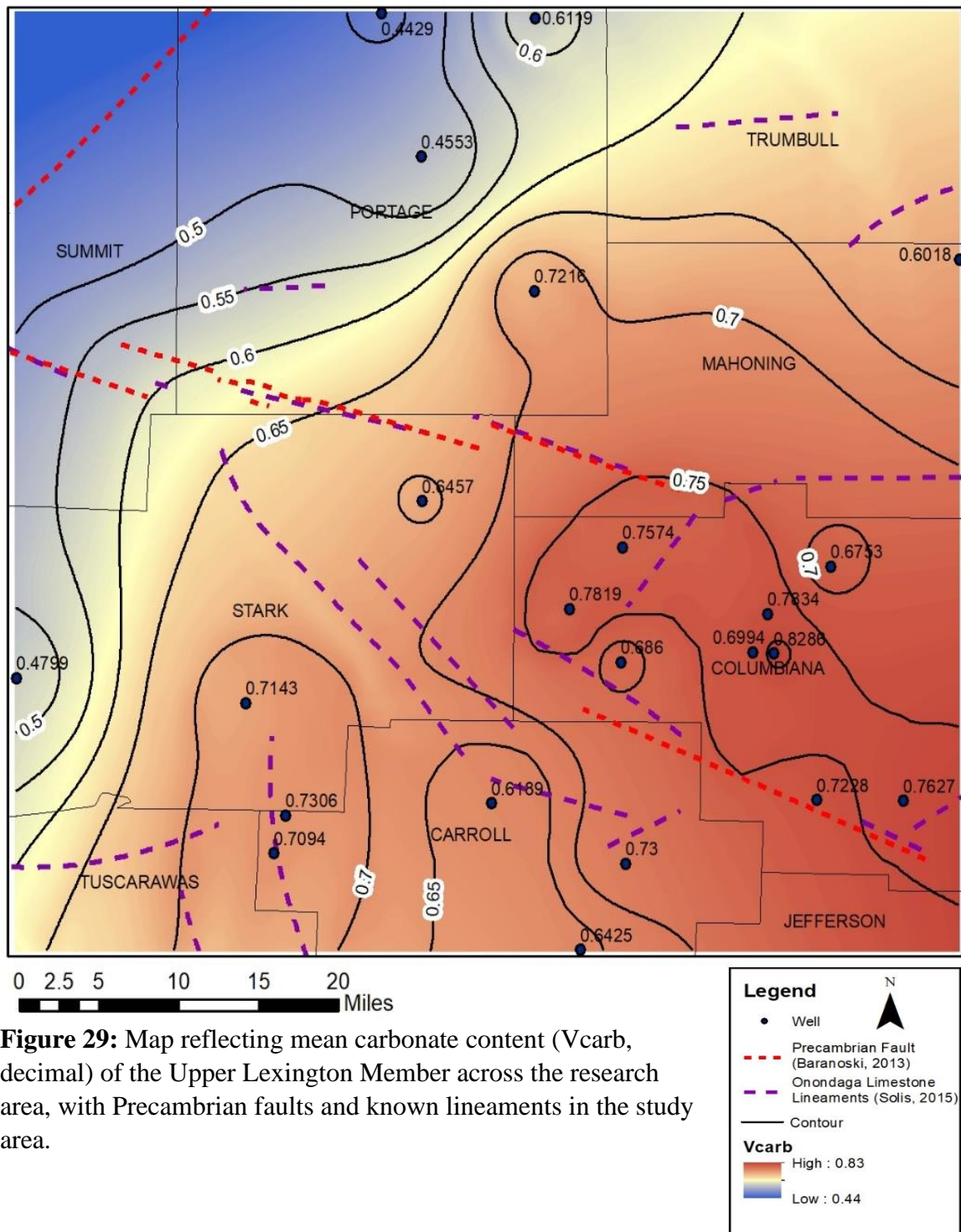


**Figure 28:** Map reflecting the mean clay content (Vclay; decimal) of the Upper Lexington Member across the research area, with Precambrian faults and known lineaments in the study area.

### Upper Lexington Member Average Carbonate Map





### Upper Lexington Member Average Siliciclastic Map

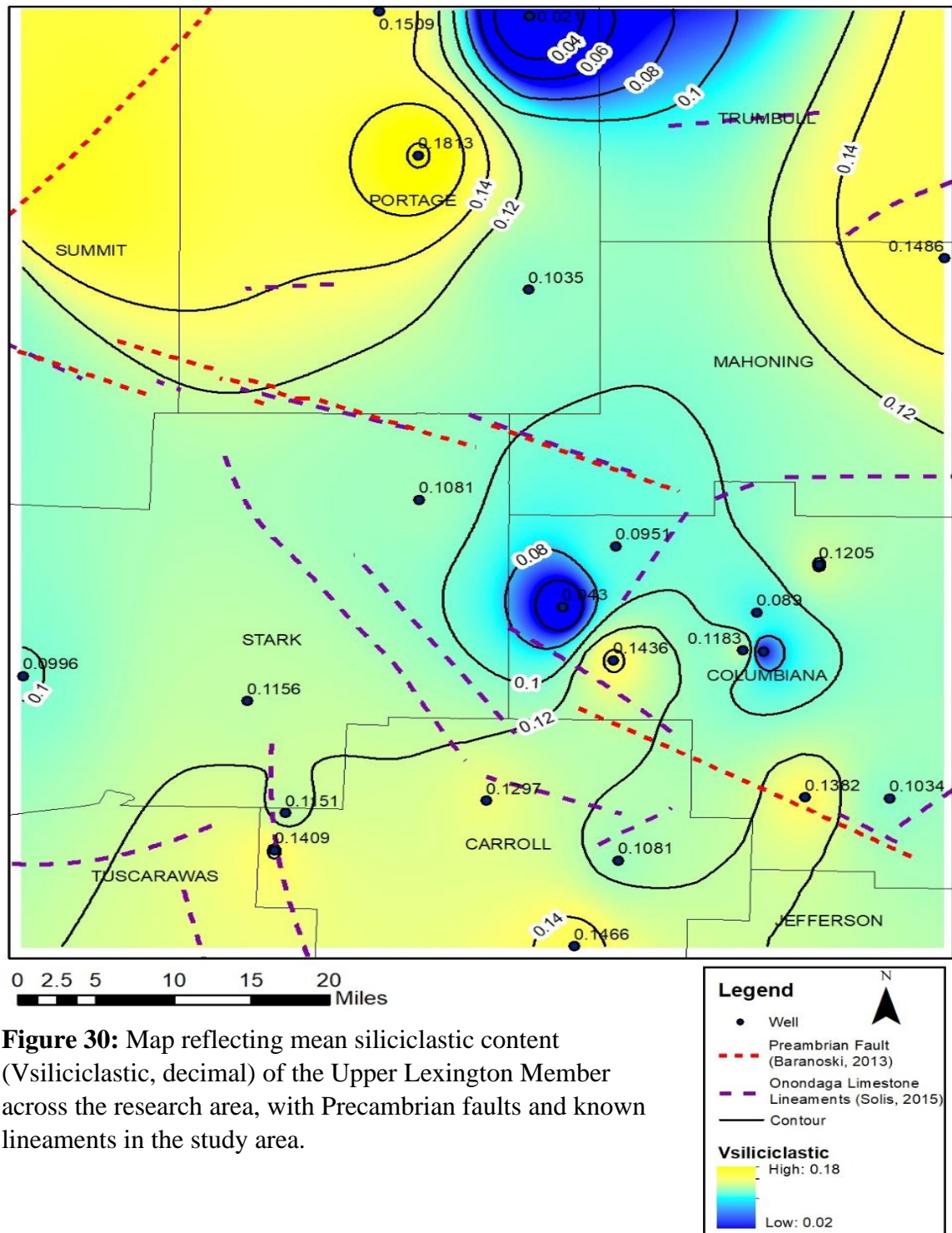


**Figure 30:** Map reflecting mean siliciclastic content (Vsiliciclastic, decimal) of the Upper Lexington Member across the research area, with Precambrian faults and known lineaments in the study area.

### Upper Lexington Member Average Pyrite Map

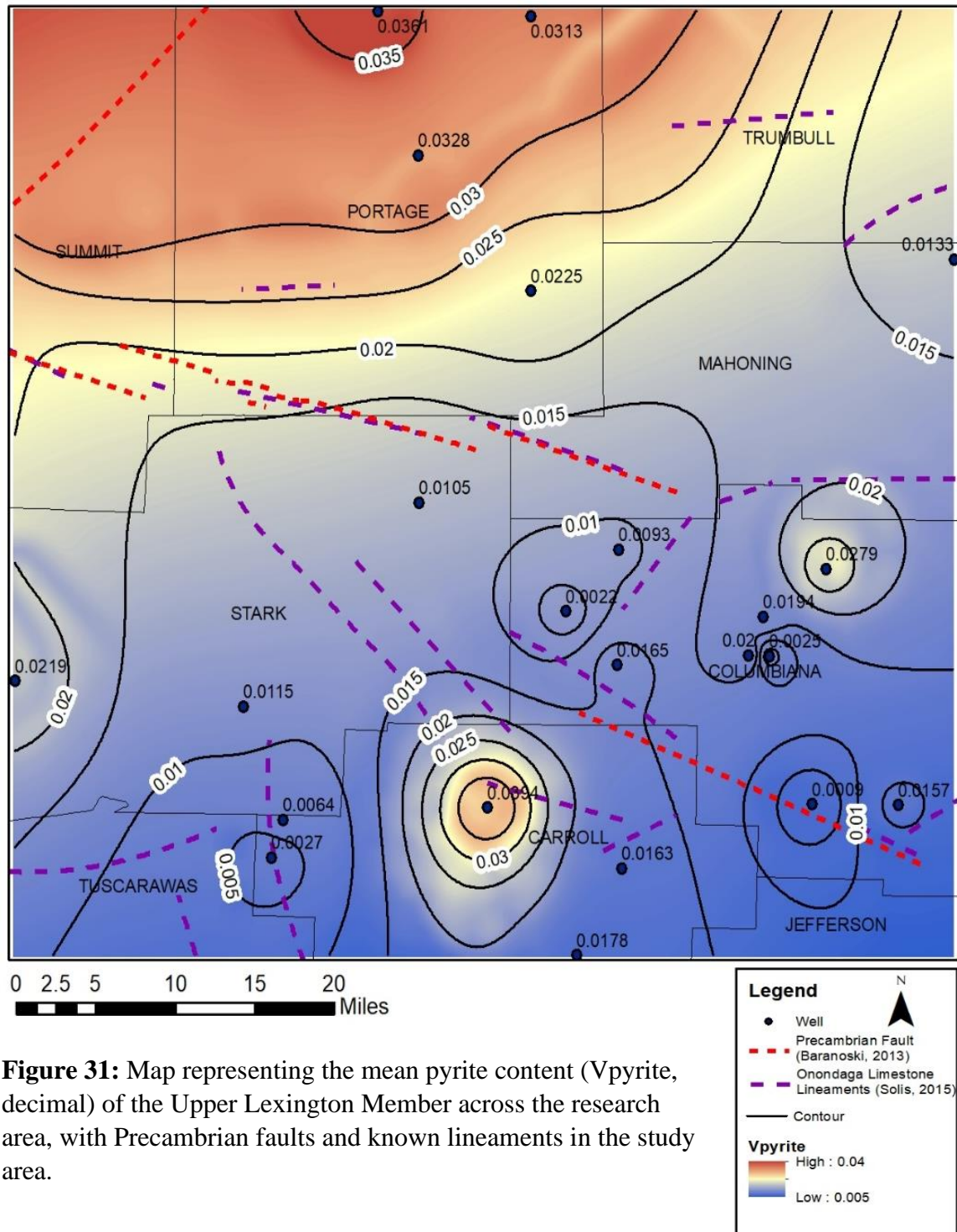


**Figure 31:** Map representing the mean pyrite content (Vpyrite, decimal) of the Upper Lexington Member across the research area, with Precambrian faults and known lineaments in the study area.

Upper Lexington Member Average TOC (Wt %) Map

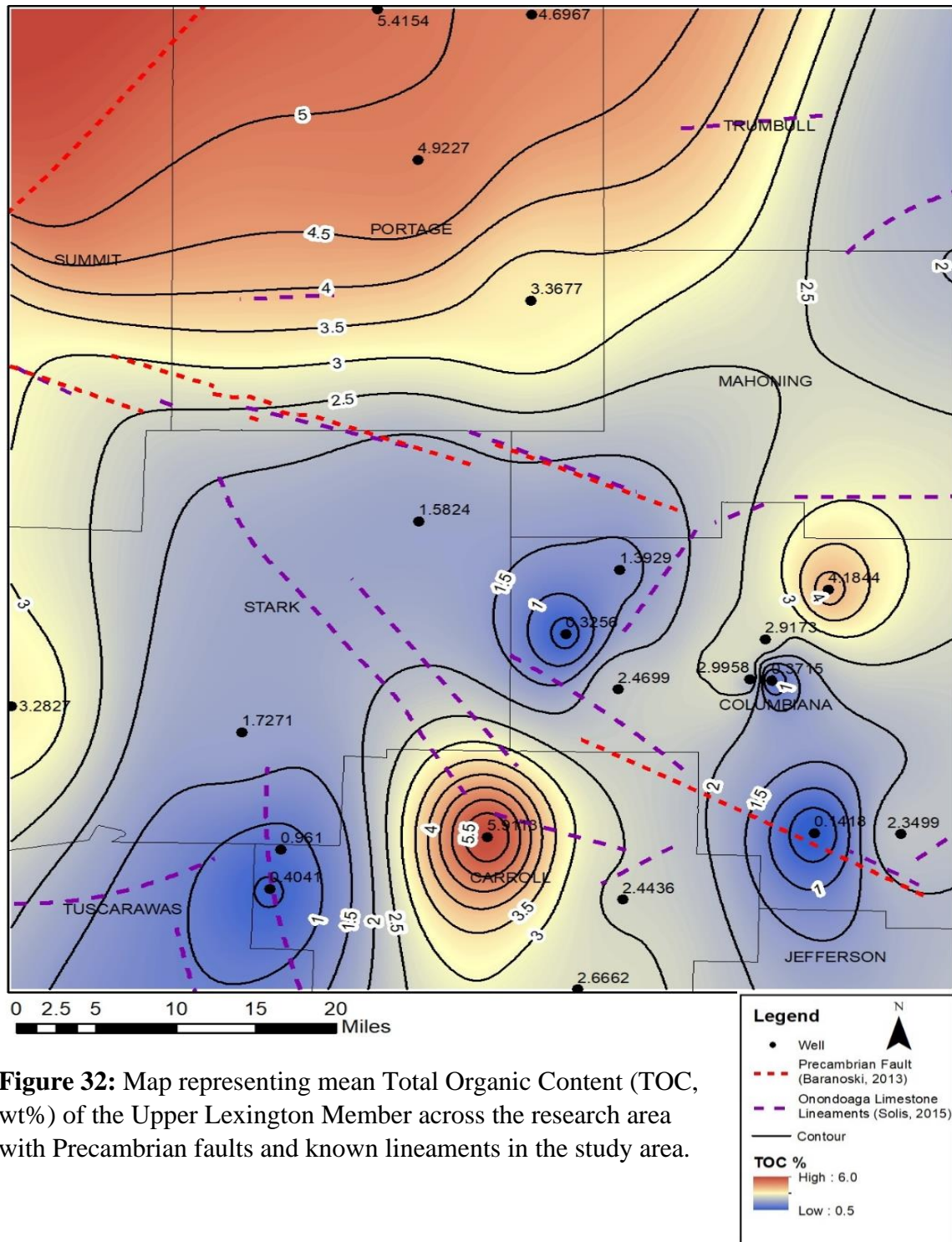


**Figure 32:** Map representing mean Total Organic Content (TOC, wt%) of the Upper Lexington Member across the research area with Precambrian faults and known lineaments in the study area.



### Upper Lexington Member Average Porosity Map

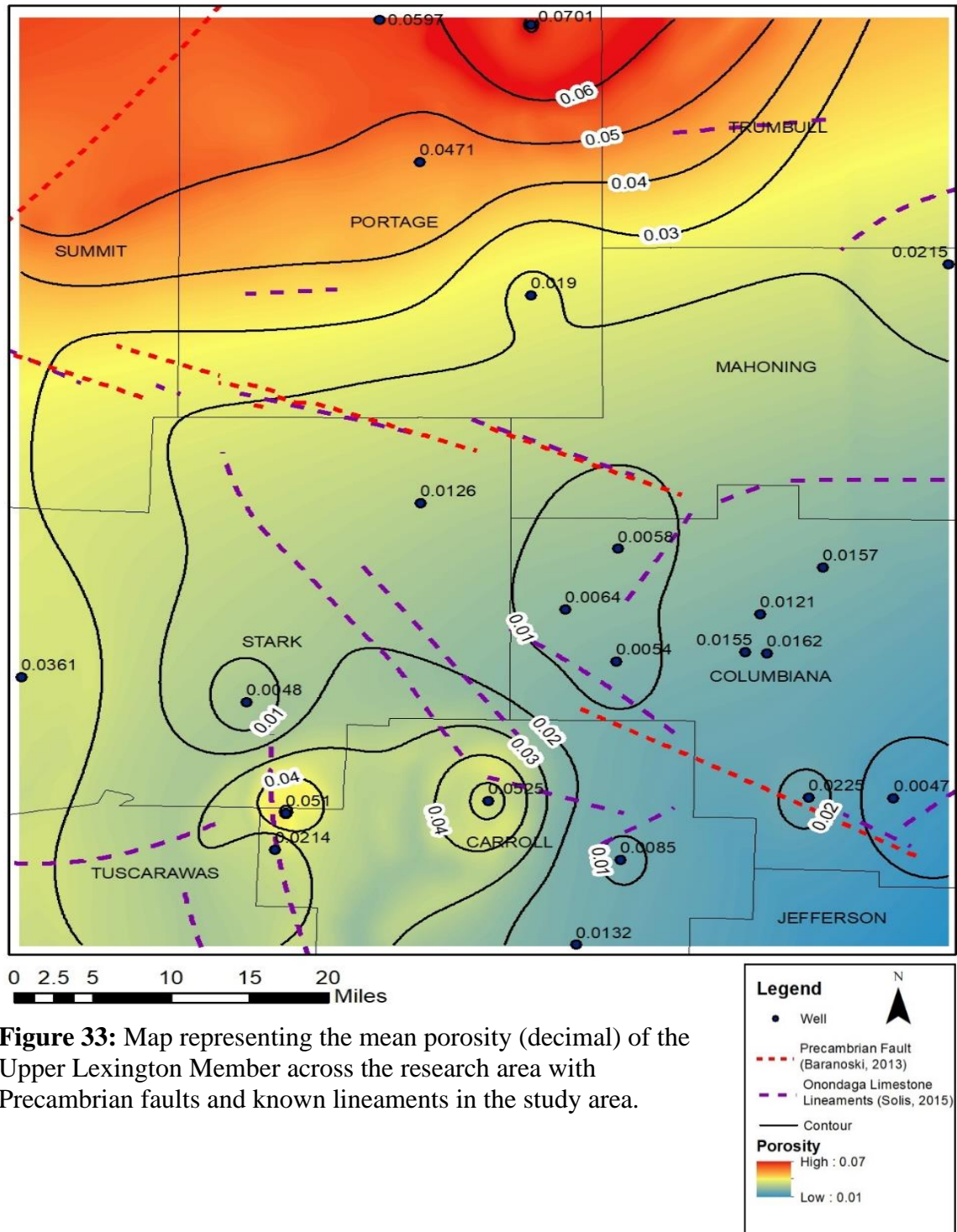


**Figure 33:** Map representing the mean porosity (decimal) of the Upper Lexington Member across the research area with Precambrian faults and known lineaments in the study area.

#### **6.2.4 Point Pleasant Formation**

Clay content ranges from 3-44%, with a general increase observed in the northern-most wells with values more than 40% (Figure 34). Wells within northeast Stark County and central to southeastern Columbiana exhibit low clay values, with some as low as 3%. These wells require further analysis and XRD data to verify or disprove these values given the large variance across the research area. A NW-SE trend of decreased clay content is prominent within the area and coincides with the orientation of known faults and lineaments. This zone is flanked by increased clay content to the immediate north and southwest, providing support for the interpretation that this interval of decreased clay content is a structural high spanning from Columbiana to Stark counties.

Carbonate content ranges from 10-56%, with the highest values occurring in Columbiana County where values consistently exceed 40% and reach as high as 56% (Figure 35). In contrast, northern Portage County has the lowest carbonate values, decreasing to 10-17%. A rapid increase in carbonate content is observed in southeast Portage County, where values reach 40% and continue to increase to the southeast. This NW-SE trend of increased carbonates coincides with the reduced clay content, further supporting the presence of a structural high that is bounded by known faults and lineaments.

Siliciclastic content ranges from 12-32%, with northwestern Portage County and Carroll County containing the highest values in the area (Figure 36). A noticeable NW-

SE siliciclastic poor trend is observed, spanning from southeastern Columbiana into Stark County and western Mahoning County and coinciding with an increase in carbonate content. While strongly correlated to clay content, siliciclastic values reach as high as 20% in the clay rich region. This supports the presence of a structural high composed of siliciclastic rich carbonates, and a significant decrease in clay deposition.

Pyrite content ranges from 1-5.5%, with a localized region of pyrite content present in northern Stark County and western Mahoning County (Figure 37). Immediately south of this area pyrite content drops rapidly, with values of 3% or less present, and a minimum of 1.5% located in western Columbiana County. Pyrite content appears heterogeneous, and does not correlate to a specific mineralogy or interpreted structural high or low.

TOC content is observed to range from 2-8%, exhibiting a similar pattern to the pyrite content distribution (Figure 38). A sweet spot is located in western Mahoning and northern Stark counties, with additional well data needed to determine the extent of the sweet spot. Directly south of the sweet spot TOC values drop considerably, with most wells reporting less than 5%. TOC is observed to be heterogeneous, with no clear correlation to a specific mineralogy or structural feature.

Porosity values range from 2-10%, with the highest values recorded in northern Portage County and western Mahoning County (Figure 39). The TOC sweet spot is observed to correlate with an area of increased porosity for the formation. However, high

porosity is shown to not be a determining factor for organic content alone, with multiple wells exhibiting high porosity but low TOC. Instead, porosity appears to correlate with an increase in clay and siliciclastic content within the interpreted depositional lows.

### Point Pleasant Formation Average Clay Map

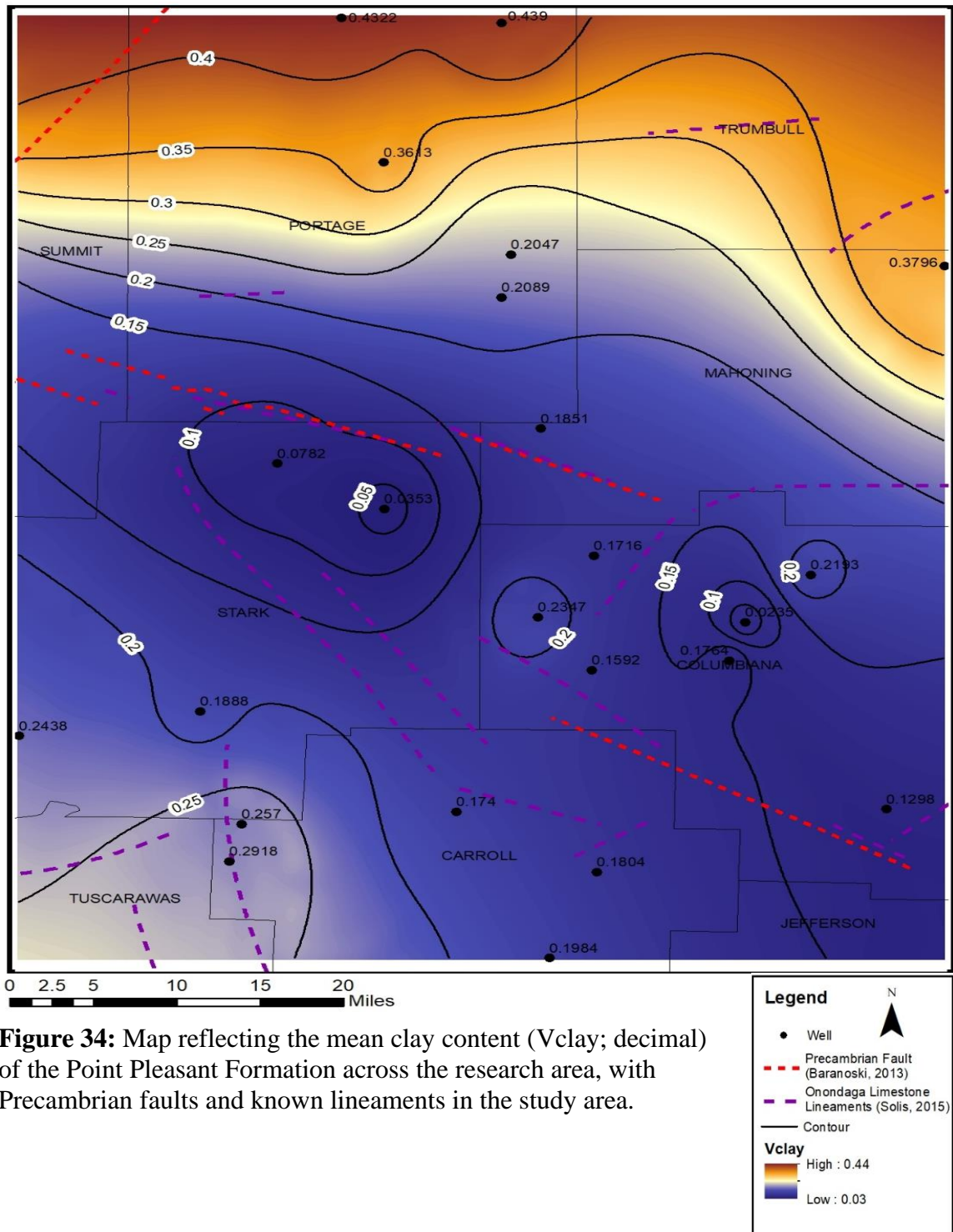


**Figure 34:** Map reflecting the mean clay content (Vclay; decimal) of the Point Pleasant Formation across the research area, with Precambrian faults and known lineaments in the study area.

### Point Pleasant Formation Average Carbonate Map

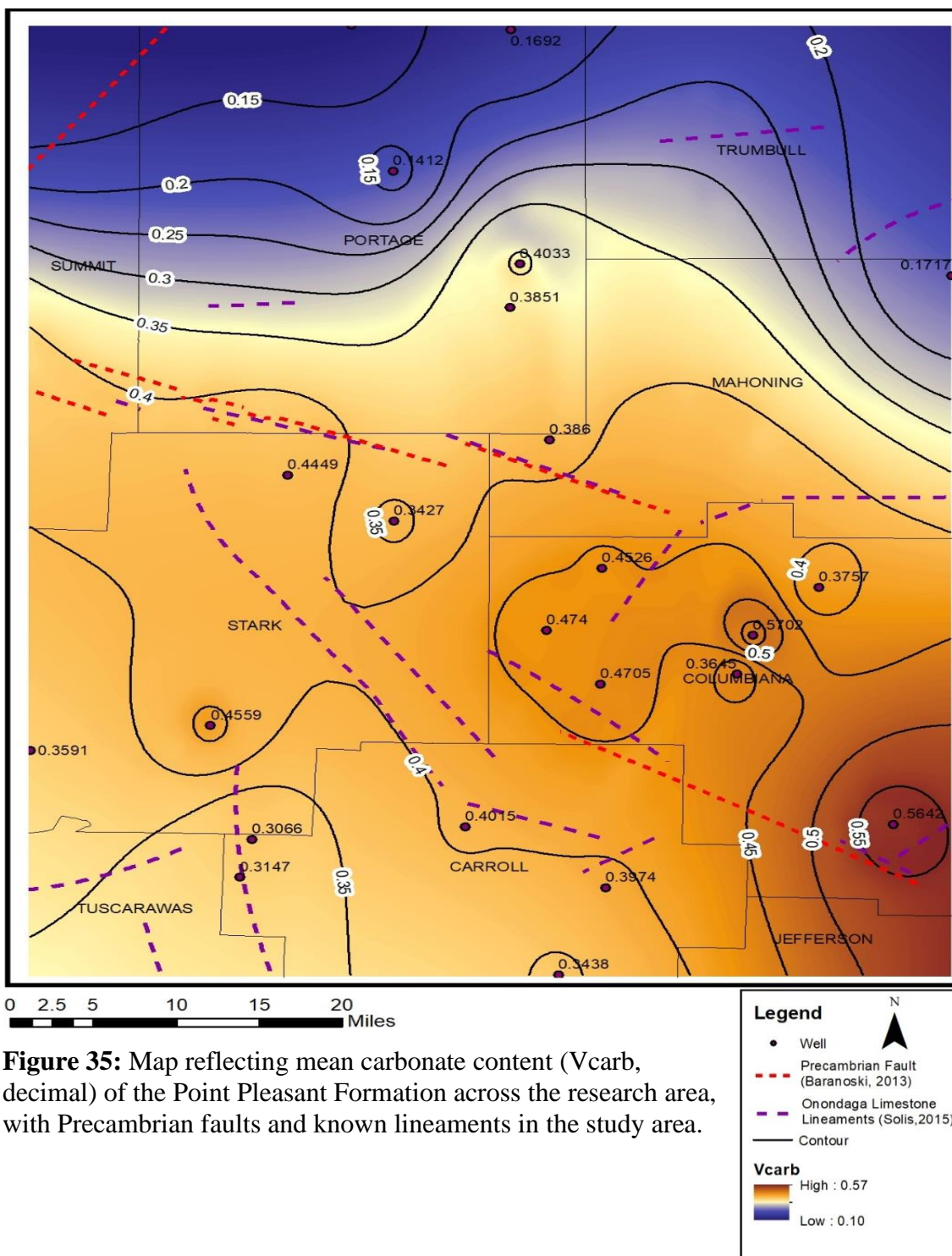
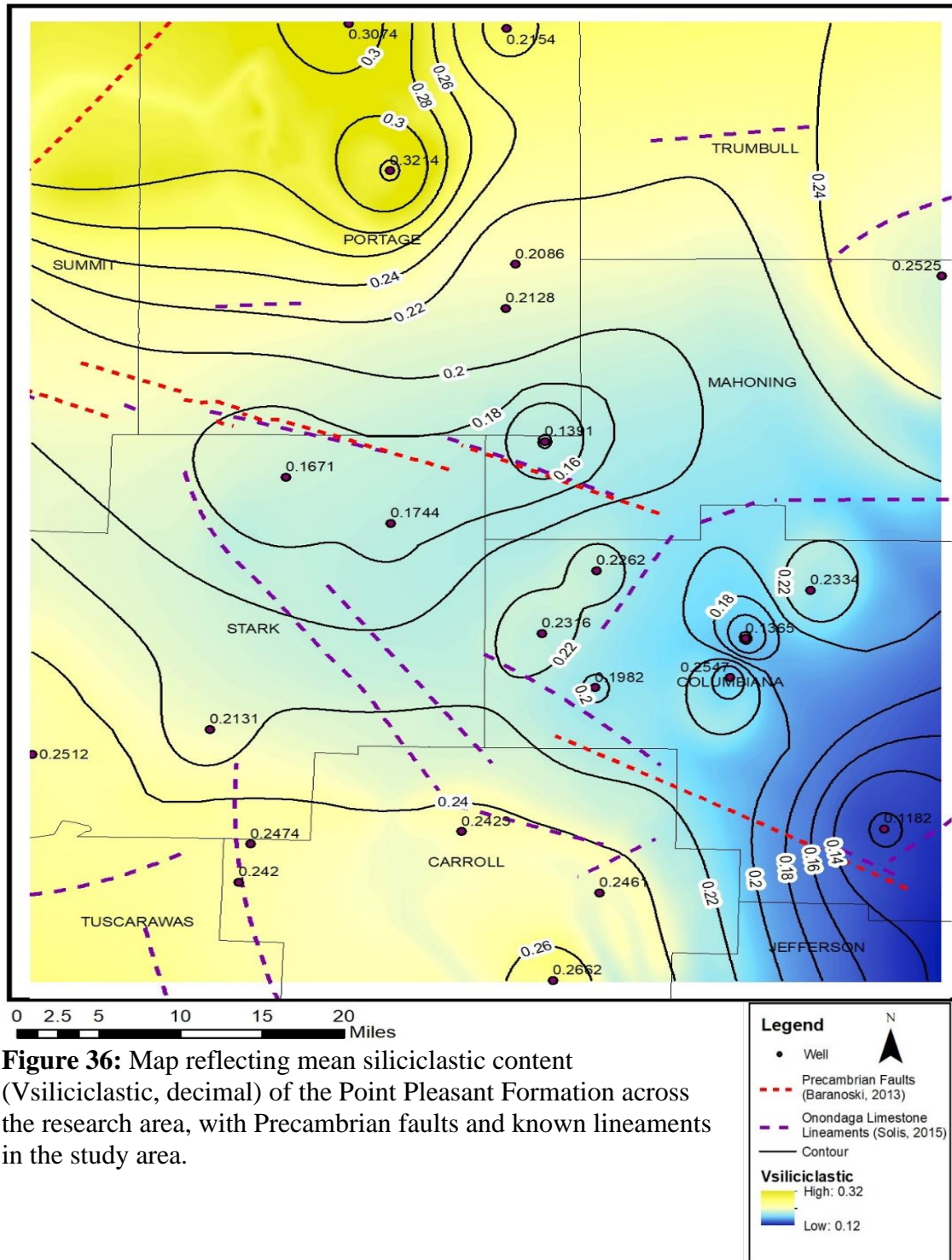


**Figure 35:** Map reflecting mean carbonate content (Vcarb, decimal) of the Point Pleasant Formation across the research area, with Precambrian faults and known lineaments in the study area.



### Point Pleasant Formation Average Siliciclastic Map



### Point Pleasant Formation Average Pyrite Map

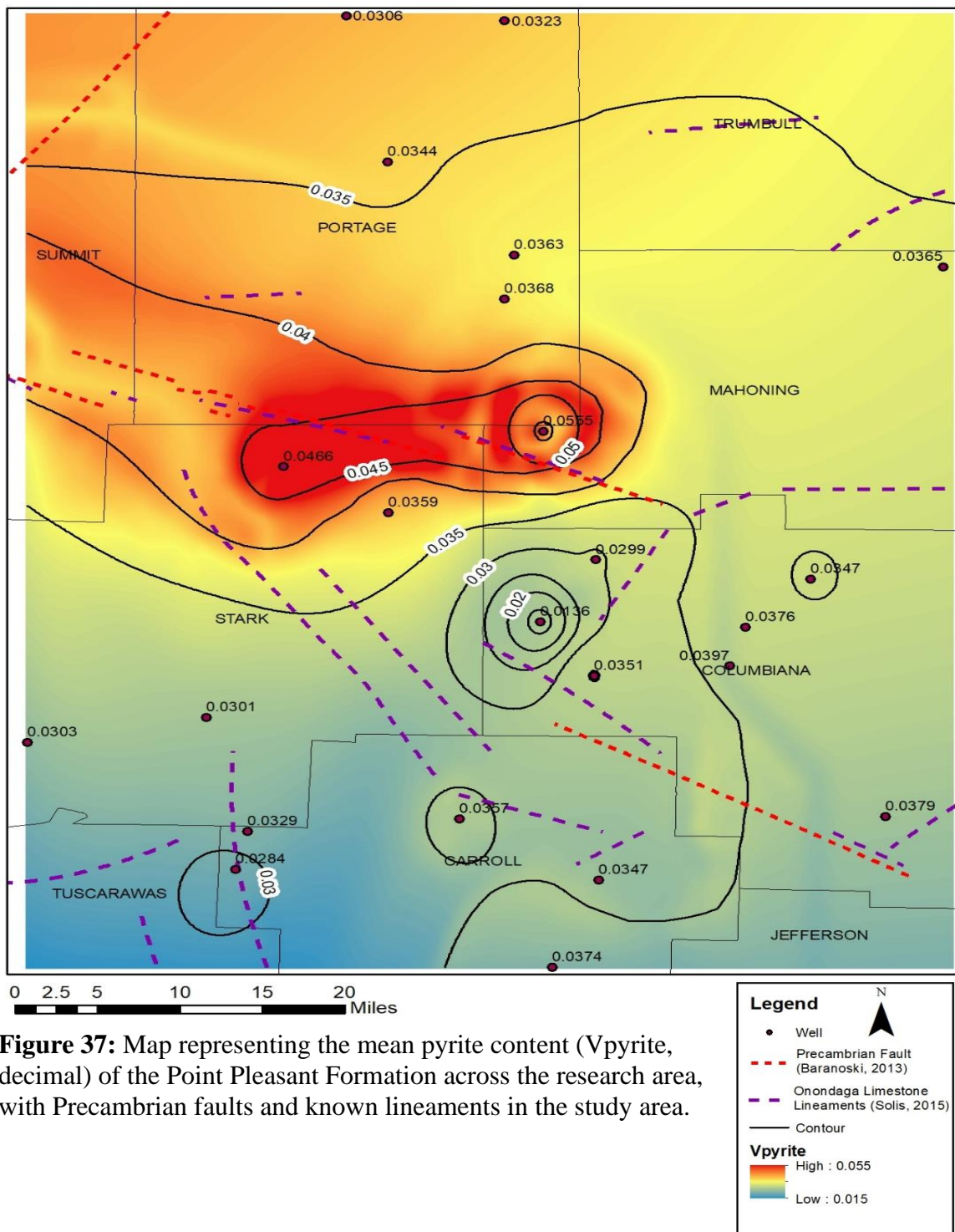


**Figure 37:** Map representing the mean pyrite content (Vpyrite, decimal) of the Point Pleasant Formation across the research area, with Precambrian faults and known lineaments in the study area.



**Point Pleasant Formation Average TOC (Wt%) Map**

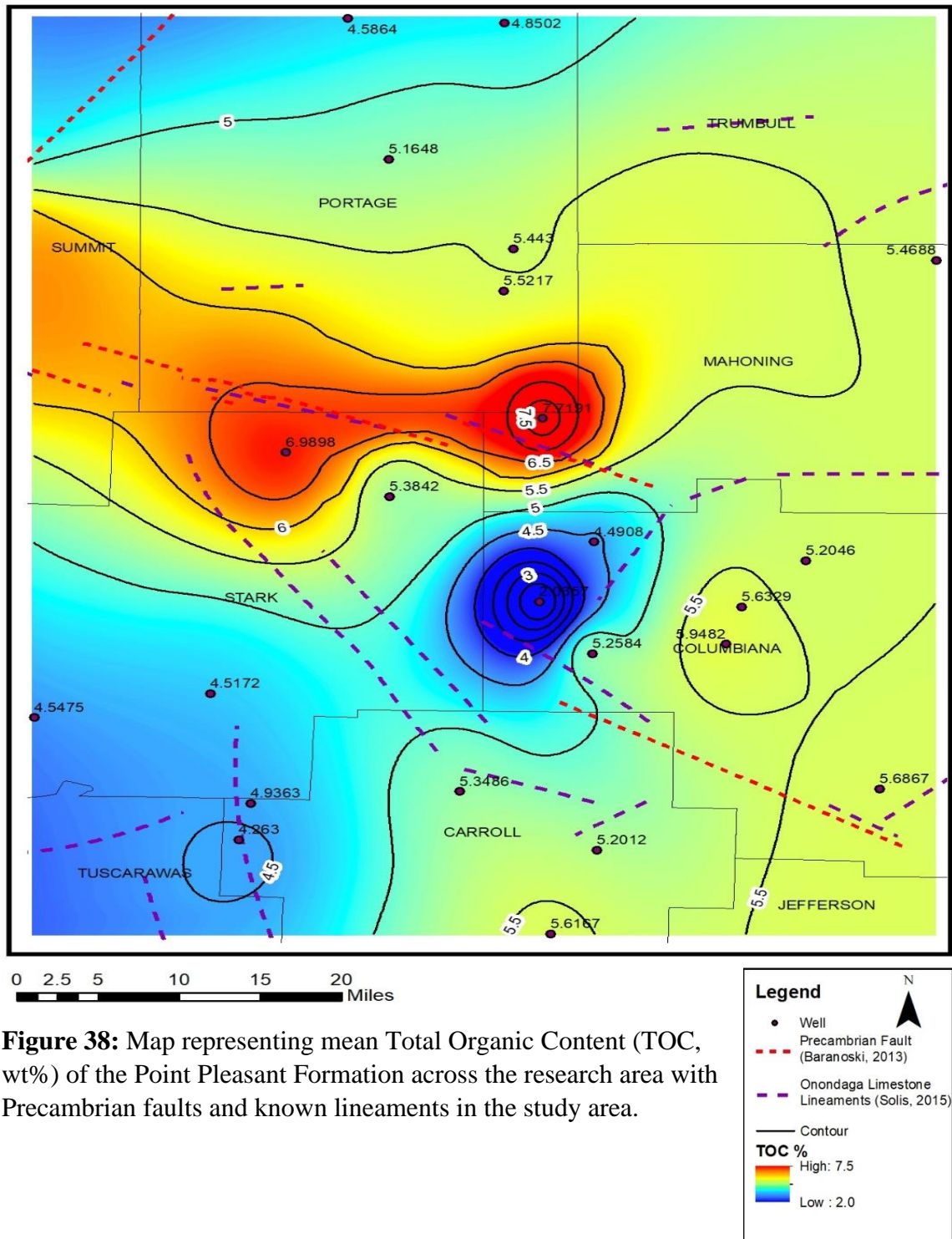


**Figure 38:** Map representing mean Total Organic Content (TOC, wt%) of the Point Pleasant Formation across the research area with Precambrian faults and known lineaments in the study area.

**Point Pleasant Formation Average Porosity Map**

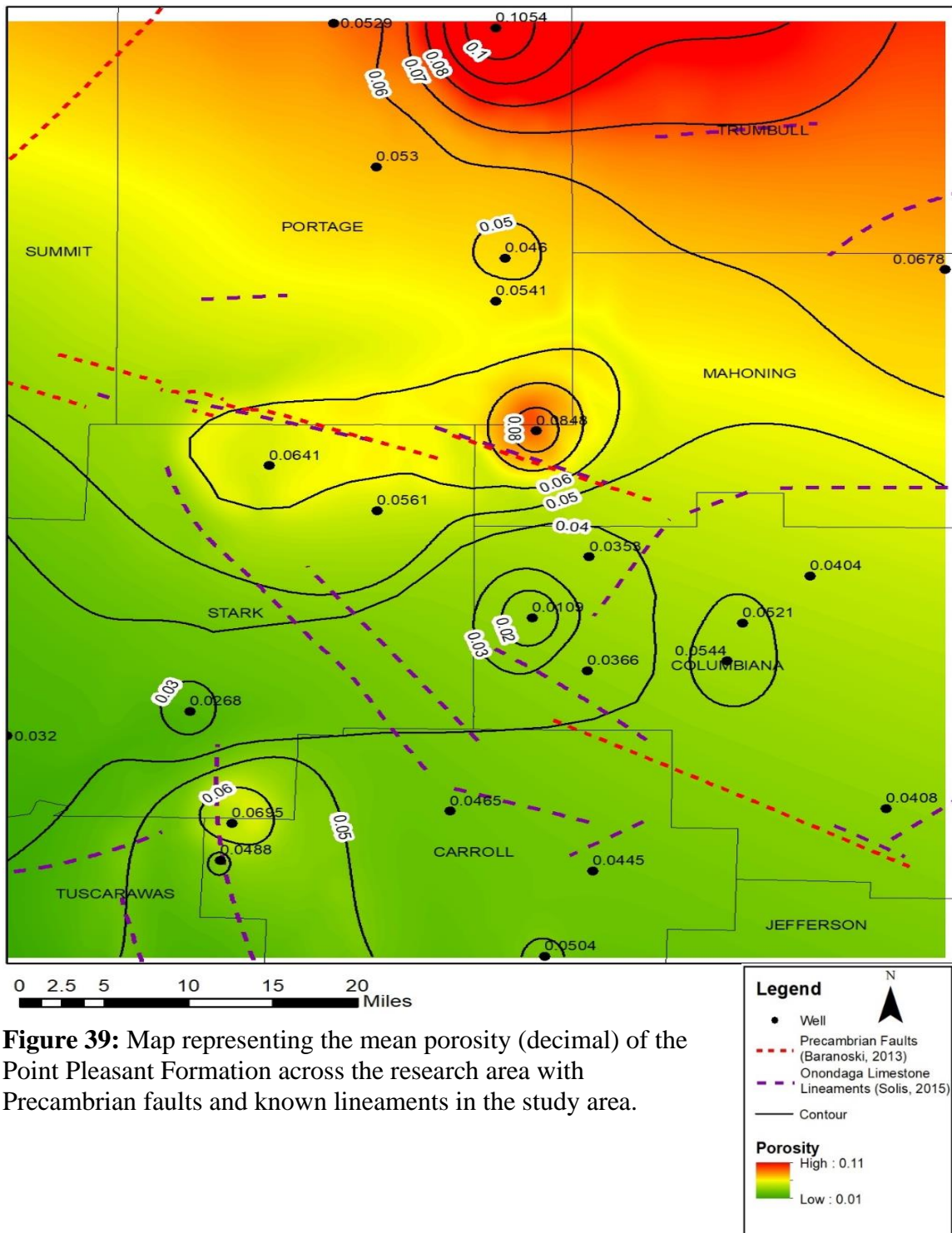


**Figure 39:** Map representing the mean porosity (decimal) of the Point Pleasant Formation across the research area with Precambrian faults and known lineaments in the study area.

### **6.2.5 Utica shale**

Clay content ranges from 33-56%, with clay rich zones located in northern Portage, western Carroll, and northeastern Mahoning counties (Figure 40). A clay-poor zone is located in the center of the research area, spanning from central Carroll to southern Portage, with values averaging less than 40%. Additional well data is needed to verify the extent of this zone, with Stark and eastern Columbiana lacking sufficient well data to verify the clay distribution. NW-SE oriented faults and lineaments are observed to cut through the interpreted clay-poor zone, but do not significantly affect clay content. A SW-NE oriented lineament is present in western Columbiana County and appears to correspond to a sharp change in clay content, with a 10% increase in clay content to the east of the lineament reported. Clay content appears to gradually increase to the north and southwest of this clay poor area, indicating this to be a possible bathymetric low. This region corresponds to the southern edge of the Sebree Trough.

Carbonate content ranges from 3-19%, with a carbonate-rich area located in northwestern Columbiana County and spanning to southeastern Portage County. Within this area, values exceed 15% and coincide with the clay-poor region (Figure 41). Surrounding this area, mean carbonate content decreases considerably, with values often less than 10% to the north and south of this area. Fault and lineaments appear to correlate with shifts in carbonate content. The carbonate-rich zone is adjacent to and bisected by several NW-SE faults and lineaments, with increased carbonate content observed. These

faults and lineaments appear to separate the carbonate-rich zone to the north from the carbonate-poor zone to the south.

Siliciclastic content ranges from 31-43%, with a general increasing siliciclastic content towards the southern portion of the research area (Figure 42). Siliciclastic content does not appear to correlate as strongly to clay content as it did in the underlying units indicating a possible shift in the depositional environment. Faults and lineaments are not interpreted to play a significant role in the siliciclastic distribution, instead following a strong north to south trend. This trend appears to deviate from the strong correlation to clay content in previous units, however, siliciclastic content is observed to typically be between 35-40% for the majority of wells, indicating there is little variance in siliciclastic content in the area.

Pyrite content ranges between 1-5%, with a pyrite-rich area located in central Carroll County that extends into central Columbiana County (Figure 43). Within this area, pyrite values often exceed 3% and reach in excess of 5% in central Carroll County. Adjacent to this in western Carroll County is a pyrite-poor region with values between 1-2% that continues into Portage County, where values increase slightly. This pyrite-rich region appears heterogeneous, with no apparent correlation to a specific mineralogy or structural feature.

TOC content ranges from 1.5-7.5%, with a sweet spot located in Carroll County and spanning into western Columbiana County (Figure 44). Values within this sweet spot

are consistently over 4% and reach a max of 7.5%. Western Carroll County exhibits a sharp drop in TOC, with values decreasing to less than 2%. The organic lows and highs appear heterogeneous and do not correlate to a specific mineralogy or observed structure. Instead, the organic rich areas reflect areas in which the water column was anoxic, allowing for the preservation of organic material and subsequent pyrite diagenesis.

Porosity ranges from 2-9%, with the highest values occurring in western Carroll and northeastern Mahoning counties (Figure 45). As well data is sparse in Mahoning, additional data is needed to verify the high porosity of the well present there. Porosity values appear to correlate to clay content, but not as strongly as it did in the underlying members of the Lexington Limestone. The NW-SE faults and lineaments appear to bisect the two high porosity zones. However, additional wells are needed to support the presence and extent of both porosity zones.



### Utica Shale Average Clay Map

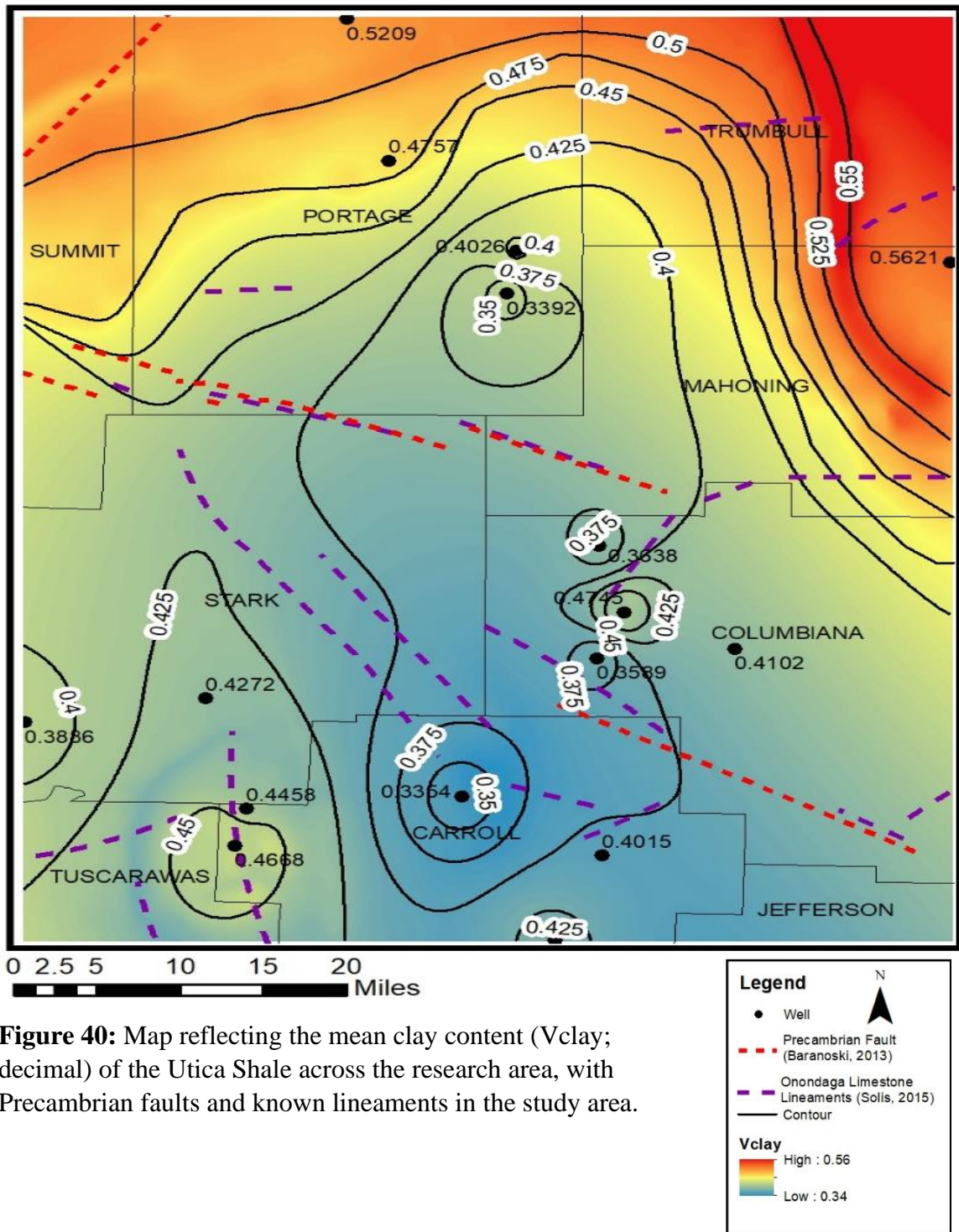


**Figure 40:** Map reflecting the mean clay content (Vclay; decimal) of the Utica Shale across the research area, with Precambrian faults and known lineaments in the study area.

Utica Shale Average Carbonate Map

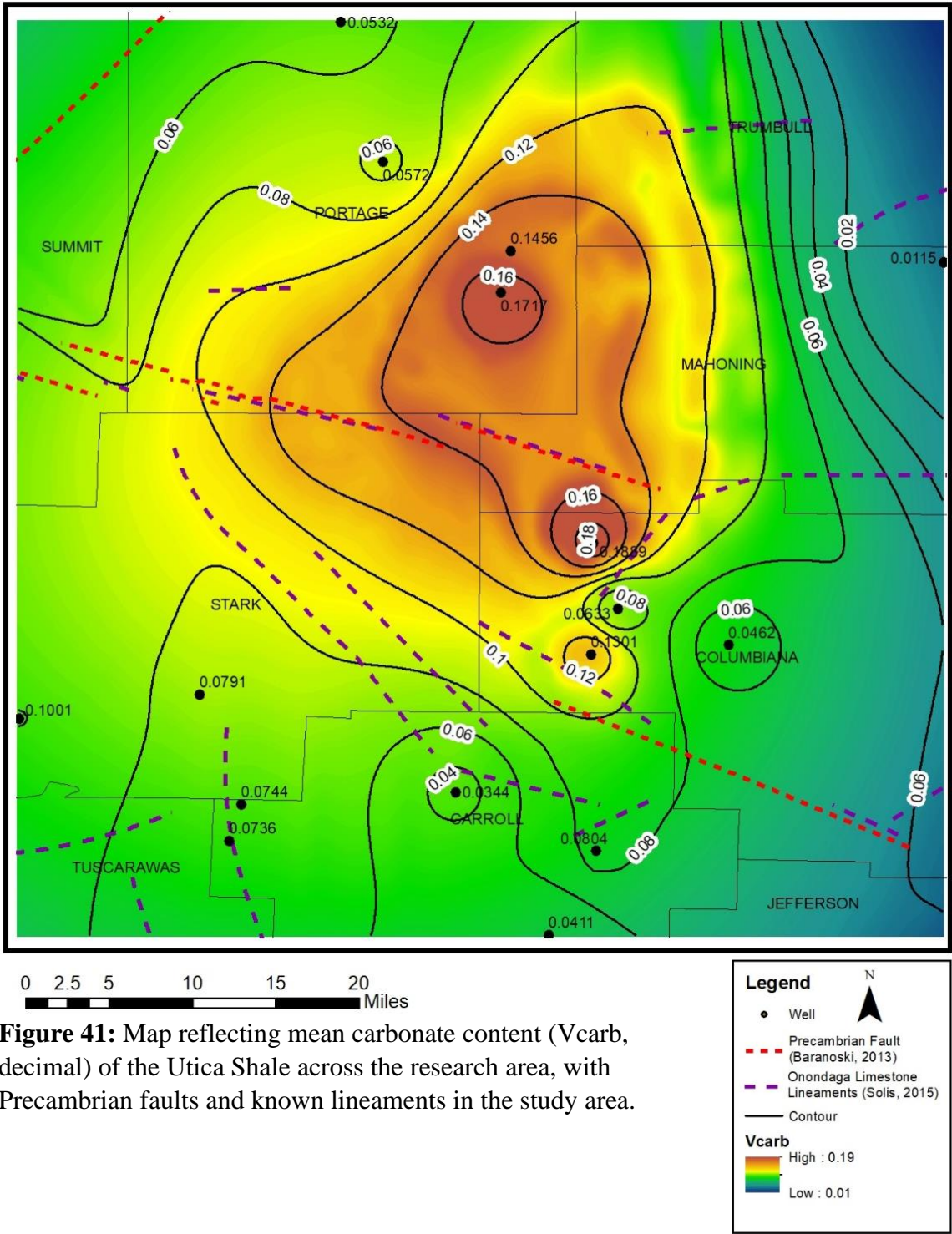


**Figure 41:** Map reflecting mean carbonate content (Vcarb, decimal) of the Utica Shale across the research area, with Precambrian faults and known lineaments in the study area.



### Utica Shale Average Siliciclastic Map

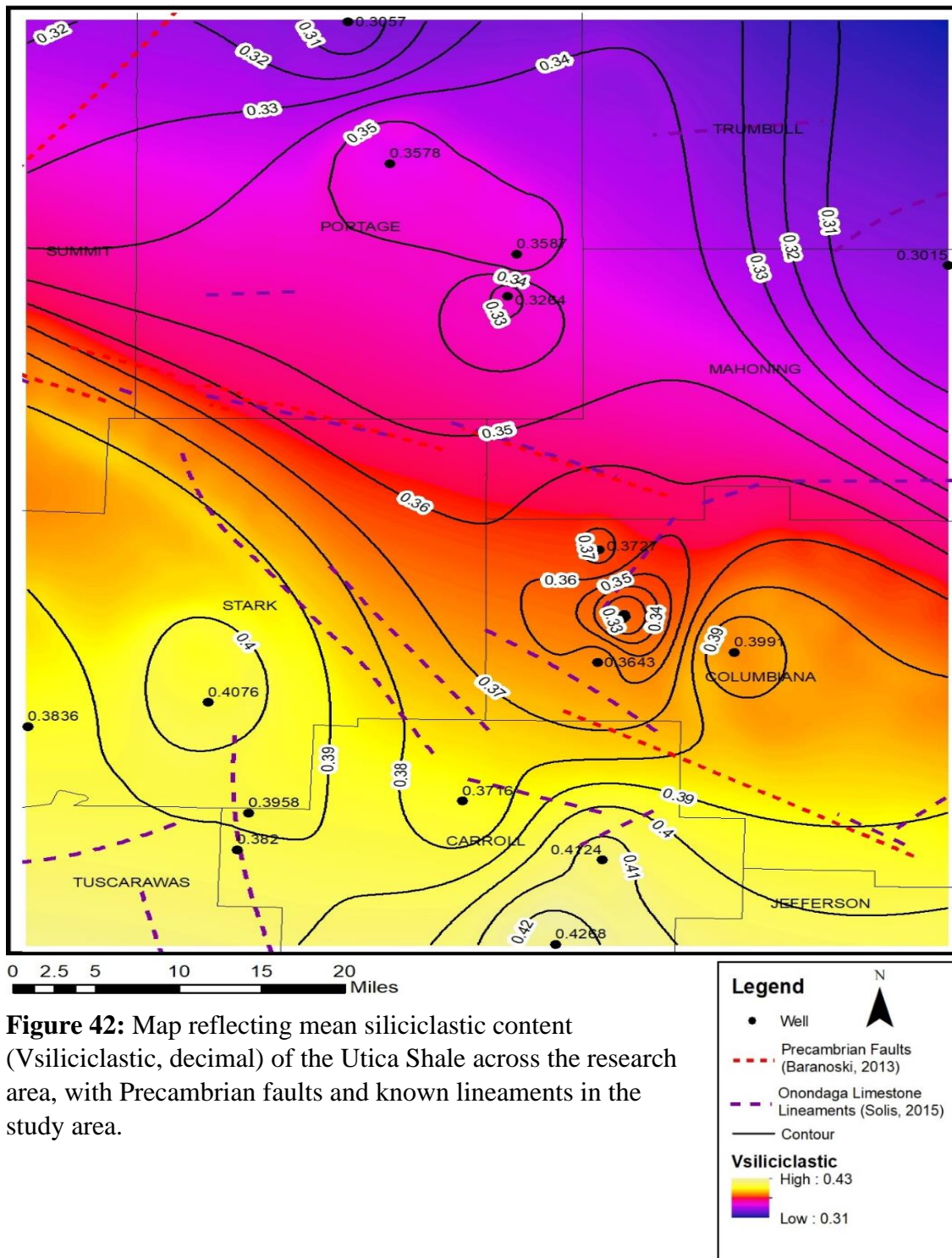


**Figure 42:** Map reflecting mean siliciclastic content (Vsiliciclastic, decimal) of the Utica Shale across the research area, with Precambrian faults and known lineaments in the study area.



### Utica Shale Average Pyrite Map

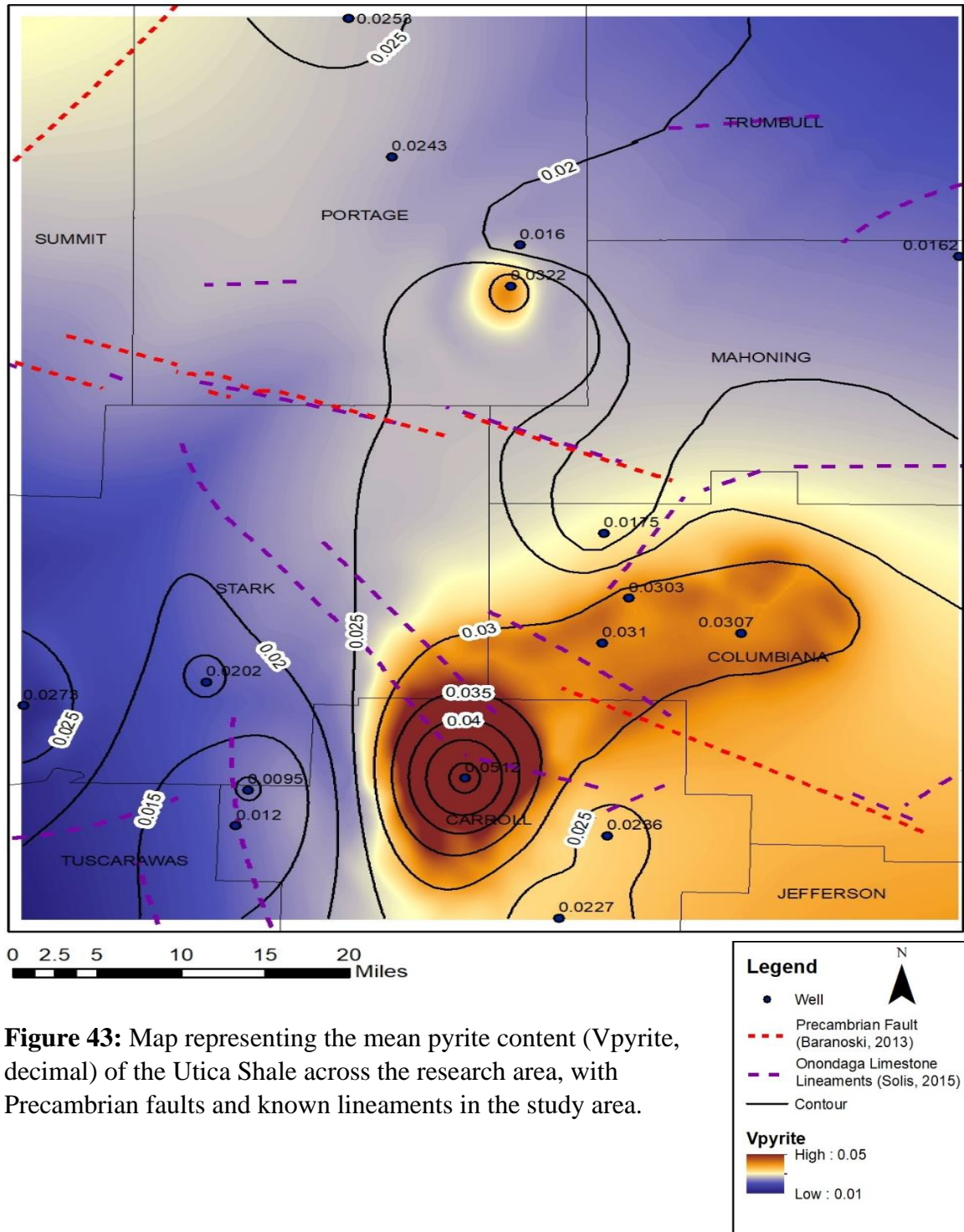


**Figure 43:** Map representing the mean pyrite content (Vpyrite, decimal) of the Utica Shale across the research area, with Precambrian faults and known lineaments in the study area.

### Utica Shale Average TOC (Wt%) Map

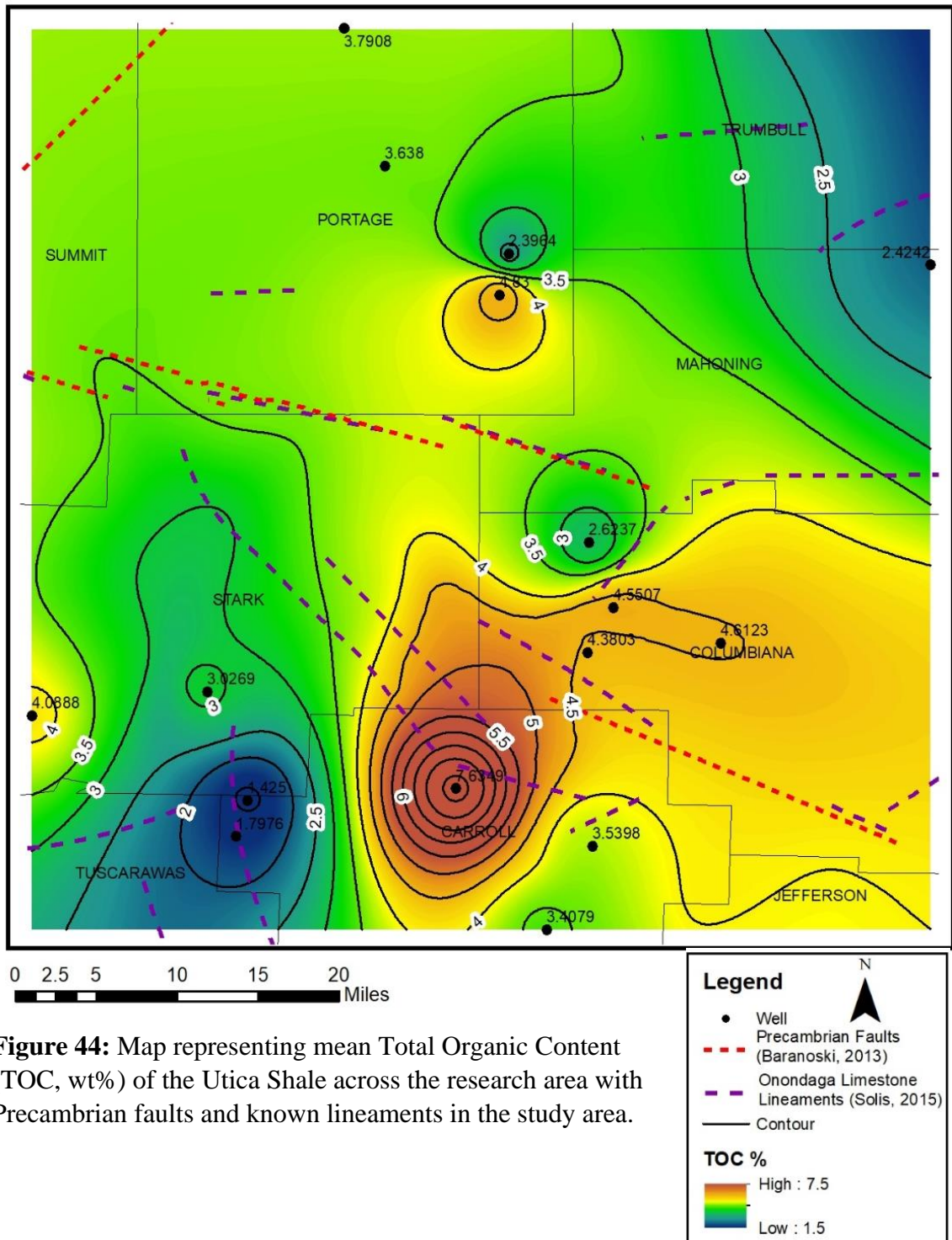
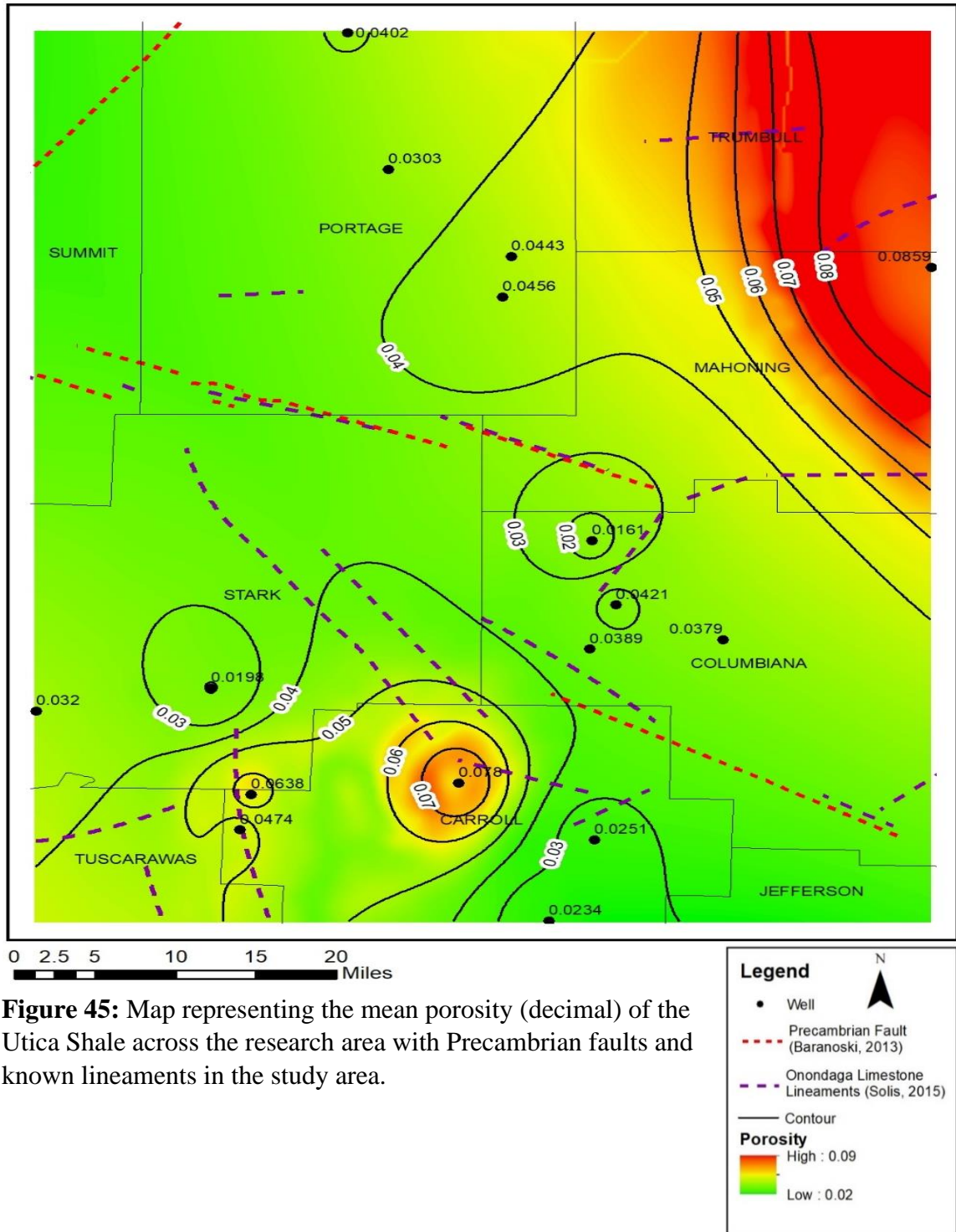


**Figure 44:** Map representing mean Total Organic Content (TOC, wt%) of the Utica Shale across the research area with Precambrian faults and known lineaments in the study area.

## Utica Shale Average Porosity Map



## **7 DISCUSSION**

### **7.1 Model Error**

Several sources of error exist within the model, with insufficient data available to calibrate every well. The result is the potential for the model to underestimate or exaggerate some mineral contents at these wells, with the interpreter deciding if the resultant model is usable based on log responses and curve statistics. Some wells in the research area exhibit regions of unusually high or low values with little to no XRD/pyrolysis data to verify these values. Therefore, these areas must be treated with caution when interpreting the maps. Additionally, well distribution in the research area remains problematic as some areas are sparse in wells, further complicating the ability to map mineralogy across the area.

Comparing the mineral model to XRD and pyrolysis data indicates that the mineral model used at the Tracker Well failed to accurately represent the dolomite content. This resulted in dolomite being consistently underestimated, and subsequently resulted in an increase in the siliciclastic and limestone percentages. This error is relatively small, with dolomite comprising less than 5% on average according to XRD data available in the research area (Patchen and Carter, 2015). However, this prevents not only an accurate representation of dolomite, but also skews the data into overestimating limestone and siliciclastics. While the unified carbonate model utilized for the multi-well

analysis reduces this error, XRD data still indicates a slight overestimation of siliciclastics. Further refinement of the mineral endpoints is required to reduce the margin of error for precise mapping and saturation modeling.

As the Tracker Well was the only well with ample XRD, pyrolysis, and tight rock analyses data, these data were used to construct all formulae from it alone rather than attempt regressions from a culmination of wells (ODNR, 2023). While this produced a model that most accurately reflected the Tracker Well mineralogy, applying this model to different wells may not have been as effective. XRD and pyrolysis data is not available for every well, and wells that do have it may not have as many points as desired. As a result, verifying model accuracy is not possible on every well. Additionally, regressions were not divided by geologic unit but instead performed on the entirety of the Lexington Limestone, Point Pleasant, and Utica shale present at the Tracker. This was an intentional decision based on similar clay mineralogy present throughout the play and the desire to simplify the model.

Tool error played a significant role in the research area, with some wells exhibiting anomalous data with unrealistic density values and NPHI in counts per second. Rescaling of these curves to match the statistics of a known reliable curve is possible, but in the process introduces error by not conveying the true log statistics at that well. Adjustment to the confidence of these rescaled curves and synthetic curves were

performed to better fit core data available. If XRD disagreed with the model, or curve statistics varied significantly, these wells were omitted from the mapping.

## **7.2 Lithology Variations and Far-Field Tectonics**

The research constructed a petrophysical model for the Utica shale play in the research area in an effort to better understand the connection between mineralogy, basin subsidence, far-field tectonics, eustatic sea level change, and distribution of organic content. Coupling mineralogy, TOC, and porosity with the known lineaments and faults, structural highs and lows can be delineated and their controls on mineralogy inferred.

Across the Appalachian Basin, faults and lineaments are numerous and generally follow a NW-SE orientation (Figure 16). These are interpreted to originate from the Precambrian basement and have been reactivated by far-field tectonic stresses over time (Bloxson et al., 2022). These faults and lineaments appear to correlate with changes in mineralogy in Ordovician strata and are interpreted to represent structural highs and lows. Structural highs would result in the deposition of carbonates with little siliciclastic content or thin shale intervals. Areas that are clay-rich are interpreted as structural lows and typically coincide with increasing siliciclastic content. These mineralogy changes appear relatively abrupt, and trend along known Precambrian faults (Baronoski, 2013) or lineaments (Solis, 2015) in the research area, indicating a potential sudden change in the depth of deposition. Furthermore, the influence of the faults and lineaments on the Upper Ordovician strata further supports the reactivation of basement structures during the

Taconian Orogeny, i.e., far-field tectonics (Bloxson et al., 2022). Structural features appear to highly influence the area depositional environment on a local scale, with eustasy affecting overall deposition throughout time in the basin.

During Lexington time, deposition of a shallow, cool-water carbonate platform began (Curdsville, Logana, and Upper Lexington). The region was tectonically active during this time, with presence of bentonite beds in the underlying Black River Formation and thin, discontinuous bentonite beds present at the base and throughout the Curdsville (Patchen and Carter, 2015). Fossil content is present throughout the formation, with the organic rich Upper Lexington containing abundant bryozoans, brachiopods, mollusks, and trilobites, with stromatoporoids and colonial corals present in zones at this time (Patchen and Carter, 2015). Mineral maps support that carbonate deposition was dominant during this time period across all members, with a general increasing clay content observed towards the contact with the Point Pleasant, indicative of increased water depth. Noticeable variations in mineralogy exist within the research area, with increased clay content being observed in some zones. These clay-rich segments appear to reach as high as 20% on average and correspond to a slight increase in siliciclastic content and sharp decrease in carbonate content. These zones are interpreted to be structural lows based on proximity to nearby faults and the abrupt change exhibited over the relatively small geographic area.



Porosity maps indicate that these clay-rich zones have relatively high porosity, reaching in excess of 5%. Carbonate-rich zones by contrast typically have a porosity of 1-3% and consistently reported low porosity values for all members of the Lexington Limestone. This suggests that within the research area, porosity is largely controlled by shale content and closely follows the structural features and bathymetric lows present in the area. The northern portion of the research area is consistently high in porosity and is representative of increased clay content in a paleobathymetric low known as the Sebree Trough (Kolata et al., 2001). During deposition of the Point Pleasant, the underlying carbonate platform was drowned with deepening of the basin and increased siliciclastic deposition (Ettensohn, 2010). Clay content gradually increased as carbonate deposition ceased. During this time, the Taconian Tectophase of the Taconian Orogeny was active, and the creation of a foreland basin and peripheral bulge developed in response to deformational loading on the continental margin (Ettensohn and Lierman, 2012). Over time, the bulge moved in response to deformational loading, resulting in rapid subsidence of the foreland basin, leading to shallow transgressing seas being replaced by deeper water deposits. It was at this time the shallow-water deposits of the Lexington were drowned, and the foreland basin became underfilled and sediment starved, with clays and silts becoming the predominant input representing the Point Pleasant Formation.

While large scale tectonic controls were responsible for the drowning of the carbonate platform and replacement with shales, localized far-field stresses were present and play a key role in the research area. Cratonward transmission of far-field stresses



resulted in a linear channel of deeper water, dark shales, known as the Sebree Trough. Development of the trough occurs in the midst of shallow-water carbonate shelves (Ettensohn and Lierman, 2012). The Sebree Trough is present in the northern edge of the mapping area and is represented on the map as a clay rich region with decreased carbonate content. The effects of the Sebree Trough are significant resulting in abrupt facies changes that dominate the mineralogy maps in the northern portion of the research area.

While the Sebree Trough dominates the northern portion of the research area, the southern portion contains numerous faults and lineaments representative of the reactivation of basement structures by far-field tectonics. These appear to have a stronger effect on mineralogy for the Point Pleasant than the underlying Lexington, with the presence of a carbonate-rich zone oriented NW-SE, bounded by faults with similar orientations. To the north and south of this zone, clay content increases abruptly, reaching in excess of 40%. The presence of the carbonate-rich zone gives support to a structural high bisecting the research area. Comparing this to the underlying Upper Lexington indicates the interpreted highs and lows for it continue into the deposition of the Point Pleasant. Porosity values continue to correlate to increased clay content, with values reaching as high as 10%. The stronger influence of faults and lineaments on the Point Pleasant Formation compared to the Lexington Limestone corresponds with the increased tectonic activity towards the east with the Taconian Tectophase in full effect.

During the deposition of the Utica shale, clay content continued to increase as carbonate deposition slowed. The carbonates within the Utica shale were mostly sourced from storm deposits known as tempestites (Potter, 2007). The increased carbonate content to the source suggests increased storm deposits and proximity to the carbonate sources south of the study area. The Utica appears to deviate from the previous formations, no longer corresponding as strongly to known faults or lineaments. Instead, clay and carbonate content are more heterogenous, with shifts in mineralogy present but not dominant. A prominent region of low clay content is present, spanning from northern Carroll to southern Portage counties, and containing a mean clay content of less than 40%. Carbonate content is observed to increase as high as 20% within this region, supporting an increase in storm activity and deposition of tempestites. Siliciclastic content is observed to consistently increase to the south, reaching as high as 30%, despite large shifts in clay and carbonate content throughout the research area.

Bloxson et al. (2022) through well log analysis indicates during Lexington time, the northern half of the research area to be dominated by carbonate deposition, with increasing clay content to the south (Figure 46A). Comparing the facies maps by Bloxson et al. (2022) to the findings here supports that the region is dominated by limestone. However, only the Curdsville member supports the increase of clay content to the south, with both the Logana and Upper Lexington clay maps indicating a slight increase in clay content to the northern part of the research area. This distinction may be due to dividing the Lexington into its respective members in this paper, whereas Bloxson et al. (2022)

performed well log analysis on the entire formation. This study did not create isopach maps for the research area. This complicates the analysis as it is not possible to relate the underlying thickness of the geologic units in this study with their effects on the deposition above it. Through conjoining the facies analysis with the isopach mapping, it would be possible to determine the relationship between structural high/lows, formation thickness, and the resulting deposition of carbonates and shales within the area. Without isopach maps, it is only possible to see how each member varies in mineralogy, but not how it relates to the underlying formation thickness and the effect it has on it.

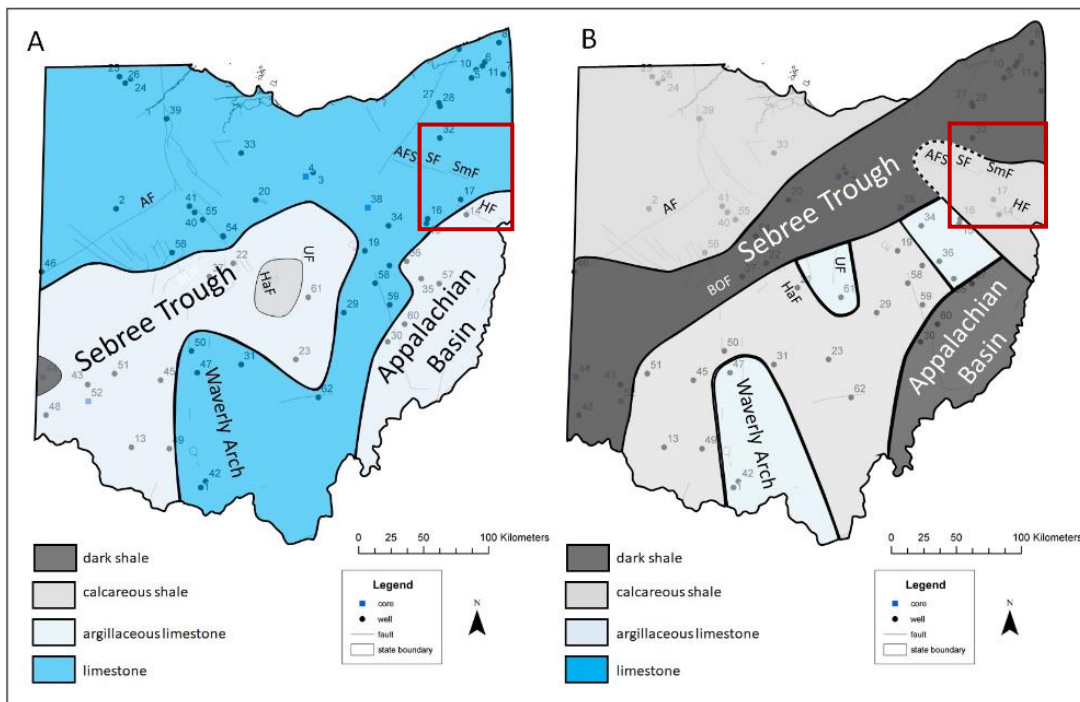


**Figure 46:** Generalized facies distribution across the state for the (A) the Lexington and Trenton limestones and (B) the Point Pleasant Formation and Utica shale as determined by the well log analysis. A red box has been added in eastern Ohio to represent the research area. Modified from Bloxson et al. (2022).

The well log analysis performed by Bloxson et al. (2022) for the Point Pleasant/Utica shale interval interprets the northern portion of the research area to be a dark shale, whereas south of the faults and lineaments it is interpreted to be a calcareous shale (Figure 46B). The mineralogy maps for the Point Pleasant from this research strongly support their findings, with mean clay content as high as 40% north of the faults. To the south, a rapid drop in clay content occurs, with carbonate content increasing as high as 57%. Clay and carbonate content maps for the Utica shale show similar patterns, with the northern portion of the research area being clay rich and supports the black shale facies assignment by Bloxson et al. (2022; Figure 46B). A notable distinction is that clay content appears to increase at the southern extent of the research area, leading to a decrease carbonate content. This shift is not directly visible on their map for the research area, although a shift into the dark shale facies assignment to the immediate south of the area is visible and would support the findings here.

TOC is observed to be both vertically and horizontally heterogeneous within the research area, occurring as discrete areas with little to no observable correlation with shale or carbonates. These shifts in TOC reflect the water anoxia present at the time of deposition. Intervals with high TOC are areas in which anoxic conditions were present and had the necessary organic material for TOC preservation. TOC poor areas indicate there may not have been ample life in the water column, or a lack of anoxic conditions to effectively preserve organic material. Pyrite content is observed to correlate with increased TOC and is representative of increased water anoxia in these areas. Given the

high density of pyrite, it is crucial to account for it within the model in order to accurately reflect the mineralogy. The heterogeneity in TOC and pyrite suggests localized sub-basins, bounded by faults or lineaments, allowed for increased preservation of organic matter in these areas. This further suggests the effects of far-field tectonics in Ohio, which is far from the center of tectonic loading in the Appalachian Mountains.

### **7.3 Eastern Ohio Fault Systems**

Within the northern portion of the research area, the Akron-Suffield-Smith Township fault system is present, running from Portage into Mahoning. Additionally, the Highlandtown fault system extends from northern Carroll to southern Columbiana. Previous studies in the research area have estimated the orientation, dip, and offset of the faults through formation structure maps and seismic mapping (Gray et al., 1982; Riley et al., 1993). These faults have previously been interpreted to be high-angle normal faults with the upthrown sides to the northeast (Baranoski, 2013; Gray et al., 1982). These systems have also undergone sinistral strike-slip movement, resulting in compression within the Stark-Columbiana region and correlate to an increase in lineaments observed (Figure 47; Solis, 2015; Waid, 2018).

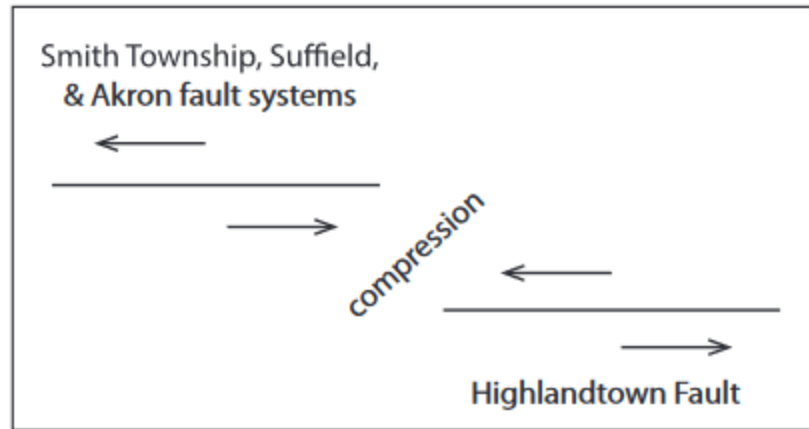


**Figure 47:** Diagram illustrating the contractional overstepping between the Akron-Suffield-Smith fault system and the Highlandtown fault system. From Waid, 2018.

While it is not possible to determine strike-slip faults from this facies analysis alone, this research is able to identify and describe the effects normal faults and lineaments have on Late Ordovician strata, and lineament up-thrown and down-thrown sides labeled accordingly (Figure 48). Facies maps indicate that northeastern Stark is remarked by a slight decrease in carbonate content and an increase in clay content within the Lexington Limestone members compared to the surrounding area, indicating a potential depositional low. Interestingly, the overlying Point Pleasant Formation maps indicate this region decreases in clay content, possibly as a result of increased carbonate deposition in the underlying Lexington decreasing water depth. This indicates this may only be a structural low during Lexington time, with insufficient well control to determine the effects into Utica time. Directly to the east of this region is an interpreted structural high in western Columbiana County. Across all geologic units analyzed here, this region is remarked by noticeably higher carbonate content and a decrease in clay

content as a result, indicating the offset is sufficient enough to dominate deposition during this time.

The Stark-Columbiana region is bounded by the Akron-Suffield-Smith Township fault system to the north, where it appears to form the contact with the interpreted continuation of the Sebree Trough. To the south, the Highlandtown fault system forms the southern boundary of the Columbiana structural high. Over time as strike-slip tectonic forces occurred between the two fault systems, the Stark-Columbiana region underwent contractional forces, resulting in localized uplift and a decrease in accommodation space in Columbiana. The Columbiana structural high not only affects Late Ordovician strata but is also present into Devonian time where it is remarked by thinner strata than the surrounding area based on isopach mapping (Waid, 2018).

### Fault and Lineament Interpretation Map for the Research Area

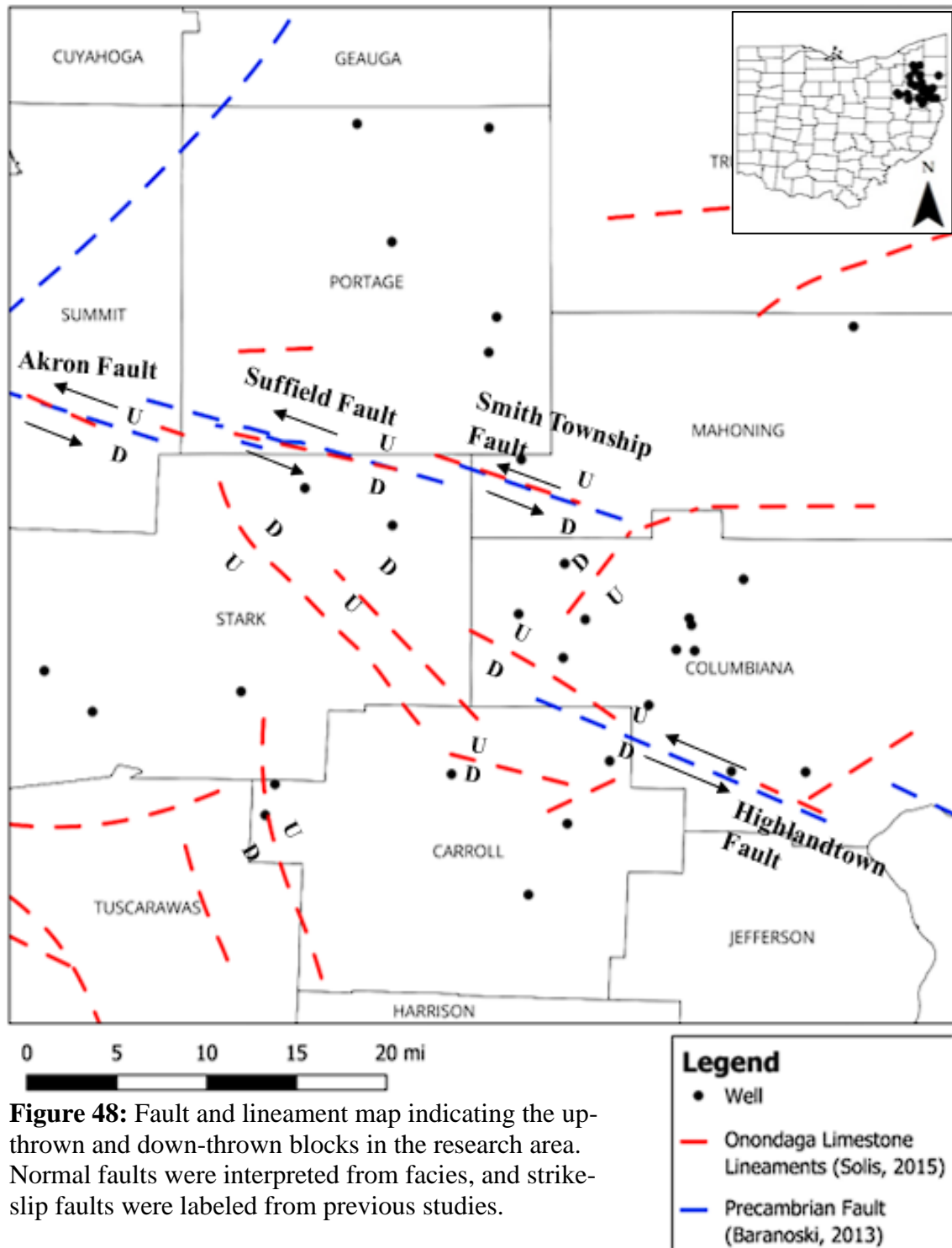


**Figure 48:** Fault and lineament map indicating the up-thrown and down-thrown blocks in the research area. Normal faults were interpreted from facies, and strike-slip faults were labeled from previous studies.



## **8 CONCLUSIONS**

While the petrophysical model is shown to correlate relatively well to XRD and pyrolysis data at the Tracker Well, the adaptation of this model to the surrounding area is presented with several difficulties. Public data within the area varies in quality, and subsequently affects model accuracy when applied to these wells.

Examining the Tracker data indicates the model largely succeeds in portraying the mineralogy, porosity, and saturation present at the well. The model illustrates how lithology and organic content change throughout the well and the implications it has on eustatic sea level change, subsidence, and water anoxia. Additionally, targets are delineated in the Upper Utica and portions of the Point Pleasant, with TOC and hydrocarbon saturation viewable alongside the lithology present. Dolomite proved difficult to model, possibly a result of changing siliciclastic composition in the shales that will need further refinement in future models.

The multi-well analysis proved less successful than the Tracker Well. Lack of resistivity data prevented saturation mapping across the area. Additionally, a unified carbonate model was utilized, which prevented detailed analysis of the carbonate mineralogy. Some wells exhibited values outside of the expected range and would require core data to verify and calibrate. TOC values appeared to be slightly higher than

expected, with further pyrolysis data needed to support the values observed. Without the presence of XRD and pyrolysis data, it is not possible to determine the extent of the error, although comparison of curve statistics to nearby wells proved useful in highlighting potential errors.

The multi-well analysis did prove useful in illustrating broad changes in mineralogy, specifically highlighting shale-rich vs carbonate-rich locations in the research area, and their relation to localized structures and the Sebree Trough. This supports the hypothesis that deposition occurred at different depths in the research area, producing the mineralogical changes observed. TOC appears to vary across all formations and does not appear to correlate to a specific mineralogy, suggesting that water depth does not play a significant role in the formation of organic-rich and organic-poor zones.

Through petrophysical analysis, this work was successful in identifying the effects of basin subsidence and eustatic sea level rise during Late Ordovician time, while also highlighting localized facies changes as a result of far field tectonics in the research area. Facies changes proved key in allowing for delineation of structural highs and lows throughout the area in conjunction with known faults and lineaments. The presence of the Sebree Trough within the northern portion of the research seems likely based on clay and carbonate content but will need extrapolation of the model on a regional scale to verify the extent of the trough into the area. The identification of organic rich portions of the

area provides insight into the anoxic conditions and how they vary locally. Additionally, these regions are of possible economic interest to the oil and gas industry, and when referenced with the clay maps can be used to assess the risk of clay swelling and fine migration for hydraulic fracturing operations. This model paves the way for further petrophysical analysis and mineral mapping for the Utica shale Play.

## **9. FUTURE WORK**

Future work includes expansion of the research area and further refinement of the model through additional wells with XRD, pyrolysis, and tight rock analysis data.

Formulae may be broken up by geologic units, further increasing model accuracy. An in-depth investigation should be performed to determine the effects the Sebree Trough has on facies and clay mineralogy within, adjacent, and outside of the trough at a regional and local scale. In depth analysis of clay mineralogy can be performed, separating the clay component into their respective minerals and mapping changes observed over the research area. Mineral volumes can be used to construct a brittleness index, allowing for relative brittleness estimation maps to be produced, assisting with hydraulic fracturing.

## 10. REFERENCES

- Baranoski, M.T., 2013, Structure contour map on the Precambrian unconformity surface in Ohio and related basement features (ver. 2.0): Columbus, Ohio, Ohio Department of Natural Resources, Division of Geological Survey Map PG-23, scale 1: 500,000, 17 p., [https://ohiodnr.gov/static/documents/geology/MapPG23\\_Baranoski\\_2013\\_text.pdf](https://ohiodnr.gov/static/documents/geology/MapPG23_Baranoski_2013_text.pdf) (accessed July 2023).
- Berry, W.B.N, Quinby-Hunt, M. S., and Wilde, P., 1995, Impact of Late Ordovician Glaciation-Deglaciation on marine life, *in* Effects of Past Global Change on Life: Studies in Geophysics: Washington, D.C., National Academies Press, p. 34–46, <https://www.ncbi.nlm.nih.gov/books/NBK231946/> (accessed July 2023).
- Bloxson, J.M., Saylor, B.Z., and Ettensohn, F.R., 2022, Subsurface relationships between the sebree trough and carbonate-siliciclastic mixing in the upper ordovician lexington-trenton and Point Pleasant-Utica Intervals in Ohio, USA, using multivariate statistical well log analysis: The Ohio Journal of Science, v. 122, p. 52–74, <https://doi.org/10.18061/ojs.v122i2.8669>.
- Cornell, S.R., 2008, The last stand of the great American carbonate bank: Tectonic activation of the upper Ordovician passive margin in eastern North America

- [Ph.D. thesis]: University of Cincinnati, Cincinnati, Ohio, 854 p.,  
[https://etd.ohiolink.edu/apexprod/rws\\_olink/r/1501/10?clear=10&p10\\_accession\\_num=ucin1226880226](https://etd.ohiolink.edu/apexprod/rws_olink/r/1501/10?clear=10&p10_accession_num=ucin1226880226) (accessed July 2023)
- Duverger, A., Berg, J.S., Busigny, V., Guyot, F., Bernard, S., and Miot, J., 2020, Mechanisms of pyrite formation promoted by sulfate-reducing bacteria in pure culture: *Frontiers in Earth Science*, v. 8,  
<https://doi.org/10.3389/feart.2020.588310>.
- Emmons, E., 1842, *Geology of New York; Part II, Survey of the second geological district*: New York State Museum, 437 p.
- Ettensohn, F., 2008, The Appalachian Foreland Basin in Eastern United States *in* Miall, A. ed., *Sedimentary Basins of the World, Volume 5: The Sedimentary Basin of the United States and Canada*, p. 105-179, [https://doi.org/10.1016/S1874-5997\(08\)00004-X](https://doi.org/10.1016/S1874-5997(08)00004-X).
- Ettensohn, F.R., 2010, Origin of late ordovician (mid-mohawkian) temperate-water conditions on southeastern Laurentia: Glacial or tectonic? *The Ordovician Earth System: Geological Society of America Special Paper 466*, p. 163-175,  
[https://doi.org/10.1130/2010.2466\(11\)](https://doi.org/10.1130/2010.2466(11)).
- Ettensohn, F.R., Hohman, J.C., Kulp, M.A., Rast, N., 2002, Evidence and implications of possible far-field responses to Taconian Orogeny: middle-late Ordovician

Lexington Platform and Sebree Trough, east-central United States. *Southeastern Geology*. 41(1): p. 1-36,  
[https://www.researchgate.net/publication/288396497\\_Evidence\\_and\\_implications\\_of\\_possible\\_far-field\\_responses\\_to\\_Taconian\\_Orogeny\\_Middle-late\\_ordovician\\_Lexington\\_platform\\_and\\_sebree\\_trough\\_East-Central\\_United\\_States](https://www.researchgate.net/publication/288396497_Evidence_and_implications_of_possible_far-field_responses_to_Taconian_Orogeny_Middle-late_ordovician_Lexington_platform_and_sebree_trough_East-Central_United_States) (accessed July 2023).

Ettensohn, F.R., and Lierman, R.T., 2012, Large-scale tectonic controls on the origin of Paleozoic dark-shale source-rock basins: Examples from the Appalachian Foreland Basin, Eastern United States, in Gao, D., ed., *Tectonics and sedimentation: Implications for petroleum systems*: AAPG Memoir 100, p. 95-124, <https://doi.org/10.1306/13351549M1003529>

Geoactive, Subsurface interpretation software: Interactive Petrophysics,  
<https://www.geoactive.com/> (accessed July 2023).

Gray, J.D., Struble, R.A., Carlton, R.W., Hodges, D.A., Honeycutt, F.M., Kingsbury, R.H., Knapp, N.F., Majchszak, F.L., and Stith, D.A., 1982, An integrated study of the Devonian-age black shales in eastern Ohio: Ohio Department of Natural Resources, Division of Geological Survey, U.S. Department of Energy Report No. DOE/ET 12131-1399, 169 p., 25 maps and cross sections,  
<https://www.osti.gov/biblio/5841004> (accessed July 2023).

- Halliburton, 2009, Halliburton's GEM Tool, <https://ir.halliburton.com/news-releases/news-release-details/halliburtons-gemtm-tool-offers-clearer-picture> (accessed April 2023).
- Kemeh, B., 2021, Geochemical characterization of the Utica Shale Play using XRF-based chemostratigraphy in Ohio [M.Sc. thesis]: Stephen F. Austin State University, Nacogdoches, TX, 125 p., <https://scholarworks.sfasu.edu/cgi/viewcontent.cgi?article=1396&context=etds> (accessed July 2023).
- Kirchner, B. and Brett, C., 2008, Subsurface correlation and paleogeography of a mixed siliciclastic-carbonate unit using distinctive faunal horizons: Toward a new methodology: *Palaaios*, v. 23, p. 174-184, doi: 10.2110/palo.2006.p06-072r.
- Kolata, D.R., Huff, W.D., and Bergstrom, S.M., 2001, The Ordovician Sebree Trough: An oceanic passage to the midcontinent United States: *Geology Society of America Bulletin*, v. 113, no. 8, p. 1067-1078, [https://doi.org/10.1130/0016-7606\(2001\)113<1067:TOSTAO>2.0.CO;2](https://doi.org/10.1130/0016-7606(2001)113<1067:TOSTAO>2.0.CO;2).
- McDowell, R.C., ed., 1986, The Geology of Kentucky-A text to accompany the geologic map of Kentucky: Washington, U.S. Geological Survey Professional Paper 1151-H, 76 p., <https://pubs.er.usgs.gov/publication/pp1151H> (accessed July 2023).



Ohio Department of Natural Resources, 2023, Tracker Well ( API:34133244490000): Oil & Gas Well Viewer, <https://gis.ohiodnr.gov/mapviewer/?config=oilgaswells> (accessed July 2023).

Passey, Q.R., Creaney, S., Kulla, J.B., Moretti, F. J., and Strouds, J. D., 1990, A practical model for organic richness from porosity and resistivity logs: AAPG Bulletin, v. 74, p. 1777–1794, doi: 10.1306/0c9b25c9-1710-11d7-8645000102c1865d.

Patchen, D.G., Hickman, J.B., Harris, D.C., Drahovzal, J.A., Lake, P.D., Smith, L.B., Nyahay, Richard, Schulze, Rose, Riley, R.A., Baranoski, M.T., Wickstrom, L.H., Laughrey, C.D., Kostelnik, Jaime, Harper, J.A., Avary, K.L., Bocan, John, Hohn, M.E., and McDowell, Ronald, 2006, A geologic play book for Trenton-Black River Appalachian Basin exploration: Morgantown, W. Va., U.S. Department of Energy Report, DOE Award Number DE-FC26-03NT41856, [http://www.wvgs.wvnet.edu/www/tbr/project\\_reports.asp](http://www.wvgs.wvnet.edu/www/tbr/project_reports.asp) (accessed July 2023).

Patchen, D. G. and Carter, K.M., eds., 2015, A geologic play book for Utica shale Appalachian basin exploration, Final report of the Utica shale Appalachian basin exploration consortium, 187 p, <http://www.wvgs.wvnet.edu/utica> (accessed July 2023).

Popova, O., 2017, Utica shale Play: Geology Review, p. 1–18, [https://www.eia.gov/maps/pdf/UticaShalePlayReport\\_April2017.pdf](https://www.eia.gov/maps/pdf/UticaShalePlayReport_April2017.pdf) (accessed July 2023).

- Potter, P.E., 2007, Exploring the geology of the Cincinnati/northern Kentucky region: Second revised edition, Kentucky Geological Survey Special Publication 8, Series XII, 128 p., [https://kgs.uky.edu/kgsweb/olops/pub/kgs/sp8\\_12.pdf](https://kgs.uky.edu/kgsweb/olops/pub/kgs/sp8_12.pdf) (accessed July 2023).
- Riley, R.A., Harper, J.A., Baranoski, M.T., Laughrey, C.D., and Carlton, R.W., 1993, Measuring and predicting reservoir heterogeneity in complex deposystems—The Late Cambrian Rose Run sandstone of eastern Ohio and western Pennsylvania: Morgantown, W. Va., National Research Center for Coal and Energy, Appalachian Oil and Natural Gas Research Consortium report for the U.S. Department of Energy, Contract No. DE-AC22-90BC14657, 257 p., <https://kb.osu.edu/handle/1811/88564> (accessed July 2023).
- Ryder, R.T., and Ruppert, L. F., 2008, Assessment of Appalachian basin oil and gas resources: Utica-Lower Paleozoic Total Petroleum System: U.S. Geological Survey Open-File Report 2008–1287, 29 p., <https://pubs.usgs.gov/of/2008/1287> (accessed July 2023).
- Schmoker, J.W., and Hester, T.C., 1983, Organic Carbon in bakken formation, United States portion of Williston Basin: AAPG Bulletin, v. 67, p. 2165–2174, doi: 10.1306/ad460931-16f7-11d7-8645000102c1865d.
- Scotese, C. R., 2003, Paleogeographic Map archive, PALEOMAP project, Arlington,

Department of Geology, University of Texas at Arlington,

<http://www.scotese.com/> (accessed July 2023).

Shaw, D.B., and Weaver, C.E., 1965, The mineralogical composition of shales: SEPM Journal of Sedimentary Research, v. Vol. 35, doi: 10.1306/74d71221-2b21-11d7-8648000102c1865d.

Smith, L.B., 2013, Shallow transgressive onlap model for Ordovician and Devonian organic-rich shales, New York State, in SPE/AAPG/SEG Unconventional Resources Technology Conference, Denver, CO, p. URTEC-1581184, <https://onepetro.org/URTECONF/proceedings-abstract/13URTC/All-13URTC/URTEC-1581184-MS/148967> (accessed July 2023).

Sohrabi, A., and Jin, J., 2013, Global palaeobiogeography of brachiopod faunas during the early Katian (Late Ordovician) greenhouse episode: Palaeogeography, Palaeoclimatology, Palaeoecology, v. 389, p. 78–86, <https://doi.org/10.1016/j.palaeo.2013.02.027>

Solis, M.P., 2016, Sinistral transpression along previously existing faults: Appalachian Basin: Ohio [abs.]: Eastern Section American Association of Petroleum Geologist, Lexington, KY, September, 2016, p. 57-58, <https://www.searchanddiscovery.com/abstracts/html/2016/90258es/abstracts/3.50.html> (accessed July 2023).

Tao, Z., Bielicki, J.M., and Clarens, A.F., 2014, Physicochemical factors impacting CO<sub>2</sub> sequestration in depleted shale formations: The case of the Utica shale: Energy Procedia, <https://www.sciencedirect.com/science/article/pii/S1876610214023601> (accessed July 2023).

United States Geological Survey, 2023, National Geologic Map Database, <https://ngmdb.usgs.gov/Geolex/search> (accessed August 2023).

U.S. Energy Information Administration - EIA - Independent Statistics and Analysis: Where our natural gas comes from: U.S. Energy Information Administration (EIA), <https://www.eia.gov/energyexplained/natural-gas/where-our-natural-gas-comes-from.php> (accessed July 2023).

Utica shale Appalachian Basin Exploration Consortium, 2015, Coordinated by the Appalachian Oil & Natural Gas Consortium at West Virginia University, [http://www.wvgs.wvnet.edu/utica/playbook/pb\\_data.aspx](http://www.wvgs.wvnet.edu/utica/playbook/pb_data.aspx) (accessed July 2023).

Waid, C.B., 2018, High-resolution stratigraphy and subsurface mapping of the lower part of the Huron Member of the Ohio Shale in central and eastern Ohio allow for detailed snapshots of basin development: Division of Geological Survey: Geological Note, v. 13, 16 p., <https://www.searchanddiscovery.com/abstracts/html/2018/pittsburgh-90335/abstracts/2018.ES.09.html> (accessed July 2023).

## 11. APPENDIX A

**Table 6:** Data table denoting well names, API, location, and wireline data present at each well.

Well Name	API	Long.	Lat.	GR	RHOB	NPHI	PEF	Resistivity	GEM
<b>(1) Tracker Well</b>	34133244490 000	-81.06	41.13	X	X	X	X	X	X
<b>(2) SASEY STEVEN #1</b>	34133206100 000	- 81.207393 25	41.3296007 5	X	X	X			
<b>(3) VASBINDER K UNIT #1</b>	34133208670 000	81.283183 19	41.0967766 1					X	
<b>(4) TROUG W R #2</b>	34133238880 000	- 81.170711 39	41.2076655 6	X	X	X	X		
<b>(5) WANTZ R UNIT #1</b>	34133240270 000	- 81.068007 78	41.3253718 6	X	X	X	X		
<b>(6) SANDERS UNIT #2</b>	34133241710 000	- 81.068325 25	41.0935359 2	X	X	X	X		
<b>(101) CLARK ET AL UNIT #1</b>	34019202860 000	- 81.107641 08	40.6577237 2	X	X				
<b>(102) MCALLISTER, JOHN O. #1</b>	34019205530 000	- 80.985317 81	40.6065404 2	X	X				
<b>(103) BRYAN UNIT</b>	34019218500 000	- 80.940593 92	40.6713017 2	X	X	X	X		
<b>(104) HICKORY CLAY #12</b>	34019219200 000	- 81.304482 61	40.6153860 8	X	X	X	X	X	
<b>(105) Lee Unit #1-DK SWIW</b>	34019220450 000	- 81.294199 14	40.6472946 7	X	X	X	X	X	

(Continued)

**Table 6:** Data table denoting well names, API, location, and wireline data present at each well.

Well Name	API	Long.	Lat.	GR	RHOB	NPHI	PEF	Resistivity	GEM
<b>(106) WHITE UNIT #1</b>	3401922059000	- 81.02648306	40.53315733	X	X		X	X	
<b>(201) BURROWS COMM.#1-2419</b>	3402920559000	- 80.89936389	40.72900894	X	X				
<b>(202) ELDEN E # DENNY#1</b>	3402920592000	- 80.988109	40.875262	X	X	X			
<b>(203) DONALD SELL UNIT#1</b>	3402920607000	- 80.85083597	40.78516119	X	X	X	X	X	
<b>(204) E.F # SANOR #1</b>	3402920620000	- 80.96642181	40.81756297	X	X	X			
<b>(205) Murgala Mike &amp; Mary</b>	3402920631000	- 80.85418019	40.81175386	X		X			
<b>(206) MURRAY, F</b>	3402920648000	- 80.87024414	40.78623389	X	X	X		X	
<b>(207) HAWKINS C&amp;M UNIT #1</b>	3402920656000	- 80.85653517	40.81878825	X	X	X			
<b>(208) Hoffman Unit 1</b>	3402920665000	- 81.0367645	40.82314789	X	X	X			
<b>(209) WILLIAMS C E &amp; M F #1</b>	3402920668000	- 80.73369083	40.65990161	X	X	X			
<b>(210) SOLOMON AQUILA E</b>	3402921476000	-80.81206	40.66062611	X	X		X	X	
<b>(211) CURFMAN, V # #4</b>	3402921592000	- 80.98972969	40.77792772	X	X	X	X		

(Continued)

**Table 6:** Data table denoting well names, API, location, and wireline data present at each well.

Well Name	API	Long.	Lat.	GR	RHOB	NPHI	PEF	Resistivity	GEM
<b>(212) R #ENTRIKIN #1</b>	34029216220 000	- 80.799224 03	40.8590385 3	X	X	X	X	X	
<b>(301) BRENNER #1</b>	34099202120 000	- 81.033936 42	40.9828026 4	X	X	X			
<b>(302) NORTH STAR(SWIW #10)#1</b>	34099231270 000	-80.68304	41.12018	X	X	X			
<b>(401) 34151210810000</b>	34151210810 000	- 81.262618 33	40.9532245	X	X	X			
<b>(402) L&amp; L FREDERICK COMM #1</b>	34151211230 000	- 81.170062 92	40.9147261 7	X	X	X			
<b>(403) EMMA SPONSELLER #4-A</b>	34151219990 000	- 81.330015 06	40.7430758 3	X	X				
<b>(404) PLOTT EJ &amp; CO INC #1</b>	34151245370 000	- 81.487100 72	40.7222632 5	X	X	X			
<b>(405) PSR #1</b>	34151254750 000	- 81.537940 25	40.7644799 2	X	X	X			

**Table 7:** Data table denoting the presence of core data at each well.

<b>Well Name</b>	<b>API</b>	<b>Long.</b>	<b>Lat.</b>	<b>XRD</b>	<b>XRF</b>	<b>Pyrolysis</b>	<b>TRA</b>
<b>(1) Tracker Well</b>	34133244490000	-81.06	41.13	X	X	X	X
<b>(2) SASEY STEVEN #1</b>	34133206100000	-81.20739325	41.32960075				
<b>(3) VASBINDER K UNIT #1</b>	34133208670000	-81.28318319	41.09677661			X	
<b>(4) TROUG W R #2</b>	34133238880000	-81.17071139	41.20766556	X			
<b>(5) WANTZ R UNIT #1</b>	34133240270000	-81.06800778	41.32537186	X		X	
<b>(6) SANDERS UNIT #2</b>	34133241710000	-81.06832525	41.09353592			X	
<b>(101) CLARK ET AL UNIT #1</b>	34019202860000	-81.10764108	40.65772372	X		X	
<b>(102) MCALLISTER, JOHN O. #1</b>	34019205530000	-80.98531781	40.60654042			X	
<b>(103) BRYAN UNIT</b>	34019218500000	-80.94059392	40.67130172	X		X	
<b>(104) HICKORY CLAY #12</b>	34019219200000	-81.30448261	40.61538608				
<b>(105) Lee Unit #1-DK SWIW</b>	34019220450000	-81.29419914	40.64729467			X	
<b>(106) WHITE UNIT #1</b>	34019220590000	-81.02648306	40.53315733			X	
<b>(201) BURROWS COMM.#1-2419</b>	34029205590000	-80.89936389	40.72900894	X		X	

(Continued)



**Table 7:** Data table denoting the presence of core data at each well.

<b>Well Name</b>	<b>API</b>	<b>Long.</b>	<b>Lat.</b>	<b>XRD</b>	<b>XRF</b>	<b>Pyrolysis</b>	<b>TRA</b>
<b>(202) ELDEN E # DENNY#1</b>	34029205920000	-80.988109	40.875262	X		X	
<b>(203) DONALD SELL UNIT#1</b>	34029206070000	-80.85083597	40.78516119			X	
<b>(204) E.F # SANOR #1</b>	34029206200000	-80.96642181	40.81756297	X		X	
<b>(205) Murgala Mike &amp; Mary</b>	34029206310000	-80.85418019	40.81175386	X			
<b>(206) MURRAY, F</b>	34029206480000	-80.87024414	40.78623389	X		X	
<b>(207) HAWKINS C&amp;M UNIT #1</b>	34029206560000	-80.85653517	40.81878825	X		X	
<b>(208) Hoffman Unit 1</b>	34029206650000	-81.0367645	40.82314789	X		X	
<b>(209) WILLIAMS C E &amp; M F #1</b>	34029206680000	-80.73369083	40.65990161	X		X	
<b>(210) SOLOMON AQUILA E</b>	34029214760000	-80.81206	40.66062611	X		X	
<b>(211) CURFMAN, V # #4</b>	34029215920000	-80.98972969	40.77792772			X	
<b>(212) R #ENTRIKIN #1</b>	34029216220000	-80.79922403	40.85903853	X		X	
<b>(301) BRENNER #1</b>	34099202120000	-81.03393642	40.98280264	X		X	
<b>(302) NORTH STAR(SWIW #10)#1</b>	34099231270000	-80.68304	41.12018				

(Continued)

**Table 7:** Data table denoting the presence of core data at each well.

<b>Well Name</b>	<b>API</b>	<b>Long.</b>	<b>Lat.</b>	<b>XRD</b>	<b>XRF</b>	<b>Pyrolysis</b>	<b>TRA</b>
<b>(401) 34151210810000</b>	34151210810000	- 81.26261833	40.9532245			X	
<b>(402) L&amp; L FREDERICK COMM #1</b>	34151211230000	- 81.17006292	40.91472617			X	
<b>(403) EMMA SPONSELLER #4-A</b>	34151219990000	- 81.33001506	40.74307583			X	
<b>(404) PLOTT EJ &amp; CO INC #1</b>	34151245370000	- 81.48710072	40.72226325			X	
<b>(405) PSR #1</b>	34151254750000	- 81.53794025	40.76447992			X	

**Table 8:** Data table denoting the mean mineralogy for the Curdsville Member wells utilized.

<b>Well</b>	<b>TOC %</b>	<b>Vclay</b>	<b>Vcarb</b>	<b>Vsilic.</b>	<b>Porosity</b>	<b>Vpyrite</b>
<b>SASEY STEVEN #1</b>	2.047	0.1012	0.738	0.099	0.0085	0.014
<b>TROUG W R #2</b>	2.4488	0.0319	0.8133	0.0816	0.006	0.0161
<b>WANTZ R UNIT #1</b>	3.5639	0.0391	0.8316	0.0006	0.0253	0.034
<b>SANDERS UNIT #2</b>	2.9998	0.0429	0.7785	0.0832	0.0136	0.0199
<b>CLARK ET AL UNIT #1</b>	5.5423	0.031	0.6549	0.1065	0.053	0.0383
<b>MCALLISTER, JOHN O. #1</b>	2.7209	0.0633	0.7623	0.0901	0.0111	0.0177
<b>HICKORY CLAY #12</b>	0.4974	0.1008	0.7497	0.1062	0.0335	0.0033
<b>WHITE UNIT #1</b>	2.3938	0.0923	0.7282	0.1074	0.0086	0.016
<b>ELDEN E # DENNY#1</b>	1.5973	0.0849	0.7881	0.078	0.0076	0.012
<b>MURRAY, F</b>	2.1042	0.0821	0.7627	0.0936	0.0057	0.0141
<b>HAWKINS C&amp;M UNIT #1</b>	2.3803	0.0225	0.8303	0.0766	0.0049	0.0155
<b>WILLIAMS C E &amp; M F #1</b>	2.3788	0.0406	0.8078	0.0837	0.002	0.0174
<b>CURFMAN, V # #4</b>	2.2472	0.072	0.7449	0.119	0.0029	0.0169
<b>R #ENTRIKIN #1</b>	4.1226	0.0458	0.7307	0.0988	0.0129	0.0266
<b>NORTH STAR(SWIW #10)#1</b>	1.7888	0.1195	0.688	0.0989	0.0283	0.0123
<b>L &amp; L FREDERICK COMM #1</b>	1.534	0.1276	0.7489	0.079	0.0052	0.0132
<b>EMMA SPONSELLER #4-A</b>	2.1386	0.0949	0.7423	0.1016	0.0041	0.0162
<b>PLOTT EJ &amp; CO INC #1</b>	4.3369	0.0148	0.7883	0.0683	0.0099	0.0276
<b>PSR #1</b>	4.0183	0.2192	0.4605	0.0986	0.0455	0.0268

**Table 9:** Data table denoting the mean mineralogy for the Logana Member wells utilized.

<b>Well</b>	<b>TOC %</b>	<b>Vclay</b>	<b>Vcarb</b>	<b>Vsilic.</b>	<b>Porosity</b>	<b>Vpyrite</b>
<b>SASEY STEVEN #1</b>	5.2371	0.2118	0.4522	0.1479	0.0573	0.0342
<b>TROUG W R #2</b>	4.787	0.1815	0.4776	0.1746	0.0447	0.0317
<b>WANTZ R UNIT #1</b>	4.4639	0.1572	0.6621	0.0138	0.0608	0.0393
<b>SANDERS UNIT #2</b>	3.6081	0.0512	0.7346	0.0947	0.0221	0.0239
<b>CLARK ET AL UNIT #1</b>	4.4325	0.0663	0.6605	0.1234	0.0335	0.0287
<b>MCALLISTER, JOHN O. #1</b>	3.0467	0.073	0.7239	0.1063	0.0168	0.0198
<b>HICKORY CLAY #12</b>	0.8249	0.1003	0.7258	0.128	0.0271	0.0053
<b>Lee Unit #1-DK SWIW</b>	0.2281	0.0731	0.7683	0.1115	0.0441	0.0012
<b>WHITE UNIT #1</b>	2.7346	0.1162	0.6601	0.1401	0.0122	0.018
<b>ELDEN E # DENNY#1</b>	1.9809	0.0761	0.7812	0.083	0.0071	0.0137
<b>DONALD SELL UNIT#1</b>	0.4609	0.0757	0.8341	0.0635	0.0174	0.0024
<b>MURRAY, F</b>	3.1015	0.081	0.7053	0.115	0.0161	0.0202
<b>HAWKINS C&amp;M UNIT #1</b>	2.9817	0.0154	0.8189	0.0718	0.012	0.0192
<b>WILLIAMS C E &amp; M F #1</b>	2.7707	0.0524	0.7766	0.0922	0.0029	0.0192
<b>CURFMAN, V # #4</b>	2.5767	0.0825	0.7139	0.1302	0.0038	0.0185
<b>R #ENTRIKIN #1</b>	4.2511	0.0527	0.7143	0.1034	0.015	0.0274
<b>NORTH STAR(SWIW #10)#1</b>	0.6184	0.1679	0.6475	0.1401	0.0339	0.0043
<b>34151210810000</b>	3.5832	0.0223	0.7935	0.0817	0.0038	0.0231
<b>L&amp; L FREDERICK COMM #1</b>	1.3903	0.139	0.7194	0.0992	0.0077	0.0128
<b>EMMA SPONSELLER #4-A</b>	1.9002	0.0985	0.7483	0.0987	0.004	0.015
<b>PLOTT EJ &amp; CO INC #1</b>	3.8789	0.0228	0.7987	0.0682	0.0037	0.0246
<b>PSR #1</b>	4.1289	0.183	0.5296	0.1039	0.0367	0.0274

**Table 10:** Data table denoting the mean mineralogy for the Upper Lexington wells utilized.

Well	TOC %	Vclay	Vcarb	Vsilic.	Porosity	Vpyrite
<b>SASEY STEVEN #1</b>	5.4154	0.1019	0.4429	0.1509	0.0597	0.0361
<b>TROUG W R #2</b>	4.9227	0.1454	0.4553	0.1813	0.0471	0.0328
<b>WANTZ R UNIT #1</b>	4.6967	0.1707	0.6119	0.021	0.0701	0.0313
<b>SANDERS UNIT #2</b>	3.3677	0.0553	0.7216	0.1035	0.019	0.0225
<b>CLARK ET AL UNIT #1</b>	5.9113	0.0211	0.6189	0.1297	0.0525	0.0394
<b>MCALLISTER, JOHN O. #1</b>	2.4436	0.0517	0.73	0.1081	0.0085	0.0163
<b>HICKORY CLAY #12</b>	0.4041	0.0926	0.7094	0.1409	0.0214	0.0027
<b>Lee Unit #1-DK SWIW</b>	0.961	0.0612	0.7306	0.1151	0.051	0.0064
<b>WHITE UNIT #1</b>	2.6662	0.0952	0.6425	0.1466	0.0132	0.0178
<b>ELDEN E # DENNY#1</b>	1.3929	0.0457	0.7574	0.0951	0.0058	0.0093
<b>DONALD SELL UNIT#1</b>	0.3715	0.0882	0.8286	0.0629	0.0162	0.0025
<b>MURRAY, F</b>	2.9958	0.0597	0.6994	0.1183	0.0155	0.02
<b>HAWKINS C&amp;M UNIT #1</b>	2.9173	0.028	0.7834	0.089	0.0121	0.0194
<b>Hoffman Unit 1</b>	0.3256	0.0624	0.7819	0.043	0.0064	0.0022
<b>WILLIAMS C E &amp; M F #1</b>	2.3499	0.0511	0.7627	0.1034	0.0047	0.0157
<b>SOLOMON AQUILA E</b>	0.1418	0.0869	0.7228	0.1382	0.0225	0.0009
<b>CURFMAN, V # #4</b>	2.4699	0.0985	0.686	0.1436	0.0054	0.0165
<b>R #ENTRIKIN #1</b>	4.1844	0.0609	0.6753	0.1205	0.0157	0.0279
<b>NORTH STAR(SWIW #10)#1</b>	1.997	0.0983	0.6018	0.1486	0.0215	0.0133
<b>L&amp; L FREDERICK COMM #1</b>	1.5824	0.065	0.6457	0.1081	0.0126	0.0105
<b>EMMA SPONSELLER #4-A</b>	1.7271	0.0687	0.7143	0.1156	0.0048	0.0115
<b>PSR #1</b>	3.2827	0.1508	0.4799	0.0996	0.0361	0.0219

**Table 11:** Data table denoting the mean mineralogy for the Point Pleasant wells utilized.

Well	TOC %	Vclay	Vcarb	Vsilic.	Vpyrite	Porosity
<b>(1) Tracker Well</b>	5.443	0.2047	0.4033	0.2086	0.0363	0.046
<b>(2) SASEY STEVEN #1</b>	4.5864	0.4322	0.1027	0.3074	0.0306	0.0529
<b>(4) TROUG W R #2</b>	5.1648	0.3613	0.1412	0.3214	0.0344	0.053
<b>(5) WANTZ R UNIT #1</b>	4.8502	0.439	0.1692	0.2154	0.0323	0.1054
<b>(6) SANDERS UNIT #2</b>	5.5217	0.2089	0.3851	0.2128	0.0368	0.0541
<b>(101) CLARK ET AL UNIT #1</b>	5.3486	0.174	0.4015	0.2423	0.0357	0.0465
<b>(102) MCALLISTER, JOHN O. #1</b>	5.2012	0.1804	0.3974	0.2461	0.0347	0.0445
<b>(104) HICKORY CLAY #12</b>	4.263	0.2918	0.3147	0.242	0.0284	0.0488
<b>(105) Lee Unit #1-DK SWIW</b>	4.9363	0.257	0.3066	0.2474	0.0329	0.0695
<b>(106) WHITE UNIT #1</b>	5.6167	0.1984	0.3438	0.2662	0.0374	0.0504
<b>(202) ELDEN E # DENNY#1</b>	4.4908	0.1716	0.4526	0.2262	0.0299	0.0353
<b>(206) MURRAY, F</b>	5.9482	0.1764	0.3645	0.2547	0.0397	0.0544
<b>(207) HAWKINS C&amp;M UNIT #1</b>	5.6329	0.0235	0.5702	0.1365	0.0376	0.0521
<b>(208) Hoffman Unit 1</b>	2.0357	0.2347	0.474	0.2316	0.0136	0.0109
<b>(209) WILLIAMS C E &amp; M F #1</b>	5.6867	0.1298	0.5642	0.1182	0.0379	0.0408
<b>(211) CURFMAN, V # #4</b>	5.2584	0.1592	0.4705	0.1982	0.0351	0.0366
<b>(212) R #ENTRIKIN #1</b>	5.2046	0.2193	0.3757	0.2334	0.0347	0.0404
<b>(301) BRENNER #1</b>	7.7191	0.1851	0.386	0.1391	0.0555	0.0848
<b>(302) NORTH STAR(SWIW #10)#1</b>	5.4688	0.3796	0.1717	0.2525	0.0365	0.0678
<b>(401) 34151210810000</b>	6.9898	0.0782	0.4449	0.1671	0.0466	0.0641
<b>(402) L&amp; L FREDERICK COMM #1</b>	5.3842	0.0353	0.3427	0.1744	0.0359	0.0561
<b>(403) EMMA SPONSELLER #4-A</b>	4.5172	0.1888	0.4559	0.2131	0.0301	0.0268
<b>(404) PLOTT EJ &amp; CO INC #1</b>	4.5475	0.2438	0.3591	0.2512	0.0303	0.032

**Table 12:** Data table denoting the mean mineralogy for the Utica shale wells utilized.

Well	TOC %	Vclay	Vcarb	Vsilic.	Porosity	Vpyrite
<b>(1) Tracker Well</b>	2.3964	0.4026	0.1456	0.3587	0.0443	0.016
<b>(2) SASEY STEVEN #1</b>	3.7908	0.5209	0.0532	0.3057	0.0402	0.0253
<b>(4) TROUG W R #2</b>	3.638	0.4757	0.0572	0.3578	0.0303	0.0243
<b>(6) SANDERS UNIT #2</b>	4.83	0.3392	0.1717	0.3264	0.0456	0.0322
<b>(101) CLARK ET AL UNIT #1</b>	7.6349	0.3354	0.0344	0.3716	0.078	0.0512
<b>(102) MCALLISTER, JOHN O. #1</b>	3.5398	0.4015	0.0804	0.4124	0.0251	0.0236
<b>(104) HICKORY CLAY #12</b>	1.7976	0.4668	0.0736	0.382	0.0474	0.012
<b>(105) Lee Unit #1-DK SWIW</b>	1.425	0.4458	0.0744	0.3958	0.0638	0.0095
<b>(106) WHITE UNIT #1</b>	3.4079	0.4329	0.0411	0.4268	0.0234	0.0227
<b>(202) ELDEN E # DENNY#1</b>	2.6237	0.3638	0.1889	0.3727	0.0161	0.0175
<b>(204) E.F # SANOR #1</b>	4.5507	0.4745	0.0633	0.3189	0.0421	0.0303
<b>(206) MURRAY, F</b>	4.6123	0.4102	0.0462	0.3991	0.0379	0.0307
<b>(211) CURFMAN, V # #4</b>	4.3803	0.3589	0.1301	0.3643	0.0389	0.031
<b>(302) NORTH STAR(SWIW #10)#1</b>	2.4242	0.5621	0.0115	0.3015	0.0859	0.0162
<b>(403) EMMA SPONSELLER #4-A</b>	3.0269	0.4272	0.0791	0.4076	0.0198	0.0202
<b>(404) PLOTT EJ &amp; CO INC #1</b>	4.0888	0.3886	0.1001	0.3836	0.032	0.0273

## **12. VITA**

Tyler West graduated from Stephen F. Austin State University in 2019 with a Bachelor of Science in Geology. After completing his degree, he continued his education at SFA and completed an internship in the oil and gas industry with a focus on petrophysics. He received the degree of Master of Science in Geology in August 2023.

Permanent Address: 1502 County Road 3120  
San Augustine, TX, 75972

Style Manual: Geological Society of America

This thesis was typed by Tyler L. West.